Cytochrome *c*-DNA and Cytochrome *c*-Enzyme Interactions for the Construction of Analytical Signal Chains

Dissertation

zur Erlangung des akademischen Grades

"doctor rerum naturalium"

(Dr. rer. nat.)

in der Wissenschaftsdisziplin "Biochemie"

eingereicht an der

Mathematisch-Naturwissenschaftlichen Fakultät

der Universität Potsdam

von

Christoph Wettstein

Potsdam, Januar 2015

Für meine Eltern, Jutta und Stefan.

Acknowledgement

LIST OF ABBREVIATIONS

General terms

AA	amino acid
AuE	gold electrode
bp	base pair
ct	calf thymus
DET	direct electron transfer
ET	electron transfer
E_f	formal potential
MET	mediated electron transfer
ML	multilayer
MWCO	molecular weight cut-off
pI	isoelectric point
U	unit
v	velocity
v_0	initial rate

Proteins

cyt *c*	cytochrome *c*
FDH	fructose dehydrogenase (FAD dependend)
PQQ-GDH	glucose dehydrogenase (PQQ dependend)

Chemicals

DNA	desoxyribonucleic acid
EDC	N-ethyl-N-(3- dimethylaminopropyl) carbodi-imide hydrochloride
FAD	flavin-adenin-dinucleotide
fructose	D-fructose
KPi	KH_2PO_4/K_2HPO_4 buffer
NaPi/cit	Na_2HPO_4/citric acid buffer
MES	2-(*N*-morpholino)ethansulfonic acid

MU	11-mercaptoundecanol
MUA	11-mercaptoundecanoic acid
PASA	poly(anilinesulfonic acid)
PEI	poly(ethyleneimine)
PQQ	pyrroloquinoline quinone
PSS	poly(sodium 4-styrenesulfonate)
TX	Triton X-100
SAM	self-assembling monolayer

Methods

AFM	atomic force microscopy
CV	cyclic voltammetry
HSQC	heteronuclear single quantum coherence
LBL	layer-by-layer
NMR	nuclear magnetic resonance spectroscopy
QCM	quartz crystal micro balance
TROSY	transverse relaxation-optimised spectroscopy

Units

A	Ampère
cm	centi metre
Da	Dalton
M	mol/L
V	Volt
k	kilo (10^3)
m	mili (10^{-3})
μ	micro (10^{-6})
n	nano (10^{-9})
p	pico (10^{-12})

LIST OF CONTENTS

LIST OF FIGURES

LIST OF TABLES

INTRODUCTION

1.1   General motivation

Electron transfer (ET) reactions play a crucial role in the metabolic pathways of all organisms. They are the most common types of biochemical reactions occurring in essential biochemical signal chains, such as the respiratory chain or photosynthesis. These cascades of ET reactions comprise a precisely organised series of proteins and protein complexes that link charge transfer reactions to other forms of chemical energy equivalents, *i.e.* sugars or adenosine triphosphate. Based upon the natural example, artificial protein assemblies were engineered, mimicking cascades of biochemical signal transduction. Such protein assemblies possess the potential of application in the field of bioelectronics, biosensors and biofuel cells.

Enabling direct electron transfer (DET) from proteins on an electrode was a breakthrough in bioelectronics, providing a simple and efficient way of connecting biological recognition elements with a signal transducer. Hereby, using electron mediators is avoided, reducing potential interferences and side reactions (Wu and Hu, 2007). The heme protein cytochrome *c* (cyt *c*) is one example of a natural electron transfer component that shows DET on different types of electrodes, such as gold, silver, platinum, carbon and metal oxides (Gorton et al., 1999).

Going beyond the adsorption of redox proteins in a monolayer, multilayer (ML) architectures can be assembled on gold electrodes (AuE) by the layer-by-layer (LBL) deposition technique (Decher et al., 1998; Lisdat et al., 2009). The basic principle of electrostatic LBL assemblies is based upon the alternating incubation of a solid substrate (e.g. an electrode) in solutions of oppositely charged molecules. The architecture is mainly stabilised by charge-charge interactions between the two building blocks, although other interactions may contribute.
Due to its ability to accept, shuttle and donate one electron, cyt *c* can be employed as a central building block of these ML assemblies. Cyt *c* has a basic isoelectric point (pI), giving its surface a net positive charge in acidic and neutral media. Negatively charged polyelectrolytes, such as sulfonated polyanilines (Lisdat et al., 2009) and surface-modified nanoparticles (NPs) (Bonk and Lisdat, 2009; Feifel and Lisdat, 2011) are used as a second building block. The LBL deposition technique is suitable for the tuning of the protein concentration on the electrode surface, while the polyelectrolyte or NP provides a biocompatible matrix for protein entrapment.

Analytical signal chains were created by coupling enzymes with cyt *c* ML systems assembled with NPs or sulfonated polyanilines (Feifel et al., 2014b; Lisdat et al., 2009). Within such systems, an electrical signal is generated by the reaction of the enzyme with the substrate and different inter-protein ET steps via cyt *c* molecules to the electrode, and *vice versa*. The functionality of such engineered ET systems is based upon protein-protein interaction and thus follows the example of nature. In the case of a sufficient stability and sensitivity, these enzyme-linked cyt *c* ML systems can be used in biosensor applications.

Recently, a cyt *c* ML system, in which the natural polyelectrolyte DNA is utilised as second building block, was characterised in a short communication (Sarauli et al., 2009). With its fibrous morphology and its negatively charged backbone, DNA has similar chemical properties, such as the previously used sulfonated polyanilines. At the same time, the biomolecule is more diverse in its molecular components. Compared to the systems based on sulfonated polyanilines, the cyt *c*/DNA ML assembly adsorbs an extraordinary high amount of electro active cyt *c* on the electrode surface. The electrostatic character of the interaction between cyt *c* and DNA was studied (Sarauli et al., 2009), however, the interaction of the two building blocks on the molecular level is still unclear. Moreover, the combination of the cyt *c*/DNA ML system with enzymes for the creation of analytical signal chains remains to be studied.

1.2   Aim of this work

The first aim of this work is to study the interaction of the two bio-molecules cyt *c* and DNA, providing the basis for the assembly of stable protein architectures on electrodes. Although the electrostatic nature of the cyt *c*/DNA interaction is known in principle, the factors influencing the interactive forces are poorly understood. Aiming on the identification of DNA's binding sites on the protein surface, the two building blocks shall be investigated in solution by means of UV-vis, circular dichroism (CD) and 2D-NMR-spectroscopy.

Targeting the creation of ET signal chains on electrode surfaces, the focus of the second part is placed upon studying the combination of enzymes with cyt *c* to utilise the enzymes' substrate specificity. In order to study the requirements for the assembly of such signal chains, two enzymes, differing in size, cofactor, surface properties and intercellular organelle locations, shall be investigated as reaction partner of freely diffusing cyt *c* and cyt *c* immobilised on an electrode surface. Concerning the immobilised state, cyt *c* monolayer and ML assemblies are addressed. If the interaction is feasible, an ET chain on the basis of a cyt *c* ML system shall be assembled and the electron pathway, induced by the respective catalytic reaction, is to be studied. Hereby, the sensor properties of the bi-protein electrode shall be characterised and the applicability of the bi-protein ML system as interface for enzyme coupling shall be evaluated.

LITERATURE REVIEW

2.1   Introduction to electrochemical biosensors

Biosensors are defined as analytical devices or units, incorporating a biological or biologically derived sensitive recognition element, integrated or associated with a physicochemical transducer (Turner, 2000). As biological recognition elements enzymes, proteins, antibodies, receptors, nucleic acids, aptamers, lectins and imprints of these molecules are employed (**figure 1**) (Chambers et al., 2008; Scheller et al., 2001).

The first example of a biosensor, published in a paper containing the term 'enzyme electrode' described the entrapment of the enzyme glucose oxidase in a dialysis membrane over an oxygen probe (Clark and Lyons, 1962). Following this approach, a similar device was developed in 1967, using again glucose oxidase as recognition element which was immobilised in a polyacrylamide gel on the surface of an oxygen electrode, enabling glucose sensing (Updike and Hicks, 1967).

To this day, glucose sensitive devices have the most substantial commercial success in this field of bio-sensing. For their classification, biosensors can be divided into the type of transducers used, *i.e.* optical, piezoelectric, electrochemical, acoustic or thermal pathways. Electrochemical biosensors are bio-electronic devices based upon reactions that accept or donate electrons or generate potentiometric detectable species (Privett et al., 2010).
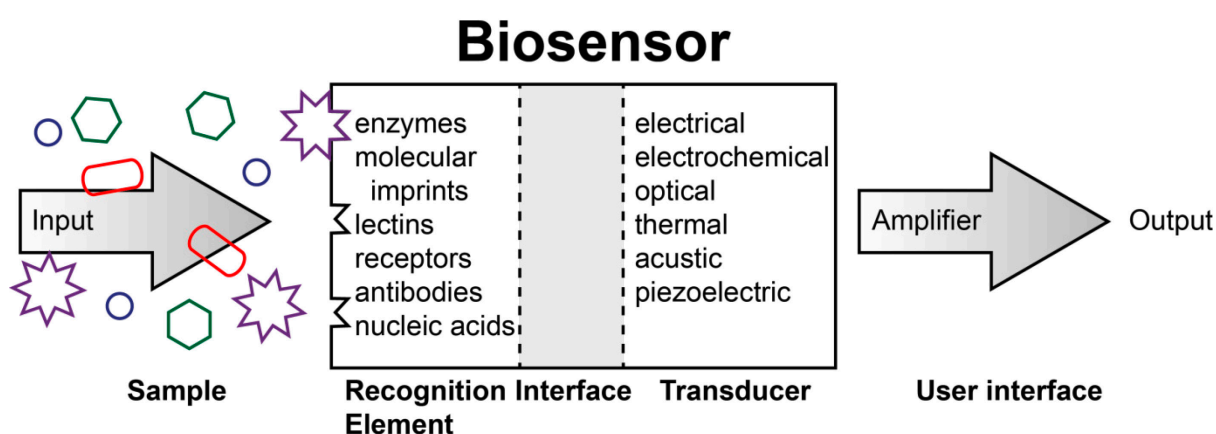
Figure 1: Schematic configuration of a biosensor listing different biorecognition and transduction elements connected by an interface (according to Chambers *et al.*, 2008).

Therefore, especially redox proteins and oxidoreductases serve as recognition elements. For the quantification of the generated signal, different potentiometric, voltammetric and amperometric methods are used, which measure either the potential or the current change, depending on the concentration of the respective analyte.

The classification of voltammetric and amperometric biosensors is based upon the three different sensor generations that were developed:

- First generation sensors measure the product of a reaction or the consumption of a co-substrate directly at the electrode.
- Second generation biosensors use mediators that shuttle electrons between the product of the catalytic reaction and the electrode to avoid interference.
- Third generation electrochemical biosensors are based upon direct protein electrochemistry between the electrode and the protein.

The basic principles of the third generation biosensors are reviewed by Wu et al., addressing redox proteins such as cyt c, as well as enzymes (Wu and Hu, 2007). Their main advantage is an advanced selectivity, given that the absence of a mediator reduces the influence of interfering reactions (Gorton, 1995). Moreover, they should operate in a potential window closer to the redox potential of the enzyme itself (Gorton et al., 1999). DET between the enzyme and the electrode surface can be achieved by using self-assembled monolayers on electrodes with a covalent enzyme attachment (Kim et al., 2012; Love et al., 2005). Another attractive feature of the systems based upon DET is the possibility of modulating the desired properties of an analytical device by modification of proteins with genetic or chemical engineering techniques (Degani and Heller, 1988; Heller et al., 1987; Wegerich et al., 2009; Willner et al., 1997). Moreover, novel interfacial materials based on nano-technological achievements, such as carbon nanotubes (Gooding et al., 2003; Katz and Willner, 2004), graphene (Pumera et al., 2010; Shan et al., 2009) or gold nanoparticles (Pingarron et al., 2008; Xiao et al., 2003), are applied as electrodes.

A variation of third generation biosensors is ET chains assembled in multiple layers on electrode surfaces. These ML architectures provide a biocompatible interface for the coupling with enzymes, awarding the electrode specificity towards a variety of substrates. Besides their sensing abilities, these assemblies enable the investigation of biological ET pathways in

a model system, since they mimic the examples of nature. In this case, cyt *c* is considered as a wiring agent between the enzyme and the electrode.

2.2   Electron transfer in nature and on surfaces

ET is the most common type of biochemical reaction and plays a crucial role in the cascades of anabolic and catabolic pathways in cells. The anabolic photosynthesis is driven by light absorption and assimilates carbohydrates as high-energetic equivalents from the low-energetic carbon compound CO_2. The respiratory chain represents a catabolic ET pathway that is located in the inner membraf mitochondria, the cells' power plants (**figure 2, left**). At the beginning of the respiratory chain, electrons are extracted from NADH (citric acid cycle) or $FADH_2$ (fatty acid oxidation) by the multi-enzyme complexes I or II. These two enzymes reduce one ubiquinone (Q) molecule by donating two electrons. The reduced Q, ubiquinol (QH_2) subsequently shuttles the two electrons via the inner, lipophilic part of the mitochondrial membrane until it reaches complex III. After docking to complex III, QH_2 transfers one electron to the Rieske-2Fe-2S-cluster, then to cyt c_1 and from there to an oxidised cyt *c* molecule, which is liberated into the inter-membrane space. The water-soluble cyt *c* diffuses along the outside of the inner membrane and reduces complex IV (cyt *c* oxidase), which then transfers electrons to O_2 to generate water. The second electron is used to reduce a Q at the Q_i-site, which binds two protons (H^+) from the matrix and transfers them to the cytosolic side of the membrane, generating an H+ gradient between the mitochondrial matrix and the cytosol. The complexes I, III and IV participate in this process. The resulting H+ reflux, from the cytosol to the mitochondrial matrix proceeds via the ATP synthase complex and is the driving force of the ATP synthesis (**figure 2, right**) (Berg et al., 2012).
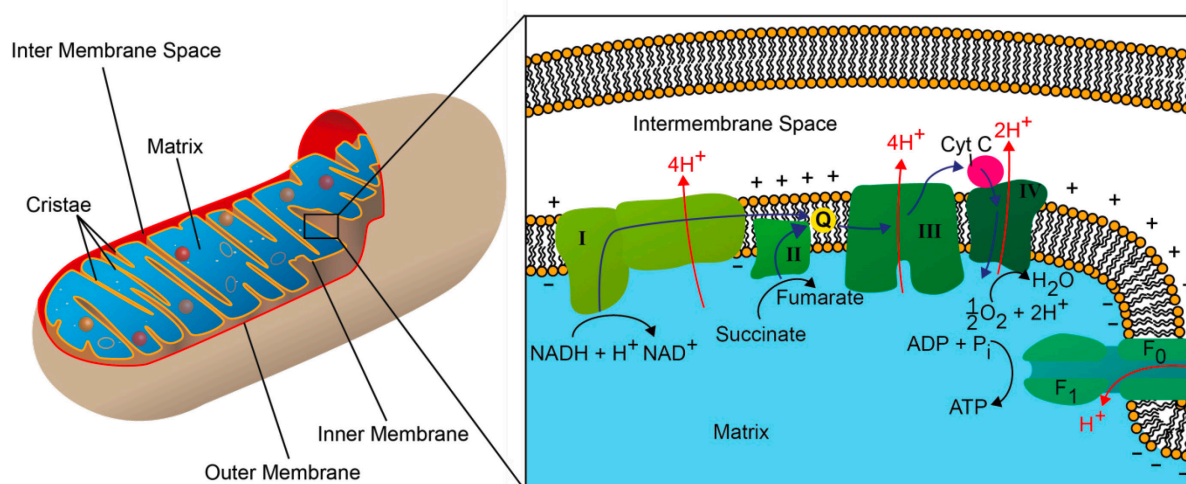
Figure 2, Left: Schematic representation of a mitochondrion. **Right:** Magnification of the inner mitochondrial membrane and schematic representation of the enzymes involved in the respiratory chain (www.robertlfurler.com). The blue arrows represent the ET from NADH via the enzyme complexes and mediator on molecular oxygen. Enzymes are labelled as follows: NADH-oxidoreductase (I), succinate-reductase (II), cyt *c*-reductase (III), cyt *c*-oxidase (IV) and ATP synthase (F0+F1).

The redox property of cyt *c* has been applied in biotechnology to construct biosensors and biofuel cells (Cooney et al., 2008; Lisdat et al., 2009; Wu and Hu, 2007). Therefore, the redox reaction of cyt *c* with electrodes of different materials *i.e.* gold, silver, platinum, carbon and metal oxides (Eddowes and Hill, 1977; Jin et al., 1996; Scott and Mauk, 1996; Song et al., 1993; Williams, 1989; Yeh and Kuwana, 1977) have been studied.

Enabling DET between proteins and electrodes is a challenging task and the most critical point in the development of third generation biosensors. Since the redox centres of proteins are deeply buried within the protein shell, ET to the electrode is slow or even impossible. Therefore, the rate constant of the ET reaction between protein and electrode is an important feature. It contains the exponential correlation between the distance of the active site to the electrode and is based on the Marcus theory (Marcus, 1993; Marcus and Sutin, 1985), for which Marcus was awarded the Nobel Prize in Chemistry in 1992.

Most protein-mediated ET processes occur over distances above the van der Waals contact, which is influenced by the sum of the attractive or repulsive forces between molecules. The semi-classical Marcus theory predicts that in this case the ET rate (k) is governed by the driving force of the reaction (ΔG^0), the nuclear reorganisation energy (λ), which comprises

both "fast" inner-shell and "slow" outer-shell reorganisation energy arising from intramolecular and solvent internuclear distances (Sutin et al., 1988), and the electronic coupling (H_{DA}) between electron donor (D) and acceptor (A) at the transition state. This can be expressed as: (Jeuken, 2003)

$$k = \frac{2\pi}{\hbar} \frac{H^2_{DA}}{\sqrt{4\pi\lambda RT}} e^{\frac{-(\Delta G^0 + \lambda)^2}{4\lambda RT}} \quad . \tag{1}$$

A broad range of theoretical approaches have been developed to predict H_{DA} in proteins. The most simple one is the square-barrier model, which treats the protein as an 'organic' glass in which H_{DA} decays exponentially with distance. Here, the effectiveness of the protein in ET is given by the tunnelling parameter β, expressed as: (Jeuken, 2003)

$$H^2_{DA} = (H^0_{DA})^2 \exp^{(-\beta \cdot (r_{DA} - r_0))} \tag{2}$$

in which H^0_{DA} is the electronic coupling at the van der Waals distance (r_0) and r_{DA} is the distance between the donor and acceptor. β ranges between 0.8 and 1.6 Å^{-1} and is dependent on the structure of the protein (Jeuken, 2003).

In order to enable DET between cyt c and the electrode, the proximity of the active site to the electrode and the proper molecular orientation of the protein on the surface are the key requirements (Scott and Mauk, 1996; Song et al., 1993; Wang and Waldeck, 2008). Moreover, if metal electrodes are used, irreversible adsorption and denaturation has to be prevented. The defined orientation as well as the prevention of denaturation is achieved by promoters, namely alkane thiols (Arnold et al., 1997; Collinson et al., 1992; Ge and Lisdat, 2002; Song et al., 1993), cysteamine (Katz et al., 1994) and DNA (Ikeda et al., 1990; Steel et al., 1998; Thiel et al., 1997). The term promoter is used to denote that these compounds do not act as ET mediators, but help (promote) ET through the establishment of correct orientation of the redox protein on the electrode (Gorton et al., 1999). Alkane thiols form self-assembling monolayers (SAM) due to chemisorption on selected metal surfaces (**figure 3**). Regarding the molecule structure, the length of the alkane chain strongly influences the

efficiency of the ET between the electrode and the protein (Arnold et al., 1997; Feng et al., 1997; Song et al., 1993). Directed adsorption of cyt *c* can be achieved by functionalising the alkane thiol with a carboxylic group (COOH) (Ge and Lisdat, 2002; Song et al., 1993; Wang and Waldeck, 2008).

The six positively charged lysine residues neighbouring cyt *c*'s cleft leading towards the heme group (Bushnell et al., 1990; Crowley and Carrondo, 2004) interact with the negatively charged carboxylic groups of the SAM. Cyt *c* forms an adsorptive monolayer on the thiol-modified electrode by charge-charge interaction (**figure 3**). Covalent immobilisation can be achieved by cross-linking primary amines of these lysines with the carboxy-group of the SAM via carbodiimides, such as 1-ethyl-3(3-dimethylaminopropyl) carbodiimide (EDC) (Ge and Lisdat, 2002; Song et al., 1993).
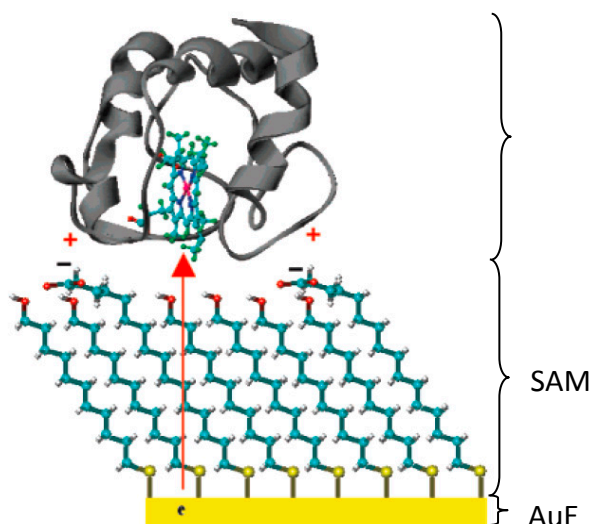
Figure 3: Schematic representation of a cyt *c* molecule (grey) bound to a self assembled monolayer (SAM) modified AuE (yellow bar with MU and MUA molecules). Charge-charge interactions stabilise the interaction between the protein's positively charged surface patches and the negatively charged carboxylic groups of the SAM. The red arrow displays the ET between the AuE and the heme site of the redox protein across the alkane thiol layer (Yue et al., 2008).

As an alternative promoter, DNA was used to enable ET reactions between redox proteins and electrodes. For instance, the enhancement of ET between cyt *c* and electrodes in the presence of DNA with both components in solution was studied by cyclic voltammetry (Ikeda et al., 1990). Charge-charge interactions were used to immobilise cyt *c* on DNA modified electrodes while promoting direct protein electrochemistry of the redox protein.

Thiolated dsDNA was found to form monolayers on gold surfaces (Steel et al., 1998; Thiel et al., 1997), which enable adsorption of cyt *c* at low ionic strength and quasi-reversible ET to the electrode (Lao et al., 2007; Lisdat et al., 1999; Shao et al., 2008). Going beyond the monolayer system DNA has been used as a building block for the assembly of cyt *c* ML systems by applying the layer-by-layer deposition technique (Sarauli et al., 2009; Wettstein et al., 2012).

Recently, surface modifications, based upon nanotechnological approaches, such as carbon nanotubes (Gobel et al., 2011; Gooding et al., 2003; Katz and Willner, 2004), quantum dots (Stoll et al., 2007) and mesoporous indium tin oxide (Frasca et al., 2010; Sarauli et al., 2012b) were applied as substrate for protein immobilisation. These materials provide a very high surface to volume ratio, which is ideal for enhancing direct electrochemistry with redox active proteins.

Besides DET reactions of proteins with electrodes and inter-protein ET (IET), this work also focuses on the arrangement of proteins on electrode surfaces by the help of DNA. Therefore, the interactions between proteins and DNA as well as protein-protein interactions are addressed in the next section

2.3   Protein-DNA and protein-protein interaction

In protein-DNA interactions, non-specific and specific binding occurs, the former of which is mainly based upon charge-charge interactions between cationic residues and the phosphate groups of the anionic DNA backbone. It often precedes specific binding and maintains a loose association between the protein and the DNA duplex, such as described for the *lac* repressor (Kalodimos et al., 2004) and restriction enzymes such as EcoRV (Winkler et al., 1993) and BamHI (Viadiu and Aggarwal, 2000). Stronger binding occurs by the insertion of an α-helix into the major groove of the DNA. This was reported for zinc-fingers (Pavletich and Pabo, 1991), heat shock transcription factors (HSF) (Littlefield and Nelson, 2001), BamHI (Viadiu and Aggarwal, 2000) and histones (Khrapunov et al., 1997). Alternatively, specific binding to a particular sequence of DNA base pairs (bp) takes place. Here, proteins, such as the restriction endonuclease (EcoRV) (Winkler et al., 1993) and transcription factors (TFs) like the glucocorticoid receptors (Luisi et al., 1991), can be exemplified. This type of interaction is often accompanied by intercalation of amino acids (AAs) between the bps, after

unwinding of the DNA. Hydrophobic binding stabilises these complexes making them 10^5 times more stable than complexes based upon unspecific binding (Berg et al., 2012).

Nuclear magnetic resonance (NMR) spectroscopy was extensively applied to elucidate the crystal structure of natural and artificial protein complexes before. For example, Volkov et al. recently reported the transient cyt *c*-cyt *c* peroxidase complex (**figure 4**) from *Saccharomyces cerevisiae* by applying paramagnetic NMR, (Vanwetswinkel et al., 2013; Volkov and van Nuland, 2013; Volkov et al., 2013; Volkov et al., 2006), whereas Jasion et al. revealed the close similarities of the same complex in *Leishmani major* (Jasion et al., 2012). Moreover, the structure of the complex between cyt *c* and cyt *bc*(1) from yeast (Hunte et al., 2002) was investigated, as well as the ET between cyt *c* and cyt *c* oxidase from human tissue (Sakamoto et al., 2011). Besides protein-protein complexes, protein-DNA complexes were also studied. Iwahara et al. applied ^{1}H paramagnetic relaxation enhancement to study non-specific binding of the HMG-box–protein to DNA and the specific binding of the SRY protein (Iwahara et al., 2004). Further, the transient complex formation between the transcription factor homeodomain of HOXD9 and a non-specific DNA sequence was investigated with respect to structural and kinetic aspects using a variety of NMR spectroscopic techniques (Iwahara and Clore, 2006; Iwahara et al., 2006).
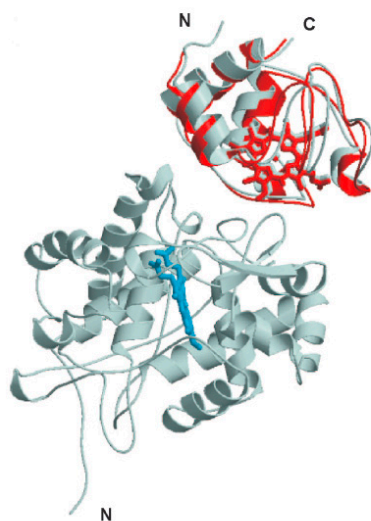
Figure 4: Solution structure of the cyt *c*-cyt *c* peroxidase complex. The lower molecule represents cyt *c*-peroxidase; the upper one is cyt *c*, while the backbone for the best solution and crystal structures are depicted in red and grey. Heme groups for both proteins are shown in sticks and the labels indicate protein termini. The complex was drawn from the inner membrane with the inter-membrane space oriented to the top of the crystal structure (PDB entry 2PCC) (Volkov et al., 2006).

Addressing biotechnological approaches, artificial protein-ligand complexes have also been investigated recently. For instance, the interaction of cyt *c* and the small protein recognition molecule, calixarene which disguises the protein surface and alters its interaction behaviour, was studied (McGovern et al., 2012). Alternatively 3D DNA designs, also known as DNA origami (Kuzuya and Komiyama, 2010), capable of holding proteins while preserving their function, were described (Andersen et al., 2008; Erben et al., 2006; Flory et al., 2014). In the field of bioelectronics especially surface confined protein arrangements are relevant.

2.4 General approaches of multilayer systems assembled by the layer-by-layer deposition technique

The construction of protein ML systems on electrodes is a popular research area, especially in the field of biosensors. For the preparation of these architectures, the LBL deposition technique is a powerful and well-investigated tool (Decher et al., 1998; Lisdat et al., 2009; Rusling et al., 2008). The primary advantage of ML films is the controlled accumulation of biological recognition elements on the electrode surface (Ariga et al., 2006; Caruso et al., 1997; Lisdat et al., 2009; Rusling et al., 2008; Zhao et al., 2006). This results in the decrease of the detection limit for the analyte and the enhancement of the signal intensity of the biosensor (Beissenhirtz et al., 2004b; Bonk and Lisdat, 2009).

Synthetic polyelectrolytes are often applied as building blocks, (Calvo et al., 2010; Decher et al., 1998; Lutkenhaus and Hammond, 2007; Song et al., 2009), while nanoparticles (Bonk and Lisdat, 2009; Feifel and Lisdat, 2011; Zayats et al., 2005) and natural materials such as DNA (Lvov et al., 1998; Rusling et al., 2008; Sarauli et al., 2009) are also used to incorporate biological compounds within ML systems. The principle of the assembly is based upon an alternating incubation of an electrode in solutions of oppositely charged molecules, stabilising the ML via charge-charge interactions between the two building blocks.

Due to its ability of electron self-exchange, the redox protein cyt *c* can be used as the central building block in the construction of ML systems on electrodes. Starting from a cyt *c* monolayer electrode, which is adsorbed to a SAM, the ML system is assembled by alternate incubation in solutions of the cationic cyt *c* and the respective anionic second building block (**figure 5**).
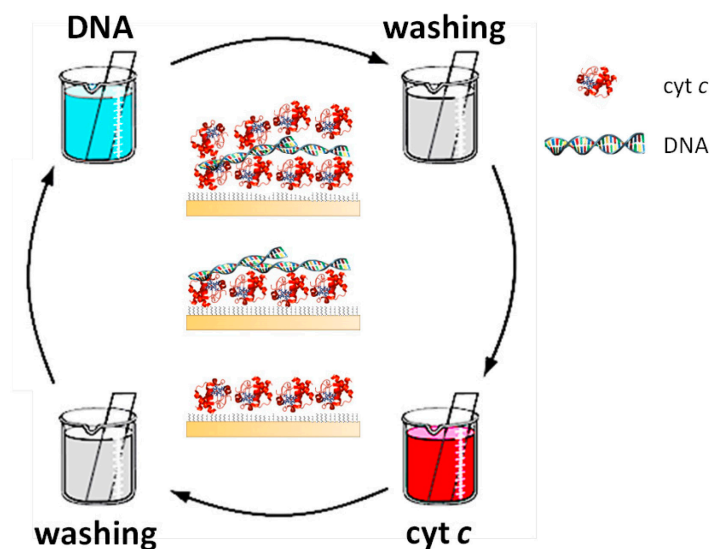
Figure 5: Representation of the assembly of a cyt *c*/DNA ML system by the LBL deposition technique. An AuE modified with a cyt *c* monolayer is alternately incubated in solutions of DNA and cyt *c* until the desired amount of protein on the electrode surface is reached. A washing step is performed in between.

Besides cyt *c*, myoglobin, the oxygen carrier protein from vertebrate muscles, was assembled in MLs. Like cyt *c*, it enables DET when immobilised on electrodes in films of varying materials. Myoglobin was adsorbed on electrodes with surfactants, such as dimethyldidodecylammonium bromide, polylysine, sodium dodecyl sulfate or cetyltrimethylammonium bromide (Bayachou et al., 1998; Guto and Kamau, 2010; Kamau et al., 2003; Nassar et al., 1995), exhibiting DET for the redox transition of the heme group. The role of surfactants in this process is suggested to be partly orientation of the protein and inhibition of oligomeric adsorbates (Wollenberger et al., 2008). Polyelectrolytes, creating multiple layers of myoglobin were used to gain higher protein loading (Lvov et al., 1998; Shen et al., 2002). However, no linear increase in the peak current or integrated charge with increasing number of layers was found, as for cyt *c*. The myoglobin closest to the electrode gave the main fraction of CV charge (Lvov et al., 1998). The E_f of myoglobin was found to be sensitive towards the nature of the film material and also to the presence of heme ligands (Wollenberger et al., 2008).

The general approach of the ML system lies in the enhanced surface density of proteins on the electrode. Given that these bio-molecules function as recognition elements of biosensors,

the increase of their surface concentration leads to a higher sensitivity (Beissenhirtz et al., 2004a; Bonk and Lisdat, 2009). Moreover, it provides a biocompatible matrix-like interface for coupling with enzymes (Balkenhohl et al., 2008; Dronov et al., 2008a; Dronov et al., 2008b; Dronov et al., 2008c; Feifel and Lisdat, 2011; Feifel et al., 2012; Lisdat et al., 2009; Spricigo et al., 2009; Wegerich et al., 2011).

A polymer based cyt c ML system was described by Beissenhirtz et al., applying the fibrous molecule polyanilin sulfonic acid (PASA) (Beissenhirtz et al., 2004b). The electro active amount of modified AuE was found to increase linearly with each cyt c/PASA layer absorbed; for example, the amount of cyt c reached approximately 650 pmol/cm² at 15 layers. The ET within the cyt c/PASA ML system was found to be quasi-reversible. Cyt c molecules located in the outer layers of ML systems generally cannot take part in the redox conversion at higher scan rates, given that the rate of potential change exceeds the rate of ET to the electrode. Thus, the ET rate constant (k_s) of this system can only be estimated to vary between 1.5 +/- 0.3 s^{-1} (for the 3-15 layers cyt c/PASA assembly) and 75 +/- 5 s^{-1}(for the cyt c monolayer) (Beissenhirtz et al., 2004b). This suggests that the electron exchange rate between the proteins within the ML is much slower than the one of cyt c and the electrode. Moreover, stronger polyanions such as polystyrene sulfonic acid and polyacrylic acid were applied, however, these polyelectrolytes prevented the generation of a fully electro active cyt c ML arrangement. Besides polyelectrolytes, surface-modified NPs were applied as second building block in cyt c ML assemblies. Bonk et al. used AuNP with an average diameter of 5 nm and a mercapto propionic acid (MPA) surface modification. The amount of electro active protein absorbed to the electrode surface increased linearly with the number of layers and a surface coverage of 100 pmol/cm² was reached at six layers. The cyt c-AuNP (MPA) ML system is stable at pH 5.0 up to an ionic strength of 100 mM phosphate buffer and provides a E_f of -24 +/- 12 mV vs. Ag/AgCl (Bonk and Lisdat, 2009). Here a k_s-range of 1.5-75 s^{-1} was determined (Bonk and Lisdat, 2009). Feifel et al. studied a ML assembly with carboxy-modified silica nanoparticles (SiNP) of different diameters. Particles with an average diameter of 5 nm resulted in the best surface coverage of 80 +/- 10 pmol/cm^2 for five deposition steps. A linear increase of the adsorbed cyt c amount in dependency on the number of incubation steps was found. The k_s is determined to be 27-75 s^{-1} for the five-layer assembly with 5 nm SiNP. Moreover, an E_f of -24 +/-5mV vs. Ag/AgCl was found. The low

width of half peak height and the narrow peak separation indicate that the cyt c molecules are present in equal states and bound in a similar microenvironment within the SiNP matrix (Feifel and Lisdat, 2011).

The described cyt c ML systems have found their application as analytical signal chains. First, the sensitivity of cyt c towards O_2 radicals enabled the application of cyt c/PASA ML as superoxide sensor. This cyt c/PASA ML showed an enhanced sensitivity for the oxygen radical, compared to the cyt c monolayer system. Its sensitivity was shown to be tuneable by the number of layers and was directly proportional to the amount of protein immobilised on the sensor surface. The highest sensitivity was reached at a six cyt c/PASA layer electrode (Beissenhirtz et al., 2004a). Second, coupling redox enzymes, which are able to interact with cyt c, to the cyt c ML systems broadened the spectrum of substrate sensitivity. Therefore, different strategies were followed:

Enzymes such as xanthine oxidase (XOD) (Dronov et al., 2007) and laccase (Balkenhohl et al., 2008) were assembled on top of cyt c/PASA ML system. Here, the inner layers contained cyt c entrapped in the PASA matrix, acting as electron mediators between electrode and enzyme. In the XOD system the cationic polyelctrolyte poly(ethyleneimine) (PEI) was employed to immobilise the enzyme on top of the cyt c/PASA ML, since XOD has an acidic pI of 5.1. Polarizing this electrode at a potential at +150 mV, and adding the enzyme substrate hypoxanthine into the measuring cell resulted in an amperometric oxidation current. Hypoxanthine is oxidised at the XOD active site and hydrogen peroxide and superoxide is liberated simultaneously. At the applied potential the cyt c ML only responds to superoxide radicals which act as shuttle molecules transferring the signal from XOD via cyt c on the electrode. Thus, a very sensitive detection of hypoxanthine, a degradation product of the purine metabolism, becomes feasible with this bi-protein electrode. In the laccase system only PASA was used as polyelectrolyte to assemble the enzyme modified cyt c ML electrode with two terminating layers of enzyme. A reductive catalytic current can be observed in dependency on the oxygen concentration, since electrons are transferred from the electrode via cyt c to laccase which then reduces oxygen to water.

The enzymes bilirubin oxidase (BOD) (Dronov et al., 2008b), cellulose dehydrogenase (CDH) (Feifel et al., 2012) and human sulphite oxidase (SOx) (Dronov et al., 2008d; Spricigo et al., 2009) were incorporated in the cyt c ML system. The key point here is that both

proteins are immobilised together onto the surface. The cyt *c*:BOD and the cyt *c*:CDH systems are fabricated by starting from a cyt *c* monolayer electrode and alternating incubation steps in a protein mixture of cyt *c*, polyelectrolyte and the respective enzyme. As polyelectrolyte the sulfonated polyanilin PASA was used for cyt *c*:BOD (Dronov et al., 2008d) and cyt *c*:SOx (Spricigo et al., 2009) entrapment while Feifel et al. used carboxy-modified silica nanoparticles for their cyt *c*:CDH (**figure 6a**) assembly (Feifel et al., 2012).

In the BOD system, the catalytic current results from reduction of cyt *c*, which is oxidised due to ET to neighbouring BOD molecules. The catalytic reduction of oxygen occurs at the BOD's active site, where electrons are transferred to molecular oxygen in a four electron-reduction process, producing water (Dronov et al., 2008b).

The ET in the cyt *c*:CDH system is based upon the oxidation of lactose at the FAD active site of the enzyme. An oxidative catalytic current is generated by the oxidation of lactose at the FAD active site of CDH. CDH transfers electrons via its cyt *b* cofactor on cyt *c* molecules located in its close environment, which then shuttle the electrons on the electrode. A further important finding of this study was that using a deglycolysated enzyme exhibits much higher current densities than the assembly with native CDH for the same number of layers (Feifel et al., 2012). A similar system was constructed with laccase instead of CDH (Feifel et al., 2014a).

a)   b)
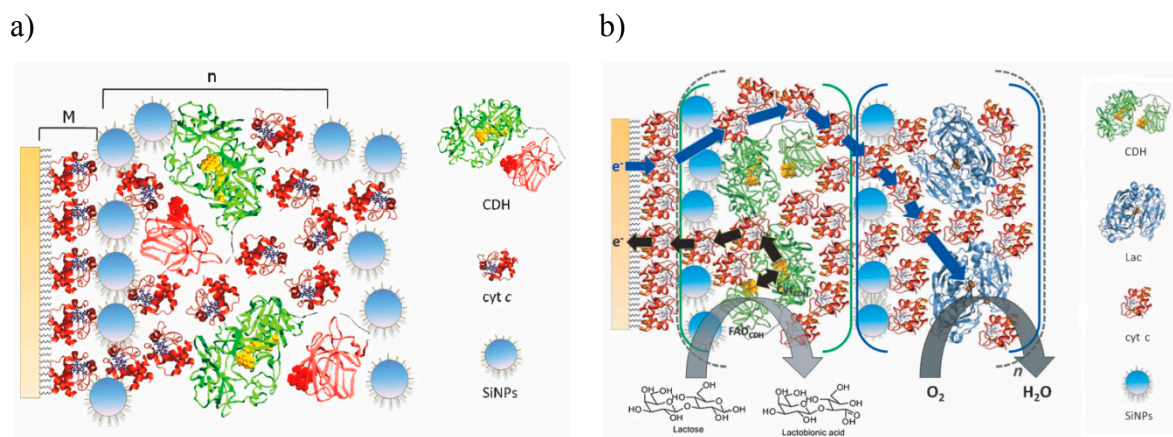
Figure 6: Schematic representation of **a)** the SiNP/cyt *c*:CDH multilayer assemblies and **b)** the SiNP/cyt *c*:CDH/SiNP/cyt *c*:laccase) multilayer assemblies prepared on a cyt *c* monolayer electrode (M). The cyt *c* monolayer is assembled on a mixed thiol layer (MU/MUA). Layered systems [SiNPs/cyt *c*:CDH]n (n = 1 - 4).(Feifel et al., 2014a; Feifel et al., 2014c)

However, it is also possible to construct such protein assemblies without a polyelectrolyte (Dronov et al., 2008d). For the cyt *c*:SOx approach solely charge-charge interactions between cyt *c* and SOx with rather separated isoelectric points were exploited to assemble a ML system on an electrode surface. Investigating this ML assembly by means of QCM, mass accumulation was detected at the electrode surface after alternating incubation of cyt *c* and the enzyme. However, no increase of the voltammteric signal of cyt *c* was found as a function of the number of layers assembled. This behaviour suggested that electron self-exchange between the cyt *c* molecules is hindered by the SOx-layer. In order to improve the ET between the layers, the enzyme was co-immobilised together with cyt *c* in a mixture by assembling alternating layers of cyt *c* and cyt *c*:CDH. For this strategy the mass accumulation on the electrode was also recorded by QCM. Moreover, voltammetric analysis showed a catalytic current in the presence of sulphite which depended on number of layers. The ET pathway of this system is based upon the oxidation of sulphite to sulphate, followed by the stepwise transfer of the abstracted electron via cyt *c* on the electrode (Dronov et al., 2008d).

Recently a ML assembly containing the enzymes CDH and laccase, embedded in a matrix of silica nanoparticles, was created. It enables the switchable and dual detection of the respective substrate, *i.e.* lactose or oxygen, in solutions (Feifel et al., 2014c). The bi-directional ET mechanism is depicted in **figure 6b**.

2.5   The cytochrome *c*/DNA multilayer system

2.5.1 Properties

In 2009 calf thymus (ct) DNA was found to be functional for the assembly of the cyt *c*/DNA ML system (Sarauli et al., 2009). Concerning the surface coverage, the assembly was found to be most efficient in acidic media of pH 5.0, but it also worked at pH 6.0. At pH 7.0 the cyt *c* monolayer coverage was not exceeded after the ML assembly. Cyclic voltammetry (CV) experiments of ML assemblies formed at pH 5.0 showed a quasi-reversible ET, a substantial amount of electro active protein (up to 320 pmol/cm^2 for a 6 bi-layer system) and only minor changes in the formal potential (E_f) of cyt *c*, indicating that at least the heme environment remains in the native state (Sarauli et al., 2009). The electron exchange rate was observed to be slower than in the cyt *c* monolayer and ML with sulfonated polyaniline. Compared to other ML systems, which were built up by using polyelectrolytes or modified nanoparticles

(Beissenhirtz et al., 2005; Bonk and Lisdat, 2009; Feifel and Lisdat, 2011) the cyt *c*/DNA system showed the highest accumulation of redox active material. These features plus the biocompatibility of the full bio-molecular system - are ideal for the application of the system as scaffold for analytical signal chain.

2.5.2 Cytochrome *c*

Cyt *c* is a small heme-containing redox protein, which acts as electron shuttle in the respiratory chain of mitochondria (Scott and Mauk, 1996). It was the first protein to be studied electrochemically and remains one of the most common redox proteins utilised in electrochemical studies and applications (Gorton et al., 1999). Its heme moiety is held through two thioether linkages to cysteines (C14 and C17), surrounded by the folded polypeptide chain, which refolds reversibly after denaturation by pH (Fisher et al., 1973). Besides this cyt *c* has a remarkable thermo-stability, its alpha helical structures remain unchanged up to 45 °*C* (Fisher et al., 1973).

Horse heart cyt *c* contains 19 positively charged lysine residues that are located in the periphery of the protein and, combined with others, award cyt *c* its basic pI of 10.0-10.5 (Malmgren et al., 1978). Six of them account for 53% of cyt *c*'s interface area (Crowley and Carrondo, 2004) encircling the heme edge (Bushnell et al., 1990) (**figure 7**) to favour fast ET by electrostatic steering (Finzel et al., 1984; Poulos et al., 1980).
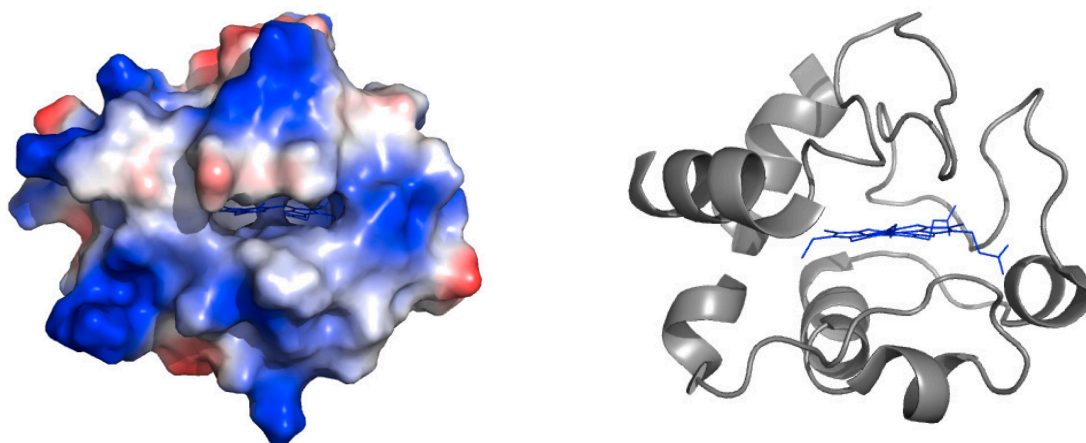
Figure 7, Left: Vacuum electrostatics of horse heart cyt *c* with view on the cavity leading towards the heme edge. Positive charges are in blue, negative charges are in red and neutral charges are in white. **Right:** Representation of secondary structure elements of the protein (grey and the heme edge in blue). The figures were generated from the crystal structure by pymol based upon pdb-file 1HRC (Bushnell et al., 1990).

The positively charged surface patches cause the 'stickiness' of the protein, resulting in strong, unspecific interactions with cell lysates (Crowley et al., 2011). Moreover, charge-charge interactions of lysines with negatively charged functionalities of reaction partners and surfaces, e.g. SAMs, can occur. This provides the basis for an efficient and oriented immobilisation on electrodes (Finklea, 1996) (also see **2.2**). In biotechnology, horse heart cyt *c* is applied as a model protein in studies of heterogeneous ET (Feng et al., 1997; Katz et al., 2006; Taniguchi et al., 1982). Due to its ability to react with reactive oxygen species, cyt *c* is used as a recognition element in biosensors (Ge and Lisdat, 2002; Gobi and Mizutani, 2000; Krylov et al., 2004; Scheller et al., 1999).

2.5.3 Deoxyribonucleic acid (DNA)

DNA is a fibrous molecule consisting of two complementary nucleotide strands interwinded in antiparallel orientation. The ribose and phosphate components form the molecule's backbone while the latter awards the DNA its net negative charge. The medial-oriented bases (purine and pyrimidine) connect the two strands via hydrogen bonds, forming a right-handed double helix with a diameter of 20 Å (Berg et al., 2012). DNA occurs in three typical conformations (**figure 8**). The B-form represents the typical right-handed double helix described by Whatson and Crick. Other forms are the A- and the Z-form. The A-form is also right-handed and similar to the B-form, but with a shorter and more compact structure. It appears in dehydrated DNA samples, for instance those used in crystallization experiments. The Z-form has a zig-zag conformation of the ribose-phosphate backbone and occurs at high salt concentrations only (Creighton, 2010). However, salts are also required to maintain the native state of the molecule in solution. Especially Mg^{2+} and Co^{2+} stabilise DNA effectively at low concentrations. A Mg^{2+} concentration of only one-hundredth that of Na^+ is required to keep DNA in its native B-form under denaturing conditions (Creighton, 2010).

Double helix is a very stable configuration. It keeps its native form (B-form) in a pH range from pH 5 to pH 9 (Creighton, 2010; Kas'ianenko et al., 1985). Destabilisation below pH 5 and above pH 9 is caused by the titration of its polar groups; for instance, ctDNA is denatured at pH 2.95 and 11.77 at 20°C, while DNA from other organisms behaves very similarly (Creighton, 2010). Low pH is known to decrease the solubility of the molecule, it also induces double strand breaks and stabilises the formation of the triple helix structure, which

was found to be implicated in the regulation of several genes, such as *c-myc* (Creighton, 2010). DNA is also relatively insensitive towards temperature changes. Its melting point depends on the GC-content and the size (number of bps) of the molecule.
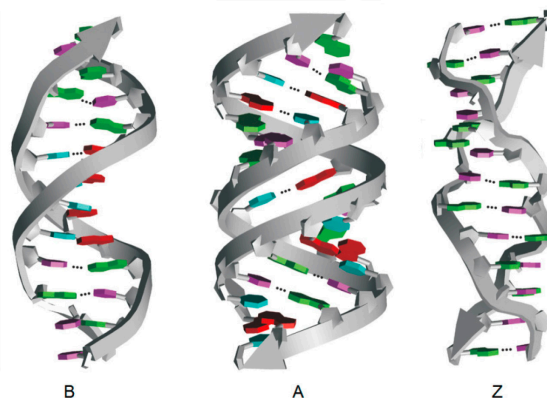
Figure 8: Schematic representation of the DNA double helix in its three possible conformations (B, A and Z). The phosphate sugar-backbone is in grey and the medial oriented purine and pyrimidine bases are in colors (according to Müller-Esterl, 2004)

2.6 Electrochemistry of enzymes

2.6.1 Fructose dehydrogenase

The enzyme fructose dehydrogenase (FDH) was first isolated by Yamada et al. (Yamada et al., 1967) from *Gluconobacter sp.* and later on purified to homogeneity and characterised by Ameyama et al. (Ameyama et al., 1981). FDH is heterotrimeric, membrane associated flavohemo-protein with a molecular mass of *ca.* 140 kDa. The subunits I, II and III have a molecular weight of 67.0, 50.8 and 19.7 kDa (Ameyama et al., 1981). Subunit I holds one covalently bound flavin-adenin-dinucleotide (FAD) cofactor (see **figure 9**), whilst subunit II has three additional *c* type hemes (heme c1-3) as prosthetic groups. The E_f of these three hemes was recently determined to be -10±4 (heme c3), 60±8 (heme c2) and 150±4 mV (vs. Ag/AgCl sat KCl) (heme c1) at pH 5.0 (Kawai et al., 2014). Consequently, the reduction of its natural electron acceptor ubiquinone and the membrane anchoring property is assigned to subunit II (Kawai et al., 2013; Kawai et al., 2014). Due to its hydrophobic surface patches, FDH tends to precipitate in solution which causes inactivation. However, storage of the enzyme in Triton X-100 containing buffer preserves the activity for 2 weeks at 4°*C* (Ameyama et al., 1981). For the reduction reaction with fructose and $K_3[Fe(CN)_6]$ a K_m value

for fructose of 10 mM was found at pH 4.5. Moreover, FDH is an acidic enzyme with a pI of 5.0 +/- 0.1, a pH optimum at 4.0 to 4.5 and a temperature optimum at 37°C (Ameyama et al., 1981).
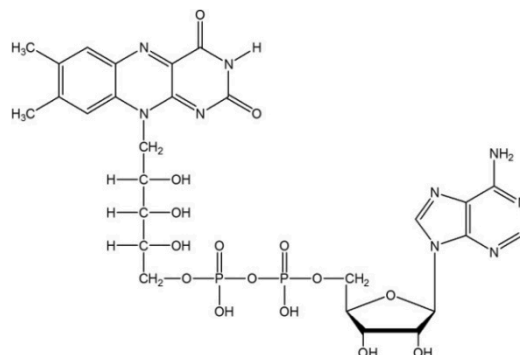
Figure 9: Chemical structure of the FAD molecule (drawn by ChemDraw) located in the active site of FDH.

Instead of FAD, pyrroloquinoline quinone (PQQ) was also described as cofactor of FDH (Ikeda et al., 1991; Marcinkeviciene and Johansson, 1993; Sasaki et al., 2011). However, to the best of our knowledge no studies addressing the identification of PQQ as the enzymes cofactor are existent. Therefore, all the references consulted here go back to the studies of Ameyama et al, who identified FAD as the cofactor.

In recent biotechnological studies the immobilisation of FDH was shown to be feasible and ET was found to proceed either directly between enzyme and electrode or via mediating molecules. Mediated ET was studied by Biscay et al, who combined FDH with a commercial screen-printed ferrocyanide-carbon electrode for the first time. This electrode displayed a low detection limit (0.05 mM for fructose), high reproducibility, long term stability for fructose determination and a linear response range from 0.1 to 1 mM with a sensitivity of 1.25 ± 0.02 A/mM. Furthermore, the pH optimum was determined to be between pH 4.0 and 5.0. The sensor was found to work reliably in fructose real samples such as cola, fruit juice and honey, and lost only 2% of its initial activity after one month of storage at 4°C (Biscay et al., 2012). Damar et al. immobilised FDH on AuE modified with and poly(amidoamine) dendrimers (PAMAM) and used ferrocyanide as mediator. Here, a pH optimum of 4.5 was defined, the sensor was found to operate in a range of fructose concentrations of 0.25-5.0 mM and an Icat(max) of 0.8 µA was achieved (Damar and Demirkol, 2011). Campuzano et al.

constructed a bi-enzyme sensor with FDH and GOD, capable of sensing glucose and fructose simultaneously, whereby tetrathiafulvalen was used as mediator (Campuzano et al., 2004).

Concerning DET reactions, carbon-based materials were found to have a positive effect on the ET efficiency, therefore, recent studies have focused on direct bioelectrocatalysis on carbon-based surfaces (Kamitaka et al., 2007a; Tominaga et al., 2009; Tominaga et al., 2007). The most efficient systems have been established on ketjen black (Kamitaka et al., 2007b) and gold nanoparticles modified with mercaptoethanol (Murata et al., 2009), achieving a current densities of 4 mA cm^{-2} and 14.3 ± 0.93 mA cm^{-2}. Based upon the potential at which DET is observed, it seems that the orientation of the enzyme with the heme site facing the surface facilitates an effective ET between FDH and the electrode (Kamitaka et al., 2007b). This is in agreement with the suggestion of Kawai et al. who determine the heme c2 to be the electron donating site to external electron acceptors in DET reactions (Kawai et al., 2014). Ferapontova et al. showed DET between cysteamine and mercaptoundecanol (MU) modified AuE, with FDH in solution. Within this study, cyt *c* was described as mediating protein for electrons towards the MU modified electrode whilst inter-protein ET was found to be most efficient at pH 7.0. Moreover, two different ET pathways were suggested. At high scan rates, the catalytic route may be proceeding from the active site directly to cyt *c* in solution. At low scan rates, catalysis may occur via the common pathways from the cofactor to the heme domain and subsequently to free cyt *c* (Ferapontova and Gorton, 2005).

2.6.2 Glucose dehydrogenase

The water-soluble glucose dehydrogenase (PQQ-GDH) is isolated from the cytoplasm of *Acinetobacter calcoaceticus*. It is a basic (pI = 9.5), redox active enzyme with a pH optimum at 7.0. PQQ-GDH has a dimeric structure (**figure 10**) comprising two identical subunit (Dokter et al., 1986). The monomers (50 kDa) have a β-propeller structure, made up of six four-stranded, antiparallel β-sheets. These are similar to the ones of other PQQ-containing dehydrogenases, such as PQQ-methanol dehydrogenase, however, by contrast with the other enzymes, PQQ-GDH has six (not eight) four-stranded antiparallel β-sheets (Anthony, 2001). Each of the monomers binds one pyrroloquinoline quinone (PQQ) cofactor and three calcium ions (Ca^{2+}). One Ca^{2+} activates the cofactor within the catalytic centre while the other two stabilise the enzyme dimer. PQQ is not covalently bound to the enzyme. Therefore, it can

reversibly dissociate from the active site. The key feature of the molecule is the ortho quinone at the C4 and C5 position of the quinoline ring (**figure 11**), which is reduced to a quinol during the catalytic reaction (Duine, 1988, 1991). The E_f of free and immobilised PQQ was determined to be -125 mV vs SHE at pH 7.0 (Katz et al., 1994). PQQ-GDH catalyses the oxidation of glucose and other aldose sugars to their respective lactones. This reaction runs in a base-catalysed proton abstraction in concert with a direct hydride transfer (Oubrie, 2003).
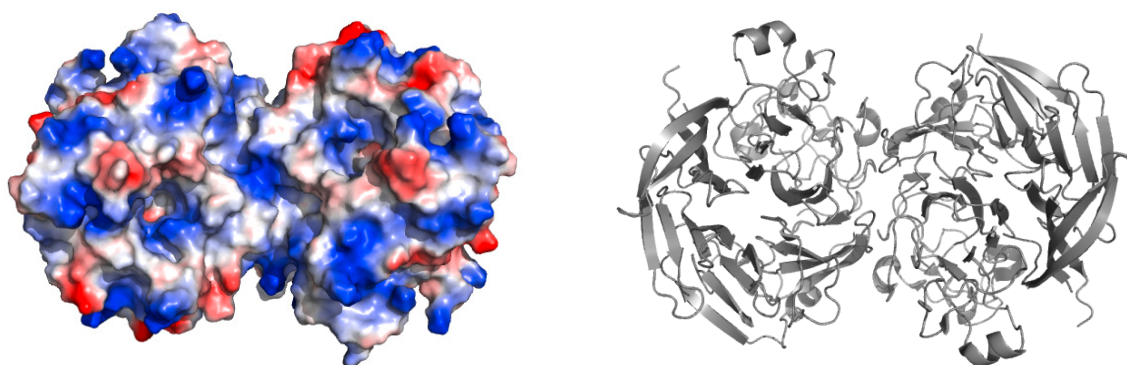
Figure 10; Left: Vacuum electrostatics of the homo dimeric PQQ-GDH molecule. Positive charges are in blue, negative charges are in red and neutral charges are in white. **Right:** Representation of secondary structure elements of the protein (grey), the PQQ cofactor is not shown. The figure is generated from the crystal structure by pymol based on pdb entry 1QBI (Oubrie et al., 1999).

For the coupling of PQQ-GDH to electrodes, different approaches were described. They are mainly based upon mediated ET and the use of phenolic compounds (Jin et al., 1995; Lisdat and Wollenberger, 1998; Loew et al., 2004), a redox polymer (Habermuller et al., 2003), ferrocene derivates (Laurinavicius et al., 2004), phenazine (Lapenaite 2006) and PQQ (Jin et al., 1998; Tanne et al., 2010; Willner et al., 1997; Zayats et al., 2005) as mediator.

Jin et al. described a ML approach consisting of covalently immobilised PQQ-GDH on AuEs (Feifel et al., 2014b; Jin et al., 1995). The enzyme was fixed on the gold surface in a monolayer, using 3,3'-dithiodipropionic acid bis-N-hydroxy succinimide ester, which contains a disulfide group for chemisorbtions onto gold and an activated succinimide esther group for protein coupling. The ML was assembled by activating the adsorbed enzyme with the bifunctional coupling agent 4,4'-diisothiocyanate-2,20-stilbene-disulfonic acid which enables the stepwise coupling of further PQQ-GDH layers. This system can be applied as recycling sensor for p-aminophenol, which is oxidised at the electrode and re-reduced by the enzyme. The linear dynamic range of the PQQ-GDH ML electrode was found to be between

10 nM and 10 mM and its detection limit was at 5 nM. A similar ML electrode, based on adsorptive immobilization of PQQ-GDH was created by the help of the anionic polyelectrolytes such as poly(sodium 4-styrenesulfonate) (PSS) and PASA (Loew et al., 2004). Quartz crystal microbalance (QCM) measurements showed that the amount of enzyme increased by about 1.88 mg/cm^2 for one PQQ-GDH/PASA bi-layer and 2.4 mg/cm^2 for one PQQ-GDH/PSS bi-layer. Adding phenolic compounds as electron mediator, resulted in an oxidation current. This reaction was increased by the catalytic glucose oxidation of PQQ-GDH in the presence of the substrate. The system was described to function as glucose sensor, only, when quinones are present in a non-limiting amount. Moreover, the amperometric response was already diffusion limited when a single layer of PQQ-GDH was adsorbed.
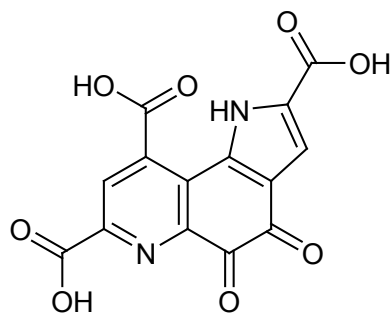
Figure 11: Chemical structure of the PQQ molecule (drawn by ChemDraw), located in the active site of PQQ-GDH.

Direct ETs have also been achieved for certain types of electrodes, including PQQ modified gold nano particles (Zayats et al., 2005), carbon black modified carbon paste (Razumiene et al., 2006), SWCNTs (Ivnitski et al., 2007), aniline derivative modified carbon nanotubes (Schubart et al., 2012), vertically aligned carbon nanotubes (vaCNTs) and buckypaper (Halamkova et al., 2012; Scherbahn et al., 2014), polyaniline modified MWCNTs (Gobel et al., 2011), porous carbon cryogel (Flexer et al., 2011) and titanium oxycarbide nanostructures (Sarauli et al., 2012a).

The soluble PQQ-GDH is not coupled to the respiration chain of *Acinetobacter calcoaceticus*, and its physiological role as well as the natural electron acceptor of PQQ-GDH remains unclear (Ferri et al., 2011). However, Dokter et al. showed that electrons can be transferred from the reduced quinol to molecules of the cytochrome family, e.g. cytochrome

b_{562} (Dokter et al., 1986). Based upon the known interaction between PQQ-GDH and cyt *c*, the basic pI and the rather small size of the enzyme, PQQ-GDH was chosen for the combination with cyt *c*/DNA ML architectures.

MATERIALS & METHODS

3.1   Materials

3.1.1 Chemicals

Chemicals		
Name	**Supplier**	**Cat.-No.**
Acetate	Sigma Aldrich	A3863
Ascorbic acid	Sigma Aldrich	255564
$CaCl_2$ (calcium chloride)	Fluka	21075
Citric acid	Sigma Aldrich	C0759
Coomassie Brilliant Blue	Sigma Aldrich	B0770
D_2O (deuterium oxide)	Sigma Aldrich	191701
D-fructose	Sigma Aldrich	F0127
D-glucose	Roth	67801
DNA from calf thymus (desoxyribonucleic acid)	Sigma Aldrich	D1501
EDC (1-ethyl-3(3-dimethylaminopropyl) carbodiimide)	Sigma Aldrich	E1769
EDTA (Ethylenediaminetetraacetic acid disodium salt dihydrate)	Sigma Aldrich	ED2SS
Ethanol	Roth	5054.3
$Fe_2(SO_4)_3 * H_2O$ (Iron(III) sulfate hydrate)	Sigma Aldrich	307718
Glycine	Sigma Aldrich	G8898
H_2O_2 (30%) (hydrogen peroxide)	Roth	8070.1
H_2SO_4 (96%) (sulphuric acid)	Roth	4623.4
H_3PO_4 ($\geq 85\%$) (o-phosphoric acid)	Roth	6366.1
HCl ($\geq 32\%$) (hydrochloric acid)	Roth	P074.3
HNO_3 ($\geq 69\%$) (nitric acid)	Sigma Aldrich	30702
K_2HPO_4 (di-potassium hydrogen phosphate)	Merck	105104
$K_3[Fe(CN)_6]$ (potassium ferricyanide)	Sigma Aldrich	244023
KCl (potassium chloride)	Merck	K41042236
KH_2PO_4	Merck	104873

(potassium di-hydrogen phosphate)		
KOH (potassium hydroxide)	Sigma Aldrich	484016
Loading dye (6X orange DNA)	Thermo Scientific	R0631
MU (11-mercapto-1-undecanol)	Sigma Aldrich	447528
MUA (11-mercaptoundecanoic acid)	Sigma Aldrich	450561
MES monohydrate (2-(N-morpholino)ethansulfonic acid)	Sigma Aldrich	69892
MV (methyl viologen dichloride hydrate)	Sigma Aldrich	856177
$Na_2HPO_4 * 2 H_2O$ (disodium hydrogen phosphate dihydrate)	Roth	4984.1
NaCl (sodium chloride)	Sigma Aldrich	746398
NaOH (45%) (sodium hydroxide)	Roth	0993.1
NEDA (N-(1-naphtyl)ethylendiamine)	Sigma Aldrich	222488
(pUC19 DNA/MspI (HpaII)	Thermo Scientific	SM0221
Oligonucleotide (41 bp)	Eurofins / Biomers	-
PQQ (pyrroloquinoline quinone)	Wako	168 17081
SDS (sodium dodecylsulfate)	Roth	2326.2
Spermine	Sigma Aldrich	S3256
Tris (Trizma® base)	Sigma Aldrich	T6066
Triton X®-100	Ferak	501104

Materials		
Name	**Supplier**	**Cat.-No.**
Gold wire (ø 0.5 mm; purity: 99.99+ %)	Goodfellow	AU005150
QCM chip (5 MHz)	L.O.T.-ORIEL	QSX301
Amicon Ultra Centrifugal filters MWCO 10000 kDa	Millipore	UCF501096Pk

Proteins & Enzymes			
Name	**Organism/Tissue**	**Supplier**	**Cat.-No.**
Cyt *c*	Horse/heart	Sigma Aldrich	C7752
Fructose dehydrogenase (EC 1.1.99.11)	*Gluconobacter japonicus*	Sigma Aldrich	F5152
		Kano Lab, Division of Applied Life Sciences, Kyoto University, Japan	-
Glucose dehydrogenase (EC 1.1.5.2)	*Acinetobacter calcoaceticus*	Roche	-

3.1.2 Buffer preparation

All solutions were prepared in 18 MΩ Millipore water.

- **KH₂PO₄/K₂HPO₄ buffer**

KH_2PO_4/K_2HPO_4 (KPi) buffer was prepared by mixing 1 M solutions of KH_2PO_4 and K_2HPO_4 in the required ratio, the pH was adjusted by adding KOH or H_3PO_4.

- **MES buffer**

MES buffer was prepared by dissolving 5 mM MES in 1 mM $CaCl_2$, the pH was set with HCl or NaOH.

- **Na₂HPO₄/citric acid buffer**

Na_2HPO_4/citric acid buffer (NaPi/cit) was prepared by mixing 200 mM Na_2HPO_4 solution with 100 mM citric acid solution in the ratio resulting in the required pH value, according to Ruzin et al. (Ruzin, 1999). The stock solution was diluted to the desired ionic strength and the required pH was set with Na_2HPO_4 solution or citric acid.

- **McIlvaine buffer (Na₂HPO₄/citric acid + Triton X-100)**

McIlvaine buffer was prepared by mixing 90 ml of a solution with 200 mM Na_2HPO_4 and 0.23% (v/v) Triton X-100 with 110 ml of 100 mM citric acid solution, the pH was set at room temperature (RT) by adding Na_2HPO_4 or citric acid solution.

- **TAE buffer**

1x TAE (Tris-acetate-EDTA buffer) was prepared by dissolving 0.04 M Tris, 0.001 M EDTA and 0.02 M acidic acid. The pH was set to 8.5.

- **SDS-PAGE buffer**

SDS-PAGE buffer was prepared by mixing a 25 mM Tris-HCl with 200 mM Glycine and 0.1% (w/v) SDS, with the pH set to pH 8.3.

3.1.3 Enzymes

3.1.3.1 Glucose dehydrogenase

Cytoplasmic PQQ-GDH from *Acinetobacter calcoaceticus* was provided by Roche Diagnostics GmbH under the terms of a cooperation project. The enzyme was recombinantly expressed in *E. coli*. For the reconstitution apoGDH was dissolved in 5 mM MES + 1 mM CaCl$_2$ (pH 5, 400 µM stock solution) and aliquots were stored at -20 °C. PQQ was dissolved in 1 M NaOH and diluted in 5 mM MES + 1 mM CaCl$_2$ to a 10 mM PQQ stock solution. According to Olsthoorn et al. the apoGDH was reconstituted with a PQQ/GDH-ratio of 1 (Olsthoorn and Duine, 1996). Therefore, the GDH stock solution was diluted to 20 µM, 20 µM PQQ were added and the mixture was incubated in the dark at RT for one hour. Given that the purity of the enzyme sample was not provided, the activity was related to the total mass of the weight solid, i.e. 2200 ± 30 U/mg

3.1.3.2 Fructose dehydrogenase

FDH from *Gluconobacter japonicus* (formerly *Gluconobacter industrius*) was provided by

a) Sigma Aldrich as lyophilised powder additionally containing salts and agents for stabilisation, *i.e.* detergents, antioxidants and sugars, to prevent inactivation. According to the provider the purchased sample of 4.5 mg FDH contained 5.1% protein. A 0.5 mg(protein)/ml stock solution with a specific activity of 1250 U/mg(protein) and an approximate molar concentration of 3.3 µM was prepared by dissolving the lyophilisate in 0.5 ml 100 mM McIlvaine buffer (pH 4.5). The enzyme solution was used without further purification for the experiments with freely diffusing. For the immobilization of FDH on the cyt *c* monolayer the buffer was exchanged to 5 mM KPi pH 7.0 to remove potentially disturbing contaminants.

b) The working group of Prof. Dr. Kenji Kano (Kyoto University, Japan) as 5.6 mg(protein)/ml enzyme solution with a specific activity of 150 U/mg(protein) and a molar concentration of 40 µM, dissolved in 100 mM McIlvaine pH 4.5 containing 300 mM sucrose for stabilization. Prior to using the enzyme, a buffer exchange to 10 mM McIlvaine pH 6.0 was performed by 2 times spinning for 9 min in a column at 12000 rpm at $4°C$. The enzyme activity was tested after the buffer exchange and was found to be stable.

The specific activity of FDH was determined prior to the use as described by the provider (www.Sigma-Aldrich.de; the protocol is based on the study of Ameyama et al. (Ameyama et al., 1981). The principle of the activity test is based upon ferricyanide reduction by FDH in the presence of fructose. The reaction is stopped by the addition of phosphoric acid, SDS and iron(III) sulfate containing solution. SDS denatures the enzyme and thus disables further reduction of ferricyanide. Iron(III) sulfate reacts with the reaction product (ferrocyanide) to Prussian blue, which is detected spectrophotometrically at 660 nm.

3.2   Methods

3.2.1 Spectroscopic investigation

3.2.1.1 UV-vis spectroscopy

- **Interaction between cytochrome *c* and DNA**

A solution of reduced cyt *c* was prepared in 20 mM KPi buffer containing 10 mM NaCl and 0.1 mM ascorbic acid, which was incubated for 10 min at RT. The pH was set and DNA (in the form of 41 bp oligonucleotides) was added in the respective concentration (**table 1**). The sample was mixed by gently inverting ten times. UV-vis measurements were started immediately after mixing the sample in order to follow agglomerate formation. Measurements with 50 and 100 mM NaCl were performed immediately after the addition of the respective amount of NaCl and 10 times inverting. UV-vis spectroscopy was performed by using a Thermo Scientific Evolution 300 spectrometer (Weltham, MA, USA) equipped with a Peltier element for temperature control. The spectra were recorded from 350 nm to 600 nm at a constant temperature of 20 °*C*, in 5 min intervals during agglomeration and 2 min intervals while disruption of the complexes.

- **Reduction of cytochrome *c* by PQQ-GDH**

UV-vis spectroscopy was performed by using a Helios α spectrophotometer. A 20 μM solution of cyt *c* and 400 nM PQQ-GDH was prepared in 20 mM MES + 1 mM $CaCl_2$ buffer. The blank value was set after 5 s of stirring and 5 s equilibration. After the addition of 5 mM glucose and another 5 s of stirring and equilibration the reduction rate of cyt *c* was followed at 550 nm.

- **Reduction of cytochrome *c* by FDH**

Kinetic measurements were performed with a Thermo Scientific Evolution 300 spectrometer (Weltham, MA, USA) equipped with a Peltier element for temperature control. As control 1 Units (U) of FDH was added to a 25 μM cyt *c* solution in 100 mM McIlvaine buffer at different pH values. Each sample was mixed by 5 s stirring and equilibrated to 37 °*C* for 5 min, prior to measuring. Subsequently, fructose was added to the cyt *c*/FDH mixture to obtain

a concentration of 50 mM, the solution was stirred for 5 s, equilibrated to 37 °C for 1 min and the reduction rate of cyt *c* was followed at 550 nm for 5 min.

- **Calculation of the initial rate of cytochrome *c* reduction**

The velocity (v) is calculated as the slope of the kinetic curve in the linear phase of the cyt *c* reduction after subtraction of the substrate free control. By applying the law of Lambert-Beer, using an extinction coefficient (ε) of reduced cyt *c* (with $\varepsilon_{(550)red} - \varepsilon_{(550)ox} = 21.1 \text{ mM}^{-1}\text{cm}^{-1}$) (van Gelder and Slater, 1962), the extinction recorded at 550 nm and the thickness of the irradiated body, the converted substrate concentration was determined. As a control, the absorbance of fully reduced cyt *c* was determined additionally by adding ascorbic acid to the pH 4.5 sample.

3.2.1.2 Circular dichroism spectroscopy

The cyt *c*/DNA (41 bp oligonucleotides) samples were prepared as described in **3.2.1.1** (also see **table 1**) and incubated for 60 min to measure the completely formed complexes. CD spectroscopy measurements were conducted using a JASCO J-720 spectrometer (Kyoto University, Japan) at RT using a 0.1 cm path length quartz cuvette. Spectra were recorded with a scan speed of 50 nm/min and 0.2 nm resolution. Each spectrum was calculated as an average of 6 scans. The buffer baseline was subtracted from the measured spectra.

3.2.1.3 Nuclear magnetic resonance spectroscopy

The samples for NMR contained 50 µM ^{15}N cyt *c*, 30 mM NaCl, 20 mM KPi, 10 % D$_2$O and 0.1 mM ascorbic acid. After each DNA (41 bp oligonucleotides) addition of 3, 6, 18 or 24 µM (**table 1**), the sample was gently inverted ten times and left to equilibrate at RT for 60 min. The pH was corrected prior to the measurement. NMR spectroscopy: Two-dimensional ^{1}H-^{15}N HSQC (heteronuclear single quantum coherence) spectra were acquired, using the TROSY (transverse relaxation-optimised spectroscopy) mode, at 303 K with 32 scans and 64 increments, on a Varian 600 MHz NMR spectrometer equipped with a HCN coldprobe and processed using linear prediction. Spectral widths of 16 ppm (^{1}H) and 40.0 ppm (^{15}N) were recorded. The ^{1}H-^{15}N HSQC resonance assignments of reduced cyt *c* were based upon those reported (Liu et al., 2003). The analysis of the DNA-induced chemical shift perturbations was performed using CARA (http://www.nmr.ch).

Table 1: Summary of the molar concentration of cyt *c* and DNA (41 bp oligonucleotides) in the samples prepared for UV-vis, DLS, CD, NMR and SEC analysis with calculation of the subsequent DNA/cyt *c* concentration ratio.

cyt *c* (µM)	DNA (µM)	DNA/cyt *c*
UV-vis / DLS		
20	2.4	0.12
CD		
10	1.2	0.12
NMR		
50	3	0.06
50	6	0.12
50	18	0.36
50	24	0.48
SEC		
100	9	0.09
100	18	0.18
100	36	0.36

3.2.2 Electrochemical characterisation

3.2.2.1 Cyclic voltammetry

Cyclic voltammetry (CV) measurements were conducted with an Autolab PGSTAT 20 (Metrohm, Germany). The modified gold wires (working electrode, WE) were placed in a custom-made 1 ml cell (**figure 12**). Immersion depth was 5 mm (surface area = 8.1 mm²) for the PQQ-GDH measurements and 2 mm (surface area = 3.3 mm²) for the FDH measurements. The WEs were equilibrated in the 5 mM KPi buffer for at least 2 min. As reference electrode (RE) an Ag/AgCl 1 M KCl electrode (Microelectrodes Inc., Bedford, USA) with a potential of +0.236 V vs. NHE (Bard and Stratmann, 2007) and a platinum wire as counter electrode (CE) were used.

The amount of redox active material adsorbed on the electrode (surface coverage Γ) was determined scanning with 100 mV/s in 5 mM KPi pH 7.0 and applying Faraday's law, which correlates the adsorbed mass to the transferred charge (Bard Faulkner 1980). The charge was calculated as the average value of the integrated area underneath the oxidation and the reduction peak

$$\Gamma = \frac{Q}{nFA} \tag{3}$$

whereby Γ = the amount of redox active material on the surface, Q = the total electric charge transferred, F (Faraday constant) = 96485 C/mol and n = the number of electrons transferred (*i.e.* one for cyt *c* (Nahir et al., 1994; Pelletier and Kraut, 1992)).
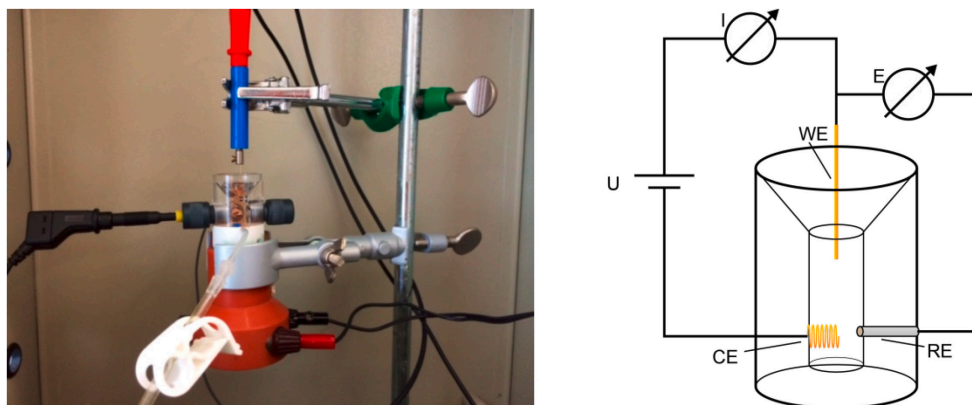
Figure 12; Left: CV experiment with three-electrode setup in a custom-made measurement cell. Reference electrode (RE) Ag/AgCl 1 M KCl, counter electrode (CE) platinum wire and working electrode (gold wire), which are immersed in a cyt *c* solution. The setup is connected to an Autolab PGSTAT 20 potentiostat. **Right:** Schematic representation of the three-electrode setup.

For the investigation of the bio-electrocatalytic reactions, two cycles were run at a scan rate of 2 mV/s and 2-5 cycles at a scan rate of 10 mV/s, starting from -150 mV or -250 mV. The last cycle is shown in the graphs and the catalytic currents were determined at a potential of 200 mV (vs. Ag/AgCl 1M KCl). It is to be mentioned that the step potential was set to 0.3 mV or 0.15 mV, while at the lower value a higher amount of redox active material can be detected on the electrode surface.

3.2.2.2 Chronoamperometry

Chronoamperometry was performed by a CHI800 Electrochemical Analyzer. The modified gold wire electrode was dipped in a custom- made 1 ml cell, containing 5 mM MES buffer with 1 mM CaCl$_2$. A fixed potential of +0.2 V versus an Ag/AgCl 1 M KCl electrode was applied. After reaching a stable baseline, the respective amount of substrate was added under

constant stirring (400 rpm). To keep the added volume as small as possible, glucose stock solutions of 1 mM, 10 mM and 100 mM were used.

3.2.3 Microgravimetric characterisation

Quartz crystal microbalance (QCM) is a mass sensitive sensor which is based upon the inverse piezoelectric effect. This means that the crystal is put in oscillation by applying an AC voltage. The frequency of the oscillation correlates to the total mass of the crystal and can be measured. The change of the frequency after mass accumulation on the crystal surface can be used to quantify the mass accumulation. The correlation between change of frequency and mass accumulation is described in the *Sauerbrey* equation

$$\Delta f = \frac{-2f_0{}^2\Delta m}{\left[A\sqrt{\mu\rho}\right]} \tag{4}$$

whereby f_0 = the resonant frequency [Hz] of the crystal, m = mass [g], A = the active surface of the crystal [cm²], μ = the shear module of the crystal [g/(cm·s²)] and ρ = the density of the crystal [g/cm³].

Here, measurements were performed by using a Q-sense E4 device. A clean, gold-covered 5 MHz quartz chip was incubated in ethanol containing 5 mM MUA/MU (ratio 1:3) for 48 h. After rinsing in ethanol and Millipore water, the chip was dried and put in the flow system. The solutions containing DNA and cyt *c* were successively pumped through the cell for 10 min and, PQQ-GDH solution (2 µM) for 30 min, with a 5 min of buffer in between. The flow rate was set at 25 µl/min.

3.2.4 Particle size analysis by dynamic light scattering

The cyt *c*/DNA (41 bp oligonucleotides) samples were prepared as described for UV-vis spectroscopy and incubated for 60 min in order to measure the completely formed complexes. Dynamic light scattering (DLS) was performed using a Beckman Coulter Delsa Nano *c* Particle Analyzer (Krefeld, Germany), working at a fixed scattering angle of 165° and with the *Marquardt* algorithm to calculate the particle size distribution. The hydrodynamic

diameter of the agglomerates was monitored by acquiring 200 data points in three cycles of each sample.

3.2.5 Size exclusion chromatography

Size exclusion chromatography (SEC) samples contained 100 µM cyt *c* and 6, 9, 18 or 36 µM DNA (41 bp oligonucleotides) (**table 1**). At pH 7.0 SEC was performed on an Äkta FPLC at 21 °*C* using an XK 16/70 column (1.6 cm diameter, 65 cm bed height) packed with Superdex 75 (GE Healthcare). A continuous flow rate of 1.5 ml/min was employed and the column was equilibrated with approximately 160 ml of buffer (30 mM NaCl, 20 mM KPi, pH 7.0). Proteins were detected by UV-vis at 280 nm.

3.2.6 Agarose gel electrophoresis

A 2 % (w/v) agarose was prepared in 1x TAE buffer. The first gel slot was filled with 4 µl of DNA ladder (pUC19 DNA/MspI (HpaII)). 0.1 µl of DNA sample (0.61 µg) was mixed with 1 µl Orange G loading dye. A current of 70 V was set. When the marker reached the edge of the gel, the current was stopped, the gel placed in an ethidium bromide (EtBr) bath (1 µg/ml) and incubated for 10 min. Finally, the stained gel was visualised by a Fusion FX7 (Vilber Lourmat) advanced imager.

3.2.7 SDS polyacrylamid gel electrophoresis

A 15 % SDS polyacrylamide gel electrophoresis (PAGE) was used to analyse the content of the SEC fractions. SDS-PAGE buffer was prepared by mixing a 25 mM Tris-HCl with 200 mM Glycine and 0.1% (w/v) SDS , the pH was set to pH 8.3 To improve detection, the SEC fractions were concentrated fivefold (miVac Duo Centrifugal Concentrator, Genevac) prior to loading. Sample volumes of 20 µl were loaded onto the gel and a potential of 140 mV was applied for 70 min. Subsequently, the gel was fixed in by microwaving in a solution of 50 % ethanol and 10 % acetate, staining, followed by incubating in a 0.05 % Coomassie brilliant blue solution (7.5 % acetate, 5 % ethanol).

3.2.8 DNA hybridisation

For the investigation of the interaction between the redoxprotein cyt c and DNA, double stranded (ds) oligonucleotides were used. The sequence of the oligonucleotide has a GC content of 50 %, comprises 41 bps (*i.e.* 5'-CCCTCATAGTTAGCGTAACGGCAAATGGCA TTCTGACATCC-3') and has a melting point (T_m) of 75 $°C$. The HPLC-purified single stranded DNA was provided as lyophilised powder, containing sodium salt. Note, that residues of triethylammonium acetate, which is used in the synthesis, may be left. The ssDNA was dissolved to 100 pmol/µl and shaken on an Eppendorf thermo mixer, at RT at 900 rpm for 15 minutes. The complementary strands were mixed in an equal molar ratio, heated to 68 °C while shaking for 15 min and cooled down to RT. To prove the hybridisation an agarose gel electrophoresis assay was performed.

3.2.9 Production and purification of ^{15}N-labelled cytochrome c

^{15}N-labelled horse heart cyt c was expressed in *Escherichia coli* BL21 (DE3) (Patel et al., 2001) and purified according to literature methods (Volkov et al., 2012; Worrall et al., 2001). The purity and concentration of the ^{15}N-labelled cyt c was estimated using 15 % sodium dodecyl sulfate polyacrylamide gel electrophoresis (SDS-PAGE) and UV-vis spectroscopy (Perkin Elmer Lambda 35 UV-vis Spectrometer). The cyt c concentration was determined using the extinction coefficient of reduced cyt c, ε_{550} = 29.5 mM^{-1} cm^{-1} (van Gelder and Slater, 1962) for the reduced (ferrous) species. Ferrous cyt c was prepared by the addition of 1 mM sodium ascorbate. For the storage at -20 $°C$, pure ^{15}N-labelled hh cyt c was oxidised with an excess of $K_3[Fe(CN)_6]$ and exchanged into NMR buffer (20 mM KPi + 30 mM NaCl, pH 6.0) prior to concentration.

3.2.10 Preparation of protein electrodes

Gold wire electrodes (AuE) were cleaned by three times incubating in piranha solution (H_2SO_4/H_2O_2 3:1) for 20 min. After each step, the electrodes were sonicated in the remaining H_2SO_4 and thoroughly rinsed with ultrapure water. In the next step, the electrodes were incubated for 4 h in boiling 2.5 M KOH, rinsed again in ultrapure water and stored in 96% H_2SO_4.

Prior to modification with the MU:MUA SAM, the AuEs were incubated for 20 min in 65% HNO$_3$, rinsed with ultrapure water, then with EtOH and dried. The prepared AuEs were incubated in 5 mM ethanolic solution of MU:MUA (3:1) for 48 h. MU and MUA form a self assembling monolayer (SAM) on the electrode surface. The negatively charged carboxylic group of MUA attracts positively charged surface patches of cyt c. MU serves as spacer between the MUA molecules to keep distance between the negatively charged carboxylic groups of MUA (Ge and Lisdat, 2002).

3.2.10.1 Preparation of cytochrome c monolayers

- For the experiments with PQQ-GDH the cyt c monolayers were prepared on the MU:MUA modified electrodes according to the published protocol of Beissenhirtz et al. (Beissenhirtz et al., 2004b). The modified electrodes were incubated in 30 µM cyt c (5 mM KPi buffer, pH 7.0) for 2 h. After washing five times in buffer the surface coverage was determined to evaluate the quality of the cyt c monolayer.
  For the covalent fixation of cyt c to the electrode surface, monolayer electrodes were incubated in a freshly prepared 2.5 mM EDC solution for 30 min.
- For the experiments with FDH the cyt c monolayers were prepared on the MU:MUA modified electrodes by running 20 cycles in a 30 µM cyt c solution (5 mM KPi pH 7.0) at a scan rate of 100 mV/s. in a potential range of -0.4 V to 0.4 V.

3.2.10.2 Preparation of cytochrome c monolayers with immobilised FDH

Cyt c monolayer electrodes were prepared as described above and incubated for 30 sec in a 200 µg/ml FDH solution with approximately 100 U/ml in 5 mM KPi pH 7.0. The buffer exchange from 100 mM McIlvaine (pH 4.5) to 5 mM KPi (pH 7.0) was performed by filling a 20 µL FDH stock solution up to 500 µL with cold KPi (4 °C) and spinning for 9 min at 12000 rpm and 4°C in a spin column with a MWCO of 10 kDa, resulting in a final volume of about 50 µL. Prior to measuring the cyt c-FDH electrode was rinsed by gently dipping five times in buffer 5 mM KPi pH 7.0.

3.2.10.3 Assembly of cytochrome *c*/DNA multilayer systems

Directly after the preparation of the monolayer, the cyt *c*/DNA ML architectures were assembled on top of a cyt *c* monolayer electrode (see 3.2.10.1) using calf thymus (ct) DNA as negatively charged building block (Sarauli et al., 2009). The freshly prepared monolayer electrodes were incubated alternately in solutions of 20 µM cyt *c* and 0.2 mg/ml DNA (0.5 mM KPi pH 5.0) for 10 min each. After each step, the electrode was washed by gently dipping it five times in 0.5 mM KPi buffer (pH 5.0).

It is to be mentioned that the assembly of the cyt *c*/DNA ML electrodes succeeded very reliably. Moreover, the ML assembly was found to be very robust in handling since dropping the electrodes, e.g. on the bench, did not seem to damage the modification severely. The modified electrodes were also found to be stable even during longer CV measurements and despite stirring during amperometry.

3.2.10.4 Coupling of enzymes with cytochrome *c*/DNA multilayer systems

Preparation of the cyt *c*/PQQ-GDH electrodes. For the assembly of the (cyt *c*/DNA)$_n$/PQQ-GDH electrode, a cyt *c*/DNA ML was prepared as described in 3.2.10.2. After the assembly of the last DNA layer, the electrode was dried at RT for 30 min. PQQ-GDH was assembled on top of the cyt *c*/DNA architecture as a terminal layer. Therefore, the cyt *c*/DNA modified electrodes were incubated for 20 min in a 2 µM PQQ-GDH solution. In between the incubation steps, a washing step (gently dipping five times in 0.5 mM KPi buffer pH 5.0) was conducted.

RESULTS & DISCUSSION

The redox protein cyt *c* and the biopolymer DNA assemble into electro active multilayer (ML) systems, providing a biocompatible matrix for the entrapment of proteins (Sarauli et al., 2009).

Aiming on the identification of DNA's binding sites on the redox protein surface, the interaction between the two building blocks is investigated in chapter **4.1**. Therefore, methods such as the UV-vis-, 2D-NMR-, circular dichroism (CD) spectroscopy, but also dynamic light scattering (DLS) and size exclusion chromatography were applied.

Besides this, the feasibility to utilise the interaction between cyt *c* and enzymes for the creation of an analytical signal chains was investigated applying two enzymes, differing in size, cofactor, surface properties and organelle locations as reaction partner of freely diffusing cyt *c* and cyt *c* immobilised on an electrode surface. In chapter **4.2** the ET reaction between the FAD dependent fructose dehydrogenase (FDH) and cyt *c* in solution as well as immobilised in a monolayer was investigated. In chapter **4.3**, the combination of the PQQ dependent glucose dehydrogenase (GDH) with the cyt *c*/DNA ML system addressed. Here, means of electrochemistry, micro-gravimetry but also spectroscopic methods such as UV-vis were applied.

4.1   Structural characterisation of the interaction between cytochrome *c* and DNA

The cyt *c*/DNA ML system, described by Sarauli et al., was assembled with DNA isolated from calf thymus (ct) as second building block (Sarauli et al., 2009). Analysing the ctDNA solution by gel electrophoresis revealed that the large DNA molecule was partly degraded to a mixture of DNA fragments varying in size from over 10kbp down to below 0.5kbp (**figure 13, right panel**). The degradation of the ctDNA molecule is related to shear forces which were caused by pipetting and stirring, as well as freezing and thawing the sample. Despite this, reproducible layer formation was possible, especially at an acidic pH value and a very low ionic strength of the buffer. In order to work with a better defined system, dsDNA molecules of a defined size, *i.e.* 41 bp oligonucleotides were used (**figure 13, left panel**).

Throughout the following interaction study, freshly hybridized ds 41 bp oligonucleotides were mixed with cyt *c* in constant ratios (**table 1**)
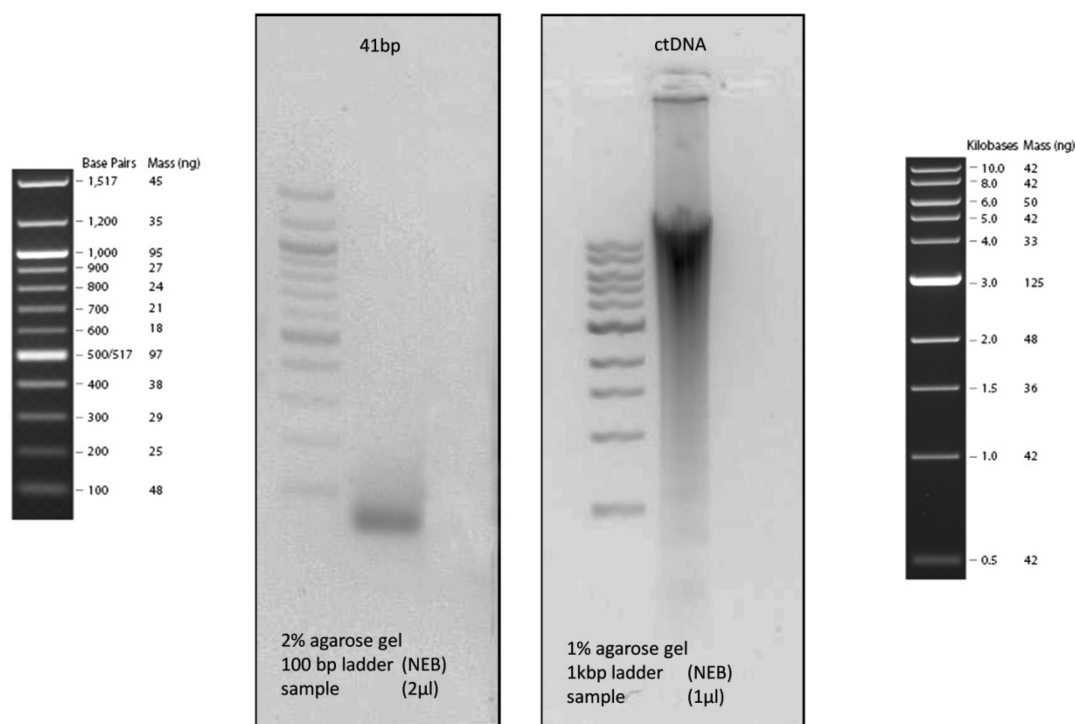
Figure 13: Agarose gel electrophoresis, 2 % agarose for oligonucleotides, 1 % for ctDNA. We used ctDNA and ds 41bp oligonucleotides diluted in 0.5 mM KPi, pH 5.0. Gel electrophoresis revels that ctDNA is severely degraded into fragments >10000 bps to <500 bps. The 41 bp oligonucleotides run slightly below the 100 bp mark. This indicates that the oligonucleotide sample is hybridised and of the expected size.

Thus far, the electrostatic character of the cyt *c*/DNA interaction has been recognised in several studies (Bi et al., 2005; Lao et al., 2007; Lisdat et al., 2001; Song et al., 2012). The ionic strength was shown to play a crucial role in the interaction of the two building blocks. The assembly of cyt *c*/DNA ML systems was found to be most efficient using a low buffer concentration and an acidic pH (Sarauli et al., 2009). Concerning the heme environment of the redox protein, no denaturation was found in the presence of DNA, neither in the cyt *c*/DNA ML, nor in the study on a cyt *c* monolayers with oligonucleotide promoters on AuEs (Lisdat et al., 2001; Lisdat et al., 1999). However, the interaction site of cyt *c* and the structure of the ML system remain unknown. Therefore, we focus on the elucidation of the cyt *c*/DNA interaction with respect to possible structural changes of the protein secondary

structures in the periphery of the molecule. This shall lead to a more precise understanding of the assembly of cyt *c*/DNA ML systems.

4.1.1 Photometric characterisation of cytochrome *c*/DNA complexes formed in solution

In order to gain insight into the interaction between cyt *c* and DNA, the reaction was studied at different pH values and salt conditions by means of UV-vis and CD spectroscopy, first. Moreover, the conditions for a reliable NMR analysis were defined here.

First, cyt *c* was mixed with the ds 41 bp oligonucleotide in a concentration ratio of 0.12 at pH 5.0 and a low ionic strength of 10 mM NaCl. The sample was observed to turn cloudy in approximately 10 seconds. The first UV-vis scan already showed an increased absorbance and a flat shape, but preserving the characteristic peaks of reduced cyt *c* at 410 nm, 520 nm and 550 nm (**figure 14a**). This indicates the formation of agglomerates in solution, which cause light scattering.
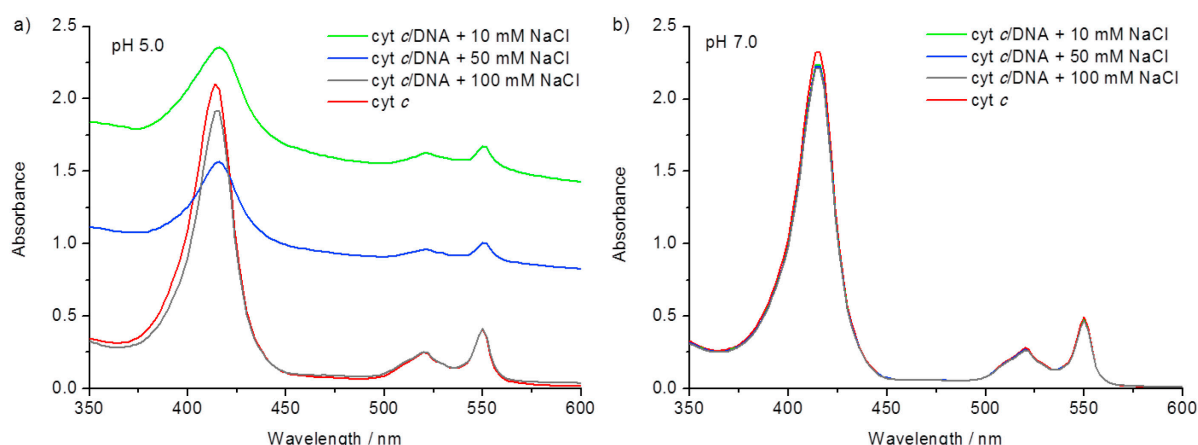
Figure 14: UV-vis absorption spectra of cyt *c*/DNA mixtures obtained at pH 5.0 **a**) and 7.0 **b**) with increasing salt concentrations at RT. Samples of the complex contained 20 µM cyt *c* and 2.4 µM DNA in 20 mM KPi, 0.1 mM ascorbic acid and NaCl, 10 mM (green) 50 mM NaCl (blue) and 100 mM NaCl (grey).

The size of the formed agglomerates was determined to an average diameter of 1250 ± 200 nm by dynamic light scattering (DLS) (**figure 15**). Following the cyt *c*/DNA spectrum over time showed a decrease in extinction, indicating the precipitation of the complexes, which was completed after about 180 min.

In the second step, the influence of the NaCl concentration on the complex formation was analysed, whereby increasing the salt concentration and mixing the sample recovered the characteristic cyt c peaks stepwise. The partial disruption of the complexes was indicated at 50 mM NaCl. At a higher concentration of 100 mM, the characteristic peaks were reset and the sample turned clear again. Although the peak intensity suggests the almost full recovery of free cyt c, DLS measurements proved the presence of small agglomerates with a size of 400 ± 200 nm despite the high salt concentration. This was the first evidence that even at a high ionic strength, interaction between the two bio-molecules occurs. The precipitation at pH 5.0 and low ionic strength correlates to the previous finding of an efficient deposition of cyt c on DNA and vice versa, resulting in stable ML assemblies (Sarauli et al., 2009). It is suggested that the interaction between the two bio-molecules not only proceeds on a surface; moreover, it is sufficiently strong to result in precipitation in solution.
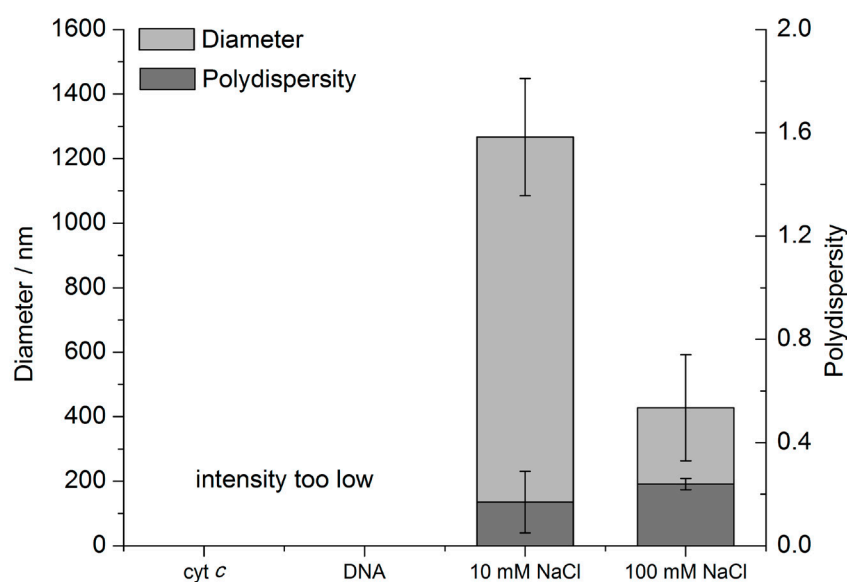
Figure 15: Dynamic light scattering measurements of cyt c/DNA samples containing 20 μM cyt c and 2.4 μM DNA in 20 mM KPi at pH 5.0, after 60 min incubation at RT and in the presence of 10 mM and 100 mM NaCl. The light grey columns depict the average particle size, the dark grey columns show the polydispersity.

When cyt c and ds 41 bp oligonucleotides were mixes at pH 7.0, the solution remained clear after DNA addition. In UV-vis no change in the cyt c spectrum occurred, even after an incubation time of 60 min (**figure 14b**), and DLS measurements resulted in a signal intensity which was below the detection limit. This suggests that either agglomeration is suppressed or only very small complexes are formed at a neutral pH value.

To investigate the pH stability of the cyt *c*/DNA complexes, a pH titration was performed on the complex from pH 5.0 to 7.0. Although the pH of the solution changed, the precipitated complexes remained insoluble. This reflects the behaviour of cyt *c*/DNA architectures described by Sarauli et al., which were assembled at pH 5.0 and even remain stable when transferred to the pH 7.0 measuring buffer (Sarauli et al., 2009).

4.1.2 Investigation of the protein secondary structure in the presence of DNA

CD spectroscopy was applied to investigate the proteins' secondary structure in the presence of DNA as a function of pH and ionic strength. Cyt *c* is rich in α-helical structure, providing a characteristic CD signal with a typical double minimum at 222 nm and 208 nm and an intense maximum at 192 nm (Cai and Dass, 2003; Dickerson et al., 1967; Fisher et al., 1973). First, measurements were performed at pH 5.0 and 100 mM NaCl, given that the formation of large, precipitating complexes was avoided under these conditions. Since Cl⁻ disturbs the CD signal in the far UV region, only the α-helical double minimum is considered here. The cyt *c* controls showed the typical negative molecular ellipticity of α-helical structures (**figure 16a and 16b**). After adding DNA, no substantial change of the spectrum was observed (**figure 16a**), indicating no alteration of the α-helical structure. The same is valid for pH 7.0 and low ionic strength (**figure 16b**).
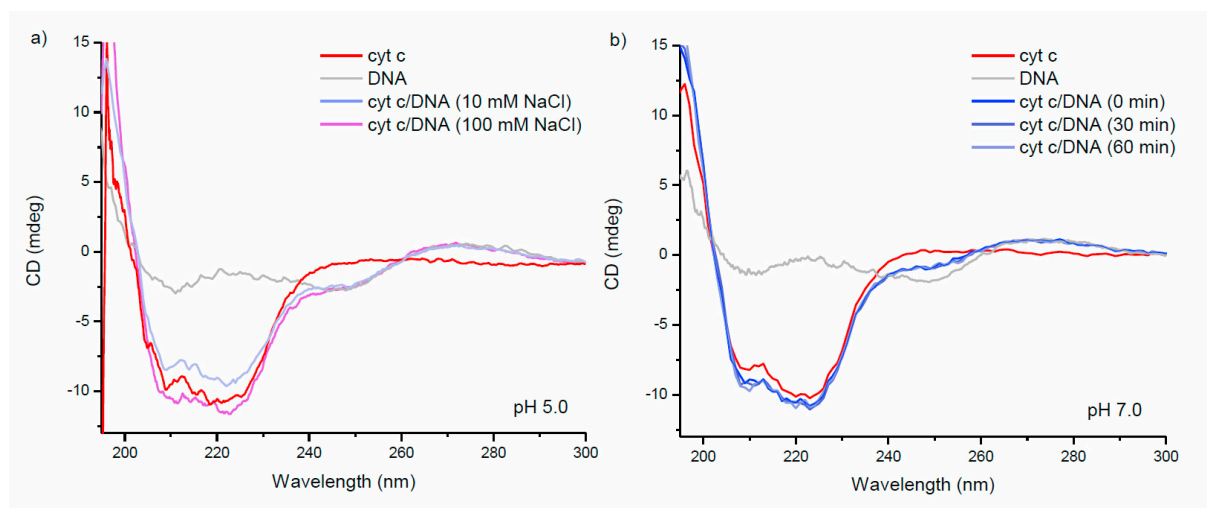
Figure 16: CD spectra of cyt *c* in the presence of DNA at (**a**) pH 5.0 and (**b**) pH 7.0. The samples contained 10 µM cyt *c* and 1.2 µM DNA in 20 KPi and were measured after 60 min of incubation. **a**) cyt *c*/DNA at pH 5.0. The α-helical signal at 222 nm and 208 nm decreases in the presence of DNA. The DNA signal at 280 nm stays constant. Increasing the salt concentration to 10 mM NaCl and 100 mM NaCl resets the cyt *c* double peaks. The

presence of Cl⁻ disturbs CD signal below 190 nm. **b**) cyt *c*/DNA at pH 7.0, with no change in negative molecular ellipticity.

It was also tested, whether CD measurements at pH 5.0 and low ionic strength can be performed. Reproducible spectra were obtained at 10 mM NaCl, although agglomeration occurred – due to the rather slow precipitation process. Although small changes in the peak intensities were observed after the addition of DNA, structural changes cannot be concluded beyond doubt due to the process of precipitation.

4.1.3 Identification of interaction sites of DNA on the cytochrome *c* surface

Since complex formation and precipitation was observed at pH 5.0 and low ion concentrations, the buffer conditions were altered to acquire reliable NMR spectra. Measurements at low pH were conducted at high ionic strength and studies at higher pH values were performed. Performing protein NMR spectroscopy, ^{15}N-labled cyt *c* was prepared and HSQC experiments were conducted at pH 5.0 with 100 mM NaCl (**figure 17**). Under these conditions, the bio-molecule interaction resulted in small complexes that were stable in solution and did not precipitate. The cyt *c*/DNA samples showed csps especially at the lysine residues K5, K8, K88 and K89. This supports the idea that cyt *c*/DNA interaction is not completely inhibited even at a high ionic strength and may explain the small agglomerates found in DLS. When performed at a lower ionic strength of 50 mM NaCl, agglomeration was not completely suppressed. Thus, spectra of lower intensity were recorded, which did not show additional interaction sites compared to the study at 100 mM NaCl. The original NMR spectra recorded at pH 5.0 and different NaCl concentrations are shown in the appendix, **figures A1-3**.
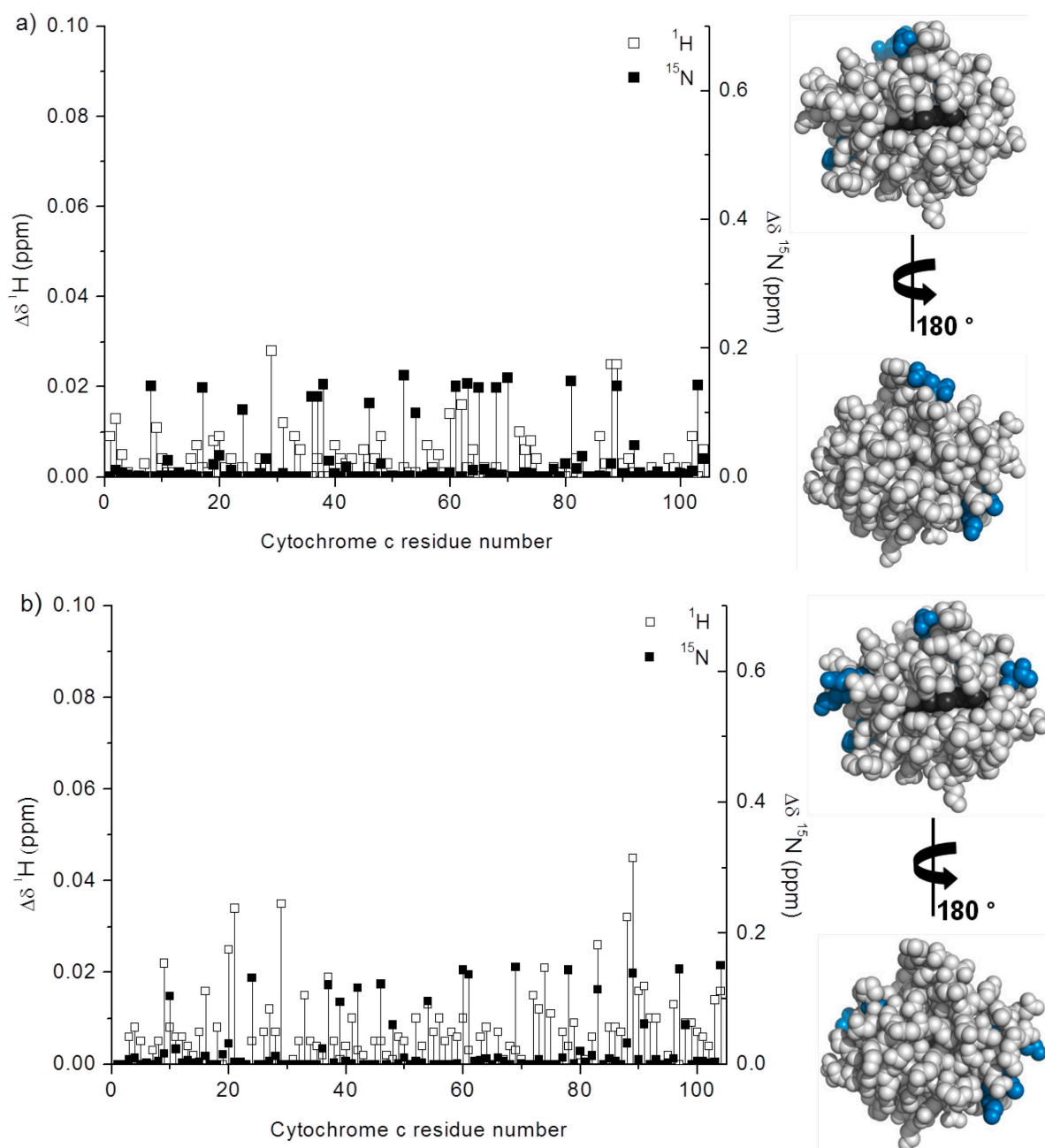
Figure 17; Left: Plot of csps recorded from cyt *c* backbone amides at pH 5.0 with 18 µM DNA (20 mM KPi, 30°*C*) and (**a**) 50 mM NaCl or (**b**) 100 mM NaCl. AAs residues are numbered from 1 to 104. Blanks correspond to proline residues 30, 44, 71 and 76 and unassigned G84. **Right:** Space filling representation of cyt *c* showing its secondary structure (grey) and residues with a significant csp ($\Delta\delta$ ^{1}H $\geq$ 0.03 or ^{15}N $\geq$ 0.15 ppm) (blue). The figures were generated by pymol based upon pdb-file 1HRC (Bushnell et al., 1990).

A second set of NMR measurements was performed at pH 7.0, given that no agglomerates were detected in UV-vis and DLS. **Figure 18a** shows a region of the cyt *c* spectrum in the presence of increasing DNA concentrations (for the full spectrum see appendix, **figure A4**).

Chemical shift perturbations (csp) occurred as a function of the DNA concentration at several resonances. The number of affected amino acids (AA) residues and the intensity of some resonances was found to be dependent on the DNA concentration and reached its maximum at a cyt *c*/DNA ratio of 0.36. The positively charged lysine residues were mainly affected, *i.e.* K7, K8, K72, K73, K86, K87 and K100, since they interact with the negative backbone charge of the DNA. Interestingly K88, which neighbours the affected K87 and T89, did not show csps here. Moreover, neutral AAs in the close environment of the affected lysine residues also tend to show csps. The DNA induced csp of Q16 and K72 is highlighted in **figure 18b and 18c.** Regarding the primary structure of the protein, the interaction sites were mainly located at the N-terminus and *C*-terminus.

In **figure 19a** the significant csps, which were recorded for all AAs at pH 7.0 are summarised and mapped onto the crystal structure of cyt *c*. The map indicates that the AA residues interacting with DNA are not exclusively part of the cyt *c*s' α-helices. Moreover, only a part of the α-helices is in interaction with DNA. Considering that cyt *c* and histones both have high amounts of α-helical structures, it may be speculated that cyt *c* helices are inserted into the major groove of the DNA molecule, as it is known from histones (Khrapunov et al., 1997). Besides this, the Q16 side chain, which is located right in front of the heme pocket of cyt *c* and known to be involved in complex formation of cyt *c* and cyt *c* peroxidase (Pelletier and Kraut, 1992; Worrall et al., 2001) is also affected by DNA binding.
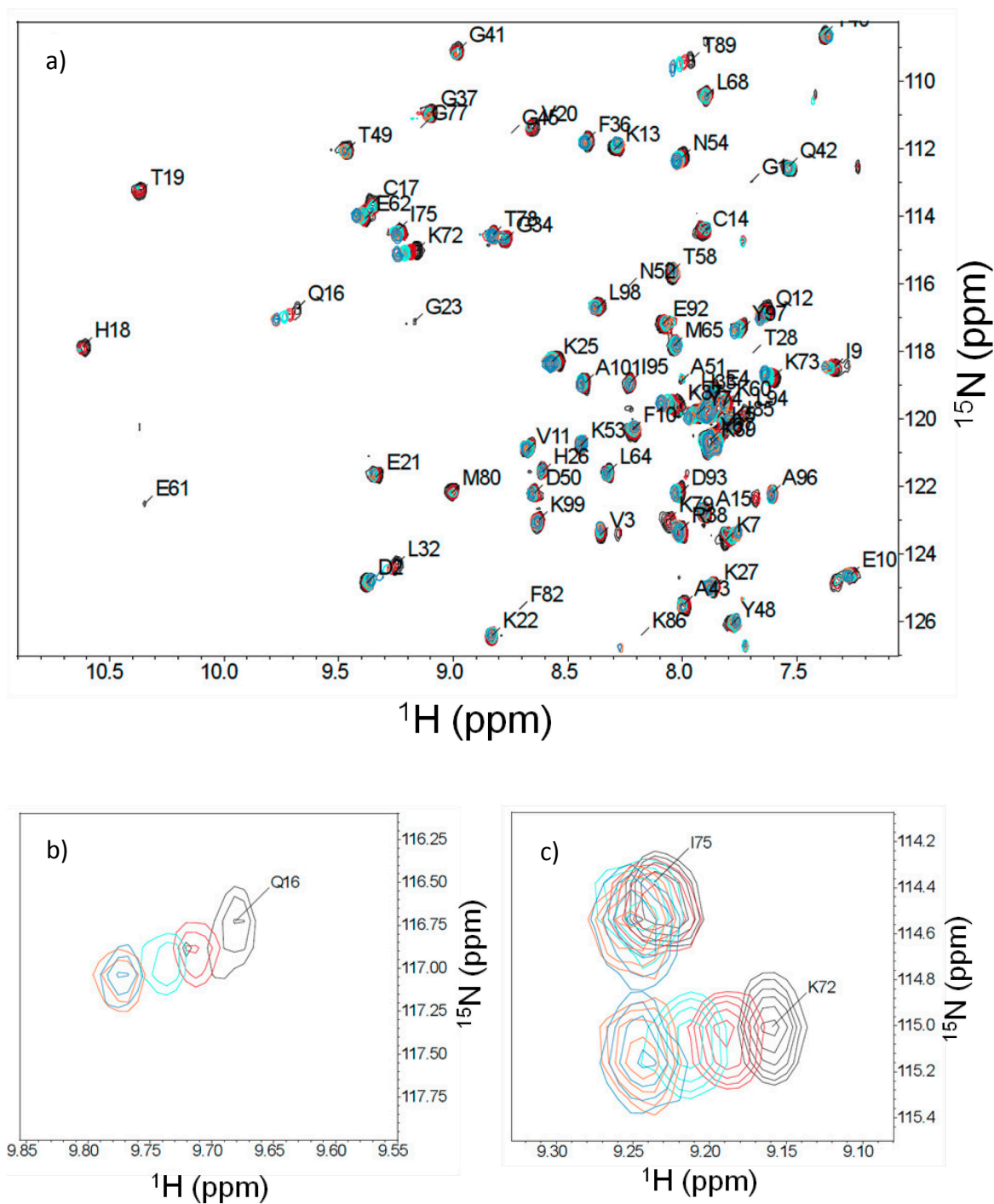
Figure 18: (**a**) Spectral region from overlaid ^{1}H-^{15}N TROSY-HSQC spectra recorded at pH 7.0 Samples containing 50 μM pure cyt *c* (black) and cyt *c* after titration with DNA: 3.0 μM (red), 6 μM (mint), 18 μM (blue) and 24 μM (orange) in KPi. Close-up of AA cross peak Q16 (**b**) and K72 (**c**) under the same conditions.

In general, several AAs found as interaction sites of DNA in this study were also elucidated in the interaction of cyt *c* with its natural binding partners. In the complex of cyt *c* peroxidase and cyt *c*, hydrogen bonds between K8, K72 and K87, and Van Der Waals interactions between I9 and E90 were identified. Moreover, the conformation of the Q16 side chain was altered after protein/protein binding to facilitate ET (Pelletier and Kraut, 1992; Volkov et al., 2006; Worrall et al., 2001). Another study performed by Brautigan et al. investigated the interaction between cyt *c* and its native interaction partner cyt *c* oxidase and determined K8, K12, K72, and K87 as the main interaction sites of the protein complex (Brautigan et al., 1978). Therefore, these AA residues seem to be favoured contact points in protein/protein and protein/nucleic acid binding.

In order to approach pH 5.0 NMR measurements were also performed at pH 6.0. Here, UV-vis did not indicate the formation of complexes, which enables NMR analysis. Moreover, it is relevant to investigate the cyt *c*/DNA interaction at pH 6.0, since cyt *c*/DNA ML systems can still be assembled at pH 6.0 (Sarauli et al., 2009) – although not as efficient as at pH 5.0. A number of significant csps already occurred at a low DNA concentration of 6 μM (figure **19b**), suggesting that more interaction sites occur in acidic medium (for the original spectrum see appendix, **figure A6**). The spectrum showed a similar pattern of AAs with csps as the pH 7.0 spectrum. However, additional csps were already observed at lower DNA concentration (**table 2**), including the basic AA residues K5, K73 and K88, as well as the neutral N70 and E91, which neighbour basic AAs. Furthermore, the neutral AAs I9, G37, G69, E92 and A101 were affected. The increased number of resonances with csps at pH 6.0 suggests that at pH 5.0 even more interaction sites may be contacted, making up the strong interaction between cyt *c* and DNA, which enables the formation of cyt *c*/DNA complexes in solution and stable cyt *c*/DNA architectures on surfaces.
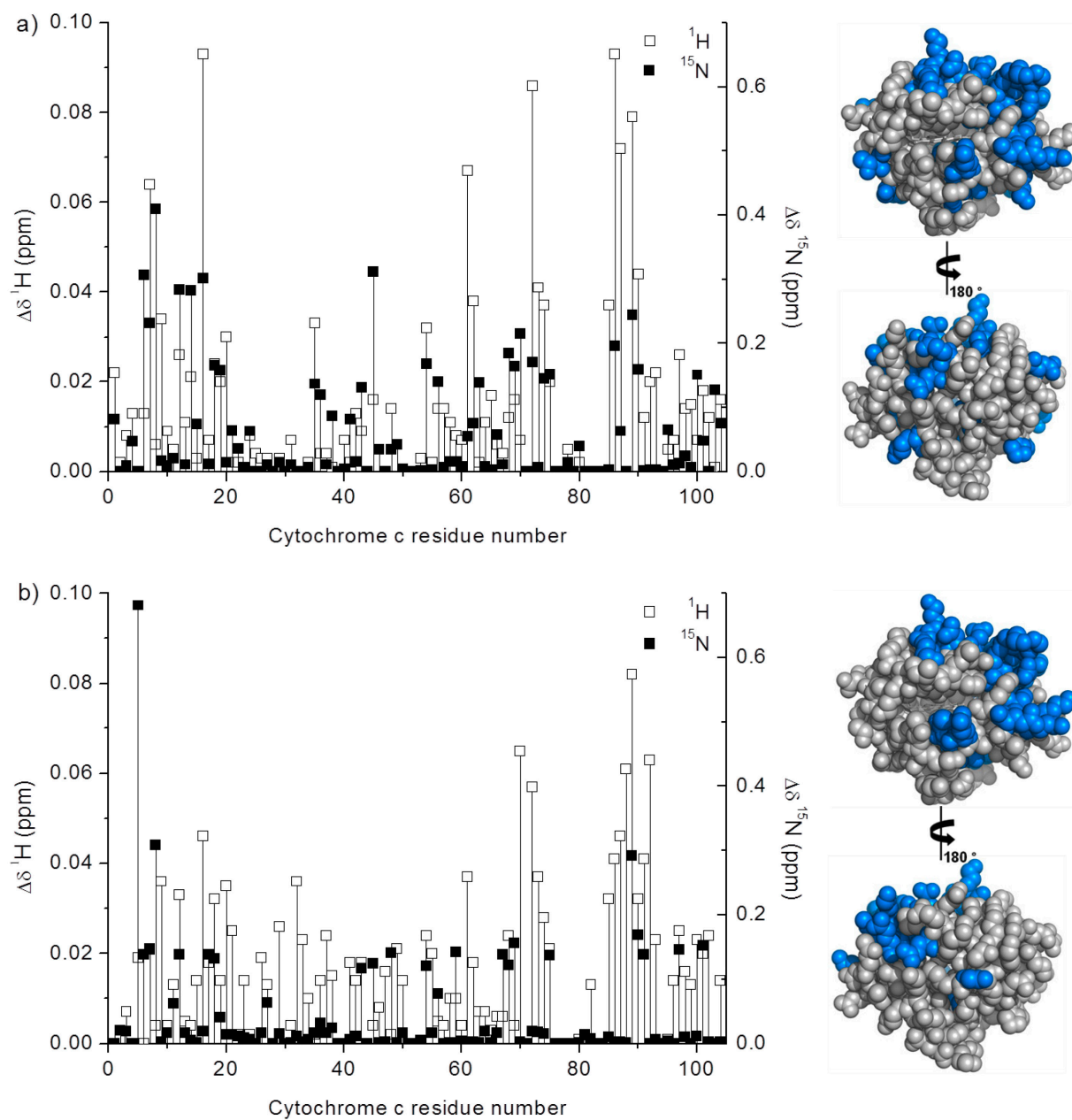
Figure 19; Left: Plot of csps recorded from cyt *c* backbone amides at (**a**) pH 7.0 with 18 μM DNA and (**b**) pH 6.0 with 6 μM DNA (20 mM KPi + 30 mM NaCl, 30°*C*). AAs residues are numbered from 1 to 104. Blanks correspond to proline residues 30, 44, 71 and 76 and unassigned G84. **Right:** Space filling representation of cyt *c* showing its secondary structure (grey) and residues with a significant csp ($\Delta\delta$ ^{1}H $\geq$ 0.03 or ^{15}N $\geq$ 0.15 ppm) (blue). The figures were generated by pymol based upon pdb-file 1HRC (Bushnell et al., 1990).

Table 2: Chemical shift perturbation (Δδ) observed for cyt *c* in the presence of different DNA concentrations at pH 7.0 and pH 6.0*

[DNA] μM	pH 7.0, 30 mM NaCl								pH 6.0, 30 mM NaCl	
	3.0		6.0		18.0		24.0		6.0	
Residue	Δδ ^{1}H	Δδ ^{15}N	Δδ ^{1}H	Δδ ^{15}N	Δδ ^{1}H	Δδ ^{15}N	Δδ ^{1}H	Δδ ^{15}N	Δδ ^{1}H	Δδ ^{15}N
K5	0.01	0.00	0.00	0.00	0.00	0.00	0.01	0.00	0.02	0.68
G6	0.01	0.10	0.01	0.15	0.01	0.31	0.02	0.31	0.00	0.14
K7	0.03	0.02	0.04	0.15	0.06	0.23	0.07	0.31	0.02	0.15
K8	0.00	0.00	0.01	0.25	0.01	0.41	0.00	0.41	0.01	0.30
I9	0.01	0.01	0.03	0.01	0.03	0.02	0.04	0.01	0.04	0.00
Q12	0.01	0.01	0.02	0.03	0.03	0.28	0.03	0.18	0.03	0.14
Q16	0.03	0.14	0.04	0.14	0.09	0.30	0.09	0.29	0.05	0.02
C17	0.01	0.01	0.00	0.01	0.01	0.01	0.01	0.01	0.02	0.15
H18	0.02	0.16	0.00	0.16	0.02	0.17	0.04	0.03	0.03	0.13
T19	0.01	0.00	0.00	0.00	0.02	0.16	0.02	0.00	0.01	0.04
V20	0.00	0.01	0.03	0.01	0.03	0.01	0.03	0.13	0.04	0.01
L32	0.00	0.01	0.05	0.10	0.00	0.00	0.04	0.31	0.04	0.01
L35	0.00	0.00	0.01	0.02	0.03	0.14	0.01	0.02	0.00	0.02
G37	0.00	0.01	0.00	0.01	0.00	0.00	0.01	0.09	0.06	0.17
G45	bbd	bbd	bbd	bbd	0.02	0.31	0.02	0.31	0.00	0.13
T47	bbd	bbd	bbd	bbd	bbd	bbd	bbd	bbd	0.02	0.00
N54	0.01	0.07	0.02	0.15	0.03	0.17	0.03	0.17	0.02	0.12
E61	0.01	0.14	0.03	0.10	0.07	0.06	bbd	bbd	0.04	0.01
E62	0.01	0.15	0.02	0.02	0.04	0.08	0.04	0.15	0.02	0.00
L68	0.00	0.01	0.00	0.00	0.01	0.18	0.01	0.00	0.02	0.12
G69	0.01	0.08	0.01	0.15	0.02	0.16	0.02	0.15	0.00	0.16
N70	0.00	0.08	0.00	0.06	0.01	0.22	0.01	0.08	0.07	0.00
K72	0.03	0.02	0.05	0.16	0.09	0.17	0.09	0.17	0.06	0.02
K73	0.02	0.00	0.03	0.00	0.04	0.01	0.04	0.16	0.04	0.02
Y74	0.01	0.00	0.02	0.06	0.04	0.15	0.04	0.16	0.03	0.02
I75	0.00	0.15	0.01	0.13	0.02	0.15	0.08	0.15	0.02	0.14
I85	0.05	0.01	0.04	0.01	0.04	0.00	0.04	0.01	0.03	0.01
K86	0.06	0.46	0.08	0.45	0.09	0.20	0.09	0.30	0.04	0.00
K87	0.03	0.07	0.04	0.08	0.07	0.06	0.07	0.07	0.05	0.00
K88	0.00	0.00	0.00	0.00	0.00	0.00	0.00	0.00	0.06	0.00
T89	0.03	0.01	0.05	0.15	0.08	0.24	0.09	0.32	0.08	0.29
E90	0.01	0.00	0.03	0.44	0.04	0.16	0.05	0.16	0.03	0.17
R91	0.02	0.00	0.00	0.44	0.04	0.00	0.05	0.00	0.04	0.14
E92	0.00	0.00	0.01	0.01	0.02	0.00	0.01	0.01	0.06	0.00
K100	0.00	0.08	0.01	0.15	0.01	0.15	0.02	0.15	0.02	0.01
A101	0.00	0.00	0.01	0.00	0.02	0.05	0.02	0.00	0.02	0.15
Σ of residues with sign. csps	12		22		29		26		26	

*A significant Δδ was defined as ^{1}H ≥ 0.03 or ^{15}N ≥ 0.15 ppm. bbd = broadened beyond detection.

At pH 7.0 and 6.0, the interaction between cyt *c* and DNA was found to be fast on the NMR timescale. Given that different cyt *c* species, either free or DNA-bound, were not detected, it is suggested that the interaction type of the two bio-molecules is transient. Complexes of this binding type have a lifetime of only some milliseconds to hundreds of milliseconds (Tolkatchev et al., 2003) and show the typical NMR spectrum of the protein, aside from the AAs affected by the ligand. On the other hand, the precipitation is a clear indicator for a very strong interaction between cyt *c* and DNA. This suggests that two different types of cyt *c*/DNA interaction occur, which are dependent on the pH value. Related to physiological conditions the transient character fits well to the cyt *c* function as shuttle molecule, capable to interact with membranes and reaction partners, but not in a permanent way, since dissociation

after ET is essential. However, under acidic conditions, the interaction is enforced, resulting in permanent complex formation and subsequent precipitation. This provides the basis for the technical application as cyt *c*/DNA assemblies. In order to gain a structural understanding of the interaction at pH 5.0, solid state NMR or X-ray crystallography may be performed.

4.1.4 Investigation of transient cytochrome *c*/DNA interactions

It was found that cyt *c* and DNA interact persistently at pH 5.0. However, NMR studies also revealed that even at pH 7.0 significant interaction occurs although an agglomeration was not detected by UV-vis-, CD spectroscopy and DLS. Thus, SEC, which is a valuable complement to NMR-based investigations (Crowley et al., 2011), was performed under NMR conditions to test whether this interaction is sufficiently strong to have practical implications. A layered deposition of both molecules cannot be realised at pH 7.0 (Sarauli et al., 2009), but it was studied how mixtures of DNA and cyt *c* behave in a size exclusion column. For this purpose, mixtures with the same cyt *c*/DNA ratios as in the NMR experiments were prepared at neutral pH and separated with a SEC column. **Figure 20** shows the overlaid chromatograms from these experiments. Note that three peaks with maxima at fractions 48 ml, 54 ml and 86 ml are present in each chromatogram. The peak at 86 ml correlates to monomeric cyt *c* (12.4 kDa) (Dixon et al., 1960) whereas the peaks at 48 ml and 54 ml are due to species with a molecular weight (MW) larger than 44 kDa. The MW of 41 bp DNA is approximately 25 kDa and is expected to elute with 70 ml to 75 ml buffer, based upon the column calibration data. However, the molecule is helical and may not behave as predicted by calibration with globular proteins. A large peak is present in each SEC chromatogram between fractions 48 ml to 55 ml. These fractions were analysed by gel electrophoresis after Coomassie staining (**figure 20**, grey panels). At low DNA concentrations (9 and 18 μM), no band was observed, indicating that DNA is not eluted with cyt *c*. However, at a higher DNA concentration (2.1), a clear band is observed, proving that cyt *c* and DNA co-elute. It should also be noted that the concentration of cyt *c* is the same in each experiment (100 μM), although the peak of the monomeric cyt *c* decreases with increasing DNA concentration. This suggests that the equilibrium shifts towards complex formation at the cyt *c*/DNA ratio identified by NMR spectroscopy. Although not detected in the previous optical measurements, these observations indicate a type of interaction that was sufficiently strong to change the elution behaviour of cyt *c* from the column. Consequently, it can be stated that despite interaction at neutral pH is

rather weak, compared to acidic pH values, it is not negligible. Thus, the AAs on the cyt c surface, which were identified in NMR experiments, represent interaction sites under physiological conditions.
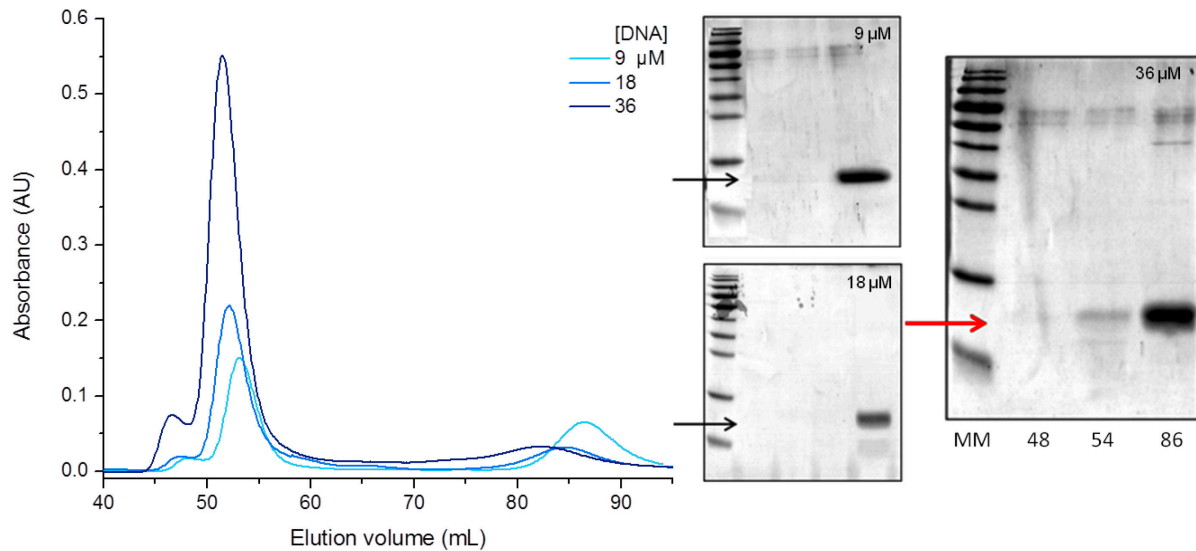
Figure 20; Left: Overlaid chromatograms from SEC experiments performed at pH 7.0. Samples contained 100 µM cyt c mixed with DNA at concentrations of: 9 µM (light blue), 18 µM (blue) and 36 µM (dark blue) (ratio from 0.09 to 0.36). **Right:** 15 % SDS-PAGE analysis of SEC fractions at 45, 54 and 80 mL, panel labelled according to DNA concentration ratio. The gel lanes are labelled: MM: molecular weight marker; fraction volume 45, 54 and 80 (mL). The black arrows mark the migration position of cyt c, the red arrow marks the co-eluted cyt c at high DNA concentration.

4.2   Interaction of FDH with a cytochrome *c* monolayer

Aiming on the formation of an analytical signal chain, the intention was to combine the membrane associated enzyme FDH with cyt *c* immobilised on an electrode surface.

The initial experiments were performed in solution to define the optimal reaction conditions between the two bio-molecules. Therefore, the reaction rate of cyt *c* with the enzyme was determined by UV-vis using the dependency on the cyt *c* concentration and different pH values. Subsequently, cyt *c* was immobilised in a monolayer on a SAM modified AuE, the enzyme was kept in solution and the interaction was studied by CV. In the final step both enzymes were to be immobilised.

4.2.1 Reaction of freely diffusing cytochrome *c* with FDH

The reaction conditions of the cyt *c* reduction by substrate reduced FDH were first investigated with both biomolecules in solution under the same conditions by applying UV-vis spectroscopy. After mixing cyt *c* and FDH under the same conditions used for the activity assay (100 mM McIlvaine pH 4.5), fructose was added and the absorbance change of the reduced cyt *c* was recorded at 550 nm (**figure 21**).
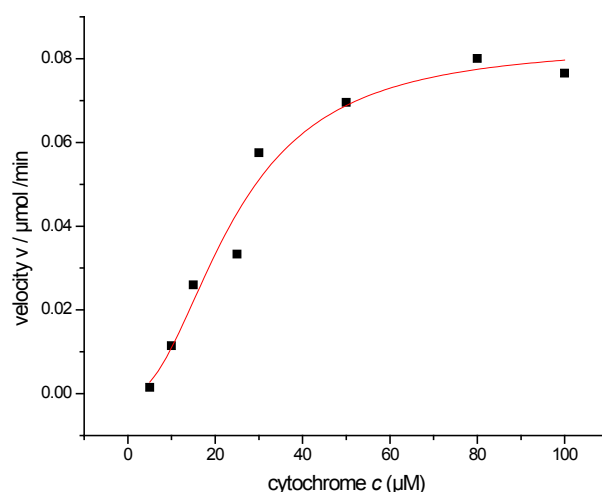
Figure 21: Velocity of cyt *c* reduction in the presence of FDH and fructose at different cyt *c* concentrations. Reduction of cyt *c* was traced at 550 nm in a 1 cm cuvette. Reaction conditions: 100 mM McIlvaine, pH 4.5, 0.5 U FDH and 50 mM fructose.

The apparent K_m value and the turnover number (k_{cat}) of the reaction between cyt c and FDH were determined. The K_m(cyt c) was found to be 24 µM and the k_{cat}(cyt c) value 0.025 1/s. The K_m(cyt c) value is lower but nevertheless in the range of the value determined using ferricyanide as electron acceptor, $i.e.$ 470 µM (Marcinkeviciene and Johansson, 1993). Comparing the values obtained with cyt c as electron acceptor to the ones obtained with ferricyanide indicates that the enzyme already works at half maximum speed at relatively low concentrations of cyt c. The very low k_{cat}(cyt c), however, suggests that the reaction with cyt c proceeds significantly less efficiently than the one with ferricyanide (k_{cat}(cyt c) = 0.025 1/s vs. k_{cat}(ferricyanide) = 95 1/s).

Furthermore, the pH-profile of the reaction was studied in the range of pH 4.5 to 7.0. The pH optimum of FDH is around 4.5, but it was reported to be active from pH 4.0 to 6.0, beyond pH 6.0 inactivation may occur due to the decomposition of the heterotrimer (Ameyama et al., 1981). However, it has also been reported that FDH reduces cyt c efficiently at pH 7.0 (Ferapontova and Gorton, 2005). Therefore, a wide pH range was selected.

After mixing cyt c and FDH, fructose was added and the absorbance change of the reduced cyt c was recorded at 550 nm. **Figure 22** depicts that the reduction of cyt c by FDH proceeds most efficiently at pH 4.0 since here the highest rate was detected. The rate decreases with increasing pH values. However, when reaching pH 6.5 and 7.0, the value increases again. During the measurement, no saturation of absorbance was observed, indicating that the kinetic data were recorded in the linear range of cyt c reduction. The reduction of cyt c was completed after 50 min of incubation. As a control, the absorbance of fully reduced cyt c was determined additionally by adding ascorbic acid to the pH 4.5 sample.

The two pH optima described here, are in agreement with the acidic pH optimum for ferricyanide reduction (Ameyama et al., 1981) and also with the neutral pH value reported for the ET reaction between FDH and cyt c in solution (Ferapontova and Gorton, 2005). According to the two pH optima, two different electron pathways are suggested; ET may either proceed from the FAD-domain via the heme group towards cyt c or directly from the FAD-domain to cyt c. A similar conclusion was drawn by Ferapontova et al. after investigating ET between cyt c and FDH by CV at different scan rates. At high SRs, the catalytic route may be proceeding from the active site directly to cyt c in solution. At low

SRs, catalysis may occur on the common pathways via the heme domain on the free cyt *c* (Ferapontova and Gorton, 2005).

Performing the standard activity assay of FDH with ferricyanide at neutral pH (usually pH 4.5) the activity obtained was 96% lower compared with the one recorded at pH 4.5. This suggests that FDH does not reduce ferricyanide efficiently at pH 7.0 with both components in solution.
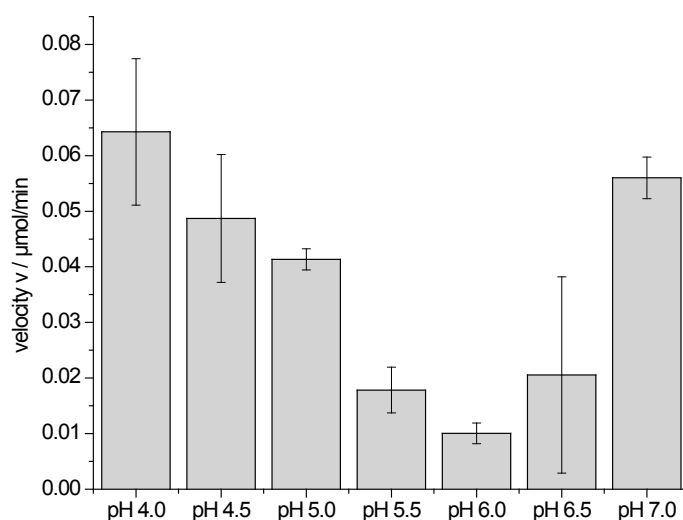
Figure 22: Velocity (v) of cyt *c* reduction in the presence of FDH and substrate in solutions of different pH values. The reaction rate was measured by following the cyt *c* reduction at 550 nm and calculated from the change in absorbance versus time, using the Lambert-Beer equation. Experimental conditions: 100 mM McIlvaine, [cyt *c*] = 25 µM, FDH = 1 U, [fructose] = 50 mM.

4.2.2 Influence of different Triton X-100 containing buffers on surface bound cytochrome *c*

FDH was reported to be inactivated due to precipitation in the absence of stabilising detergents (Ameyama et al., 1981). However, the presence of a detergent may destabilise the monolayer due to compensation of the surface charges of cyt *c* and the SAM`s carboxylic groups. Therefore, the behaviour of the cyt *c* monolayer was investigated in the presence of the detergent in different buffers (**figure 23**). Cyclic voltammograms were recorded before the buffer exchange (black lines), after the buffer exchange (red lines) and also after the incubation in Triton X-100 (TX) containing solution (green lines). To follow the stability of the monolayer in dependency on the time, cyclic voltammograms were recorded in 10 min

interval steps during incubation in 5 mM KPi buffer (pH 7.0) with 0.1% of TX (**figure 23b**) and in 10 mM NaPi/cit buffer with 0.1% of TX (**figure 23d**).
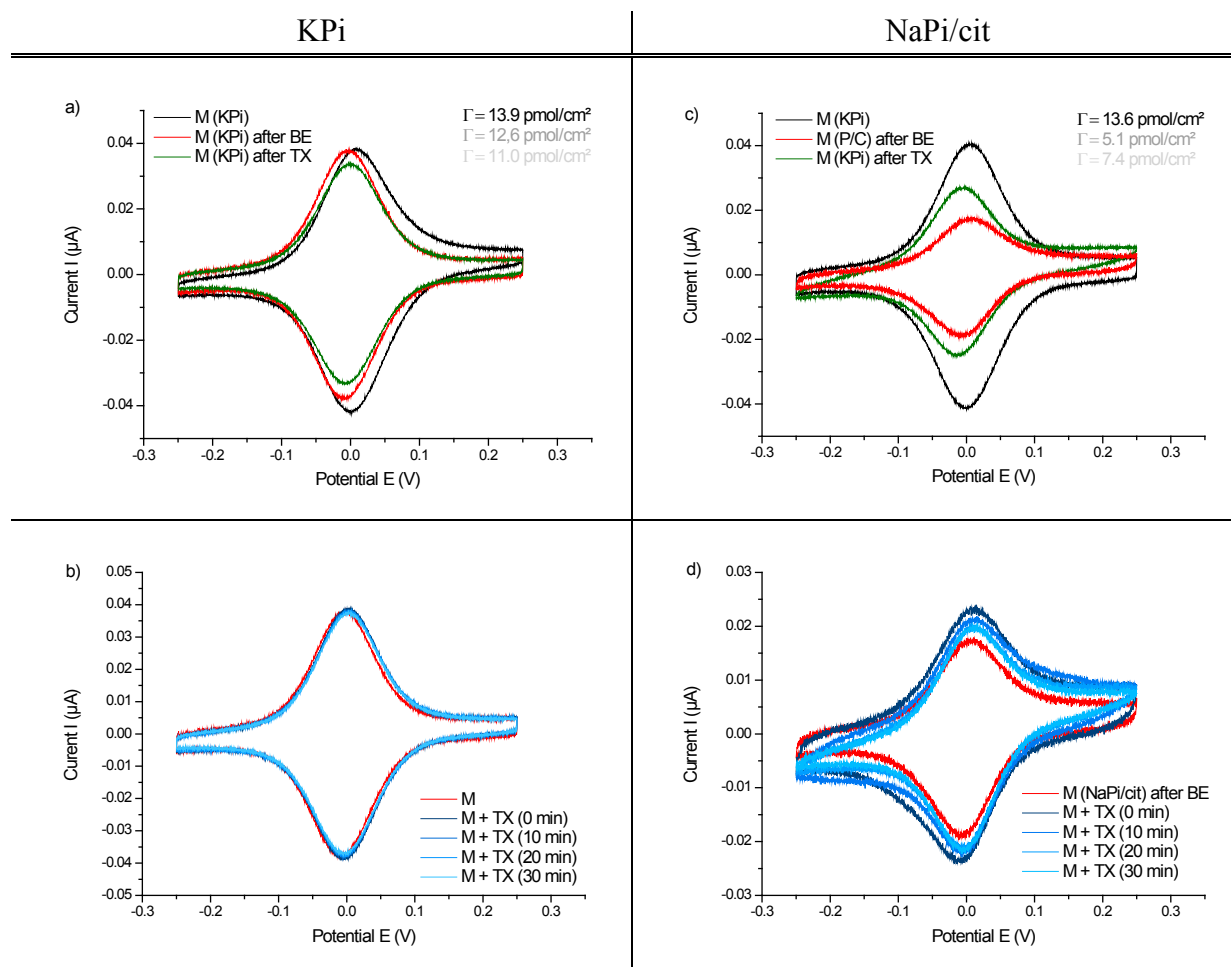
Figure 23: Cyclic voltammograms of cyt *c* immobilised in a monolayer (M) on MU:MUA modified AuE surfaces in KPi or McIlvaine buffer (pH 7.0). **a**) and **c**) M in KPi before and after buffer exchange (BE), either to KPi or to NaPi/cit as well as after incubation in TX containing buffer (KPi or NaPi/cit). M in KPi (black lines); M after BE (red lines); M in KPi after measurements in TX containing buffer (green lines). **b**) and **d**) M in TX containing NaPi/cit buffer. M after BE to KPi or NaPi/cit (red lines); M in KPi or NaPi/cit, each with 0.1% TX, incubated for 10 to 30 min (blue lines). Experimental conditions: 5 mM KPi, 10 mM McIlvaine buffer, pH 7.0, SR = 100 mV/s.

In KPi buffer a small loss of redox active material on the electrode surface was observed after the cell and the electrode were flushed with the same buffer (**figure 23a**, red line) in order to simulate the conditions of a buffer exchange. Upon addition of TX the cyt *c* signal remained stable during the time dependent measurement (**figure 23c**, blue lines). Retransferring the monolayer electrode back to TX free KPi, and comparing the surface coverage before (*i.e.* 13.9 pmol/cm²) and after (*i.e.* 11.0 pmol/cm²) the incubation, a decrease by only 2.9

pmol/cm² of redox active protein was found (**figure 23a**, green line). This suggests that the monolayer remains stable in KPi despite the presence of the detergent.

Using NaPi/cit buffer, the surface charge decreased significantly from 13.6 pmol/cm² to 5.1 pmol/cm², already when the buffer was exchanged from KPi to NaPi/cit (**figure 23c**, red line). After addition of TX and incubating for 30 min the surface coverage improves stepwise (**figure 23d**, blue lines). However, it does not reach the initial amount recorded previously with the same electrode in KPi. Retransferring the measured monolayer back to KPi showed a decreased surface coverage of 7.4 pmol/cm² (**figure 23c**, green line). This low value suggests a loss of surface confined cyt *c* of 6.2 pmol/cm² and indicates the instability of the cyt *c* monolayer in NaPi/cit buffer rather than a TX induced effect. The detergent does not seem to destabilise the monolayer assembly, however, its presence seems to have a distorting effect on the cyt *c* redox signal.

4.2.3 Investigation of surface bound cytochrome *c* with freely diffusing FDH

4.2.3.1 Direct electron transfer between cytochrome *c* monolayers and FDH at different pH conditions

- **neutral pH**

For the investigation of the interaction between immobilised cyt *c* and FDH in solution, cyt *c* was adsorbed on a MU:MUA modified AuE as a monolayer. The cyt *c*/FDH interaction was first studied at pH 7.0, since the pH profile of the reaction suggests an efficient enzymatic reduction of the redox protein at neutral pH. **Figure 24a** shows the cyclic voltammogram of adsorbed cyt *c* after addition of FDH (red line). Upon the addition of increasing fructose concentrations (green lines), a clear, substrate dependent catalytic current occurs, starting at about -80 mV and reaching a maximum of 2.0 nA under substrate saturation.

This indicates that the free FDH reduces the immobilised cyt *c* efficiently although it is trapped in a surface confined state. The catalytic currents obtained at 200 mV (vs. Ag/AgCl 1M KCl) were plotted over the fructose concentration (**figure 24b**). This plot revealed the behaviour of a typical enzymatic reaction following a Michelis-Menten-type kinetics and

enabling the determination of the apparent Km value as the substrate concentration at half maximum activity. An apparent K_m value of 250 µM was determined for the reaction of freely diffusing FDH with immobilised cyt c as electron accepting substrate. This value is more than one magnitude below the apparent K_m value of 10.0 mM, which was determined in solution at pH 4.5 and with ferricyanide as electron acceptor (Ameyama et al., 1981).

Moreover, the behaviour of commercially (Sigma-Aldrich) and non-commercially (Kano lab of the Kyoto University) produced FDH was tested with cyt c monolayers at pH 7.0. However, despite the marginally higher catalytic currents reached with the non-commercial enzyme, a similar behaviour in cyt c reduction was found for both enzyme stocks (**see appendix, figure A9**).
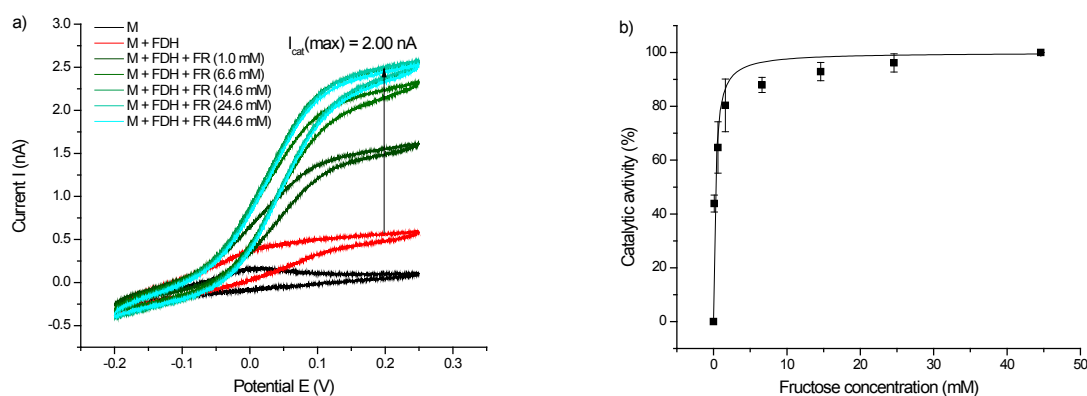
Figure 24: a) Cyclic voltammograms of cyt c monolayers (M) on a MU:MUA modified AuE surface with 4 U FDH. M (black lines), M with FDH in solution (red lines) and upon addition of 1.0 mM – 44.6 mM fructose (FR) (green lines). Experimental conditions: 5 mM KPi, pH 7.0, SR = 2 mV/s, step potential = 0.15 mV. **b**) Plot of the relative catalytic activity obtained at 200 mV (vs. Ag/AgCl 1M KCl) in dependency on the fructose concentration from n = 4 electrodes. Values (black sqaures) are fitted by $y = I_{max}\cdot[S]/(K_m+[S])$ (black line) with V_{max} = 100% catalytic activity and K_m = 250 µM.

To test whether FDH adsorbs on the cyt c monolayer after the measurement with FDH in solution, the used electrode was washed by transferring it to 5 mM KPi pH 7.0 (FDH and substrate free). Re-measuring the electrode revealed that upon the addition of the substrate a small catalytic current of 0.21 nA occurs (**figure 25**). Although only a low catalytic current was detected, the first evidence that FDH can be co-immobilised with cyt c was given here.
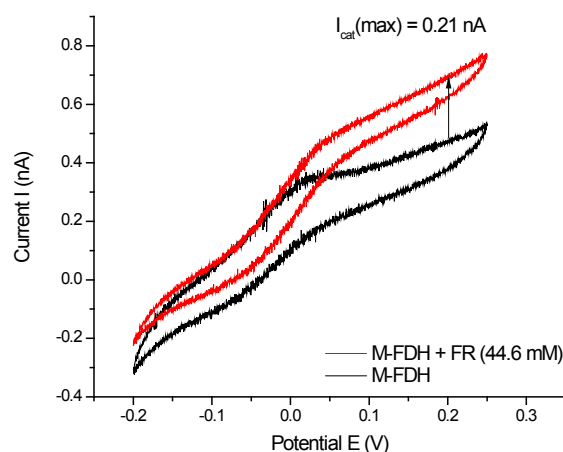
Figure 25: Cyclic voltammograms of the cyt *c* monolayer (M) on a MU:MUA modified AuE surface, previously measured with 4 U FDH and 44.6 mM fructose (FR) in solution (see **figure 24A**). M-FDH in the absence of fructose (black line) and upon addition of fructose (red line). Experimental conditions: 5 mM KPi, pH 7.0, SR = 2 mV/s, step potential = 0.3 mV.

Since FDH has been reported to be inactivated by precipitation in the absence of stabilizing detergents (Ameyama et al., 1981), control experiments were performed in Triton X-100 (TX) containing buffer (**figure 26**). With respect to the results obtained from TX-free solutions (blue line), a decrease in the catalytic activity was found after the addition of the detergent (green line). The cyt *c* electrochemistry does not seem to be affected by TX (also compare **4.2.2**), however, the ET reaction between cyt *c* and FDH may be hindered by the detergent. Although it was reported that FDH is inactivated in the absence of TX (Ameyama et al., 1981), the enzyme appears to remain active in TX-free buffer, at least in the time range of the measurements. In order to create favourable conditions for the investigation of inter-protein ET reactions and also to minimise the risk of an interference of the detergent with the test system, all electrochemical measurements were performed in TX-free buffer.

60
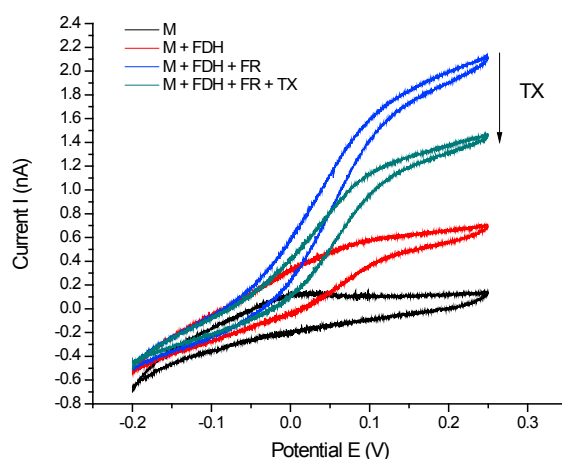
Figure 26: Cyclic voltammograms of a cyt *c* monolayer (M) on a MU:MUA modified AuE surface with 4 U FDH in solution. M (black line), M with FDH in solution (red line), in presence of 44.6 mM fructose (FR) (blue line) and upon addition TX (green line). Experimental conditions: 5 mM KPi, pH 7.0, SR = 2 mV/s, step potential = 0.15 mV.

- **acidic pH**

Given that the pH optimum of the enzyme was reported to be between 4.0 and 4.5 and the UV-vis study with both bio-molecules in solution also indicated that FDH reduces cyt *c* efficiently in this pH range, ET between FDH and immobilised cyt *c* was studied in acidic media (**figure 27**).
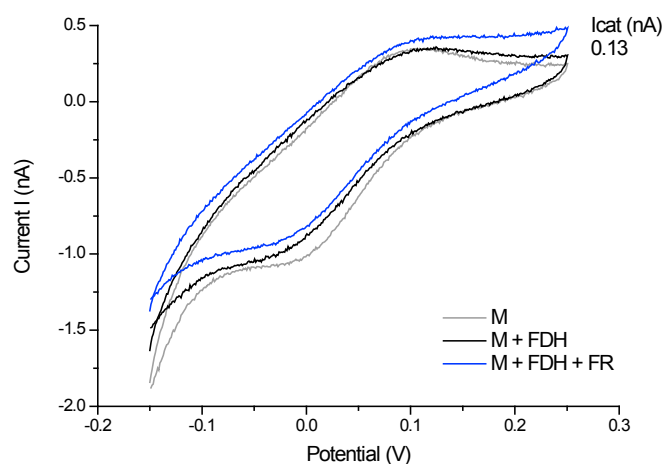
Figure 27: Cyclic voltammograms of a cyt *c* monolayer (M) on a MU:MUA modified AuE surface with FDH (4 U) in solution. M (grey line), M with FDH in solution (black line) and in presence of 44.6 mM fructose (FR) (blue line). Experimental conditions: 20 mM KPi, pH 4.5, SR = 2 mV/s, step potential = 0.3 mV).

At pH 4.5 a very small catalytic current of 0.13 nA was observed in the presence of fructose (**figure 28**). Going towards a slightly higher pH value of 5.0, the ET between FDH and cyt c seems to be improved. Upon addition of the substrate in concentrations of 1.0 - 8.0 µM a moderate substrate dependent oxidation current was observed (**figure 28a**). A maximum catalytic current of 0.55 nA was already achieved at 5.0 µM fructose and did not increase with higher concentrations. Performing the same experiment with concentrations in the nM range did not lead to a stepwise increase of the catalytic current as shown at pH 7.0 (**figure 28b**).

An evaluation of the data was tried by plotting the obtained catalytic currents over the substrate concentration (**figure 28c**). However, since the data points in the nM concentration range - defining the behaviour of the linear phase of the graph - could not be detected, the estimation of an apparent K_m value does not seem to reasonable here. It is suggested that the low substrate concentrations applied are too far below the real K_m value of the enzyme, disabling the possibility to record a proper substrate dependency in acidic media and with cyt c as reaction partner. Since the enzyme activity is expected to be high in this pH range, it is suggested that the interaction may be hindered as a result of the positive net charge of the two biomolecules below their pIs, (*i.e.* 5.0 ± 0.1 for FDH (determined by the provider) and 10.0 for cyt c (van Gelder and Slater, 1962)).

Substrate induced catalysis occurs at a fructose concentration of 1.0 µM, but it seems that the ET from FDH to cyt c is the limiting step. Several reasons can be taken into account here

i) the decreased amount of electro active cyt c on the electrode surface ii) the change in mobility of the adsorbed cyt c iii) the change in the ET rate of immobilised cyt c at pH 5.0. Indeed, a low amount of addressable cyt c was detected on the electrode surface (*i.e.* 3 pmol/cm^2), however, it is hard to discriminate whether the low catalytic currents recorded are based upon the diminished number of interaction sites or the reduced ET efficiency between the two proteins under these conditions.
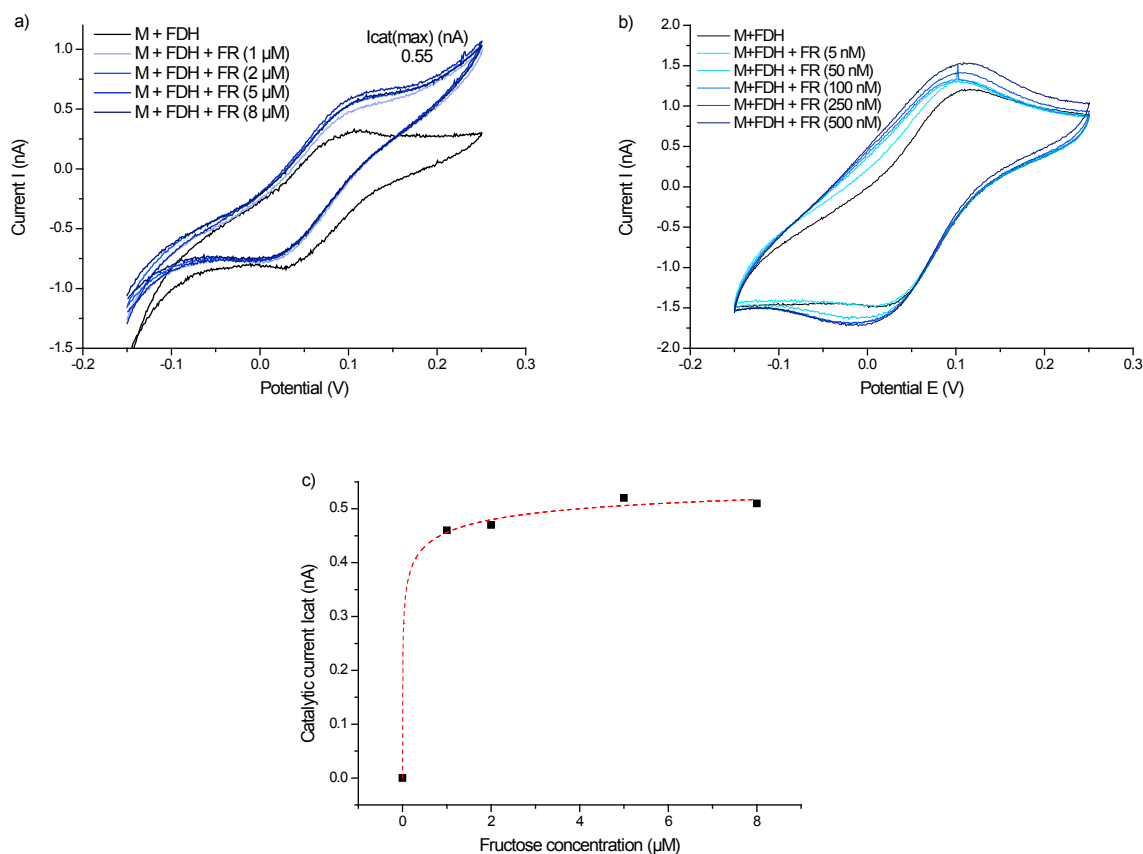
Figure 28: a) Cyclic voltammograms of a cyt *c* monolayer (M) on a MU:MUA modified AuE surface with FDH (4 U) in solution. M with FDH in solution (black line) and in presence of 1-8 μM fructose (FR) (blue lines). **b)** M with FDH in solution (black line) and in presence of 0.5-500 nM fructose (blue lines). Experimental conditions: 20 mM KPi, pH 5.0, SR = 2 mV/s, step potential = 0.3 mV). **c)** Plot of the catalytic current obtained from a) at 200 mV in dependency on the fructose concentration. Values (black sqaures) are fitted by $y = I_{max} \cdot [S]/(K_m+[S])$ (dashed line).

4.2.3.2 Ferricyanide mediated electron transfer

In order to investigate whether the ET between FDH and cyt *c* can be improved in acidic media CV measurements were performed with the redox mediator $K_3[Fe(CN)_6]$ in solution. The enzymatic reduction of $K_3[Fe(CN)_6]$ by FDH was reported previously (Ameyama et al., 1981) and utilised to assay the enzyme activity. Concerning the reaction of immobilised cyt *c* with $K_3[Fe(CN)_6]$ and $K_4[Fe(CN)_6]$, **figure 29** shows that increased oxidation and reduction currents occur upon addition of the respective redox species. This suggests that the interaction of the complex ion and cyt *c* in the immobilised state is feasible. Therefore, it is concluded that $K_3[Fe(CN)_6]/K_4[Fe(CN)_6]$ may act as mediating molecule between FDH and the cyt *c* monolayer electrode.
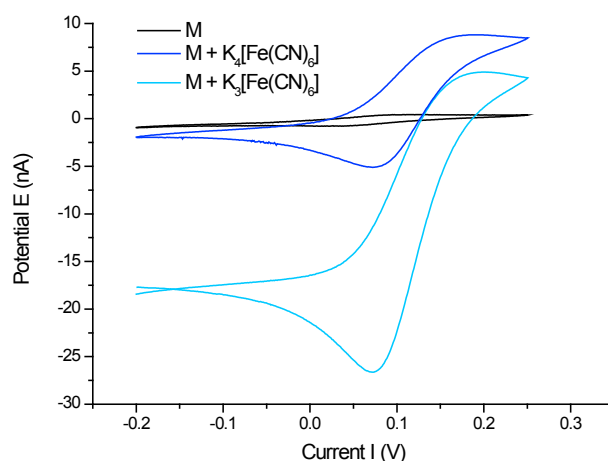
Figure 29: Cyclic voltammograms of a cyt *c* monolayer (M) on a MU:MUA modified AuE surface with $K_3[Fe(CN)_6]$ or $K4[Fe(CN)6]$ (10 µM) in solution. M (black line), M with with $K_4[Fe(CN)_6]$ (blue line) and $K_3[Fe(CN)_6]$ (light blue line). Experimental conditions: 5 mM KPi pH 7.0, SR = 2 mV/s, step potential = 0.3 mV.

Figure 30 summarises the catalytic currents obtained from the inter-protein electron transfer (IET) reaction of FDH with cyt *c* and the ferricyanide mediated ET (MET) reaction at different pH values under identical experimental conditions (scan rate, step potential and buffer). Comparing the IET reactions (left panels) at different pH 4.5, 5.0 and 7.0 indicates that the intensity of the substrate induced ET reaction improves from acidic to neutral pH (also see **4.2.3.1**). After adding $K_3[Fe(CN)_6]$ (right panels) an increased oxidative catalytic current is observed, indicating that MET occurs. Since the small redox mediator may easily diffuse between the two interacting proteins, it is suggested that the enzyme reduces ferricyanide to ferrocyanide at its active site. Ferrocyanide may then shuttle electrons on the immobilised cyt *c* (light blue to dark blue lines), causing its reduction and inducing the recorded oxidative catalytic current. For illustration of the ET pathway see **figure 31**. The efficiency of the MET reaction increases when going to a neutral pH, following the same pH dependency as the IET reaction.
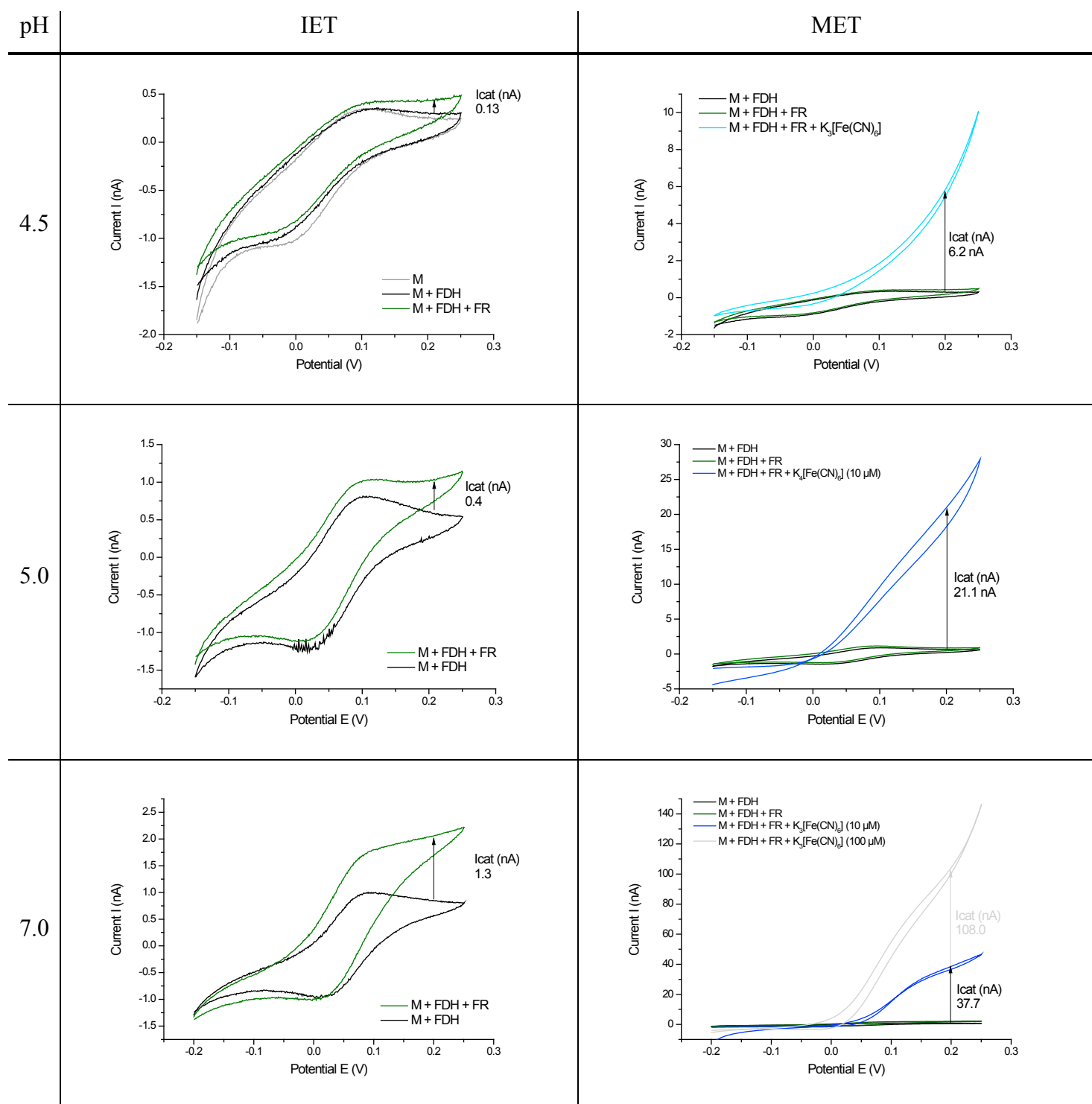
Figure 30: Cyclic voltammograms of a cyt *c* monolayer (M) on a MU:MUA modified AuE surface with FDH (4 U) in solution at different pH values (pH 4.5, 5.0, and 7.0) Inter-protein electron transfer (IET) (**left panels**): M (grey line), M with FDH in solution (black line) and in presence of 44.6 mM fructose (FR) (green line). MET (**right panels**): M + FDH + fructose after addition of $K_3[Fe(CN)_6]$ (light blue to dark blue lines). Experimental conditions: 20 mM KPi, SR = 2 mV/s, step potential = 0.3 mV.

It is generally known that ET of the redox mediator with AuEs is hindered by MU:MUA-SAMs, consequently it may be suggested that ET should only be able to proceed via the cyt *c* monolayer. However, the quality of the SAM may suffer from the buffer exchange, the permanent voltammetric scans or the exposure to high sugar concentrations. Therefore, SAM modified AuEs were treated as for the cyt *c* monolayer assembly (cycling and incubation in 5 mM KPi, pH 7.0 and buffer exchange for measurements at pH 5.0), yet in the absence of cyt *c*. Afterwards, DET as well as MET was tested at pH 5.0 and 7.0 (**figure 32a and 32b**). Figure 32 depicts that in the absence of ferricyanide, no catalytic current occurred, neither at pH 5.0 nor at pH 7.0, indicating that DET from FDH on the electrode is not possible under these conditions.

Using cysteamine as promoter, Ferapontova et al. reported that a positively charged SAM is required to achieve pronounced DET with the AuE (Ferapontova and Gorton, 2005). Here, the E_f was found to be -142.5±4 mV (vs. Ag/AgCl sat. KCl) at pH 5.0, while Khan et al. determined an E_f of 80 mV (vs. Ag/AgCl sat. KCl) at pH 4.5, using bare AuEs (Khan et al., 1991).
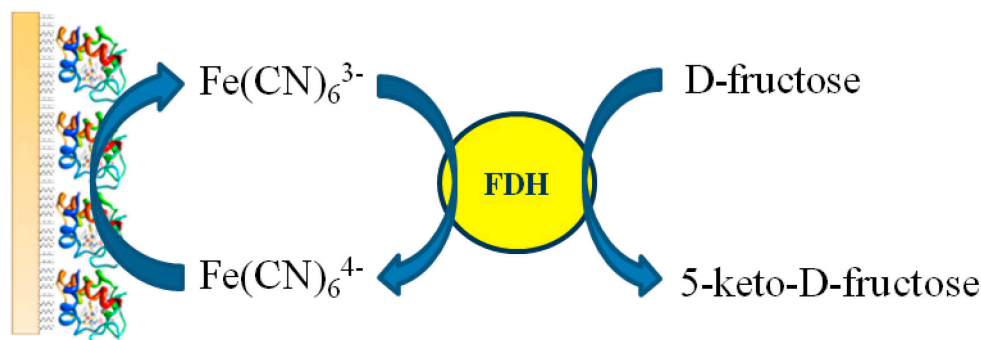
Figure 31: The scheme represents the suggested mechanism of the ferricyanide MET reaction between FDH and the cyt *c* monolayer electrode. After electron extraction from fructose, the enzyme reduces ferricyanide to ferrocyanide which shuttles electrons on the immobilised cyt *c*, causing its reduction.

Upon addition of the redox mediator small catalytic oxidation currents of 0.25 nA at pH 5.0 and 0.78 nA at pH 7.0 were observed, indicating that ET is now enabled. Comparing the catalytic currents obtained at the SAM only with the ones from the cyt *c* monolayer indicates that significantly higher currents are achieved at the cyt *c* modified electrode. This suggests that ET via cyt *c* is much more efficient than ferricyanide MET at the bare SAM modified electrode.
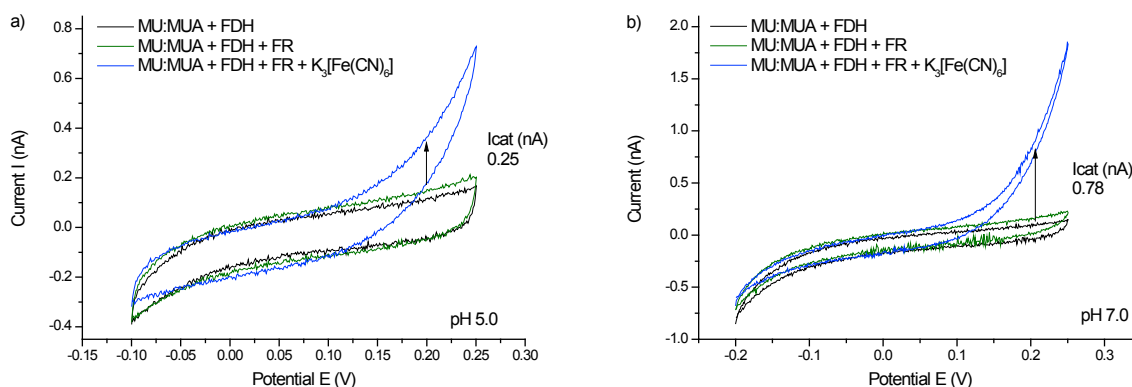
Figure 32: Cyclic voltammograms of MU:MUA modified AuEs with FDH, fructose (FR) and the redox mediator $K_3[Fe(CN)_6]$ in solution at pH 5.0 **a)** and pH 7.0 **b)**. AuE/MuMua (black line), after addition of FDH (4U) and fructose (44.6 mM) (green line) and after addition of $K_3[Fe(CN)_6]$ (10 µM). Experimental conditions: 5 mM KPi, SR = 2 mV/s step potential = 0.3 mV.

4.2.4. Investigation of FDH bound to a cytochrome *c* monolayers

In the final step of this study, both proteins were immobilised on the surface of the SAM modified AuEs. This is inspired by a previous approach in which cyt *c* and sulfite oxidase were immobilised without the help of a polyelectrolyte solely using the opposing net surface charge of the interaction partners (Dronov et al., 2008c). Given that FDH has an acidic pI of 5.0 and cyt *c* a basic one of 10, it was intended to create cyt *c*-FDH electrodes in the same manner.

First evidence for the feasibility of a direct adsorption of FDH on a cyt *c* monolayer electrode was found in **4.2.3.1.** Here, an electrode which was used to test the interaction of cyt *c* in the surface confined state with freely diffusing FDH was re-measured in substrate free and substrate containing buffer (**figure 25**). Since a weak catalytic current was generated in the presence of fructose, it was suggested that a small amount of FDH may be adsorbed to cyt *c* in the immobilised state. Therefore, cyt *c* monolayer electrodes were now incubated in an FDH solution at pH 7.0. CV was applied to investigate the cyt *c*/FDH electrodes in the absence and presence of fructose. Since the reaction between FDH and cyt *c* was found to be most efficient in media of neutral pH, CV was conducted at pH 7.0.

In order to test the influence of FDH adsorption on the redox behaviour of the cyt *c* monolayer cyclic voltammograms of each cyt *c*/FDH electrode were first recorded at 100

mV/s prior to substrate addition. Compared to a typical cyt *c* monolayer electrode, the cyt *c*/FDH electrodes showed a decreased redox activity (*i.e.* decrease in detectable electro active amount on the electrode surface) and a shift of the typical E_f of adsorbed cyt *c* (*i.e.* 0 mV vs. Ag/AgCl 1M KCl) towards -25 to -30 mV (**figure 33**). This suggests that the protein-protein interaction between cyt *c* and FDH may affect cyt *c*`s redox properties and may even lead to the desorption of cyt *c*. Alternatively, a reorganisation of the cyt *c* monolayer may take place, leading to partial loss of the redox activity.
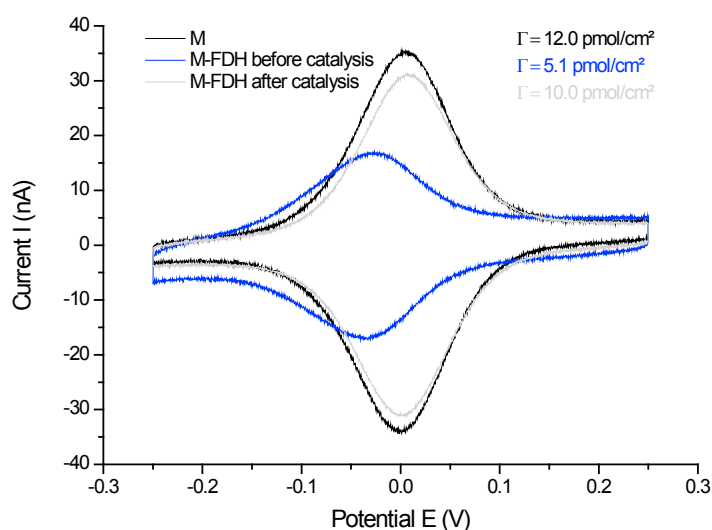
Figure 33: Cyclic voltammograms of a cyt *c*-FDH electrode (AuE/MU:MUA/cyt *c*-FDH) at pH 7.0. Monolayer (M) before FDH adsorption (black line); M with FDH immobilised on top before (blue line) and after (grey line) the addition of fructose and measurement at 2 mV/s. Experimental conditions: 5 mM KPi pH 7.0, SR = 100 mV/s step potential = 0.3 mV.

The catalytic reaction between the co-immobilised FDH and cyt *c* was subsequently investigated at a SR of 2 mV/s (**figure 34a**). The cyt *c*/FDH electrode showed a rather weak oxidation peak and lacked a reduction peak (black line), compared to a typical cyt *c* monolayer electrode. This reduced redox activity may be devoted to enzyme adsorption as suggested from the measurements performed with a higher scan rate. Adding fructose resulted in a clear catalytic oxidation current (**figure 34a**, red line) which started at -100 mV (vs. Ag/AgCl 1M KCl) and reached a maximum level of 0.7 nA at 200 mV (vs. Ag/AgCl 1M KCl). Here, a substrate dependency of the catalytic current was found as well (**figure 34b**).
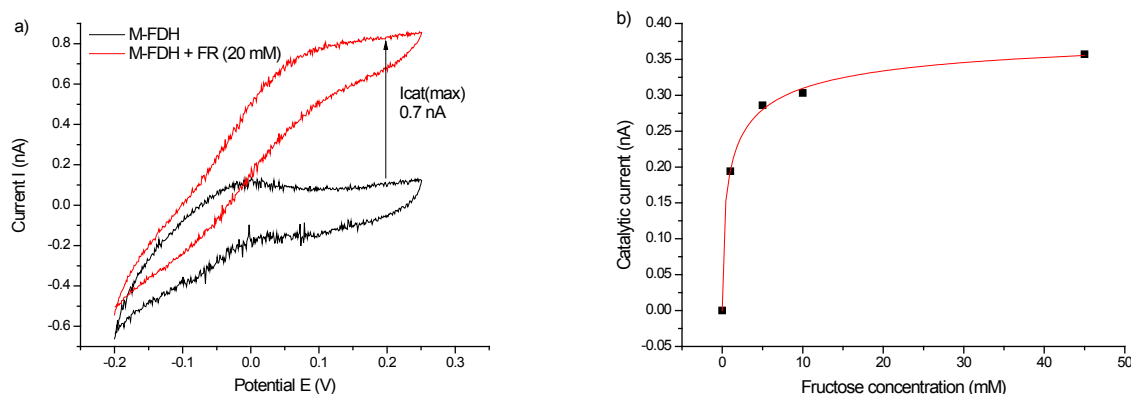
Figure 34: Cyclic voltammograms of a cyt *c*-FDH electrode (AuE/MU:MUA/cyt *c*-FDH) at pH 7.0. **a)** Monolayer (M) with FDH immobilised on top (black line) and upon addition of 20 mM fructose (FR) (red line). **b)** Plot of the catalytic current obtained at 200 mV in dependency on the fructose concentration. Values (black sqaures) are fitted by y = I_{max}·[S]/(K_m+[S]) (red line) with V_{max} = 0.4 nA and K_m = 1.1 mM. Experimental conditions: 5 mM KPi pH 7.0, SR = 2 mV/s step potential = 0.3 mV.

Plotting the obtained catalytic current over the fructose concentration revealed a Michaelis-Menten-type kinetics and reached substrate saturation at approximately 40 mM. An apparent K_m value can be estimated to be around 1.1 mM fructose. For DET reactions with FDH immobilised on carbon based electrodes such as multiwalled carbon nanotubes (MWCNTs) (Tominaga et al., 2009) and ketjen black (Kamitaka 2007), slightly higher apparent K_m values of 11.0 mM and 10.0 mM were determined. This indicates that the protein-protein reaction in the surface confined state is feasible; however, the ET efficiency is limited even at high fructose concentrations. Investigations with FDH at MU:MUA modified AuEs, performed under the same conditions, resulted in no catalytic current upon the addition of fructose (see **figure 32**). This suggests that DET is not feasible supporting the hypothesis that ET may proceeds via the redox mediator cyt *c*.

Investigating the stability of the system, the cyt *c*/FDH electrodes were re-measured at a SR of 100 mV/s after the catalytic reaction. It was found that the initial cyt *c* signal is recovered to 83% of the initial protein coverage in substrate free 5 mM KPi pH 7.0 (**figure 33**). This suggests that the cyt *c*-FDH interaction is rather weak, since FDH can be partially desorbed in the presence of high fructose concentrations. However, the amount of cyt *c* on the electrode surface is not decreased by FDH interaction, demonstrating that the cyt *c* monolayer remains

stable during the measurement and reinforcing the hypothesis that ET proceeds via cyt *c* in the cyt *c*/FDH electrode.

Despite the low catalytic activity achievd by the cyt *c*/FDH electrode, it can be concluded that a substrate induced ET between FDH and cyt *c* is feasible even with both proteins immobilised on an electrode surface. It is pointed out that the arrangement of two proteins on an electrode is possible while preserving their biological activity and enabling the interaction between the two components, resulting in the generation of a enzyme induced current mediated by a redox protein.

The combination of FDH with the cyt *c*/DNA ML system was not addressed, yet, since FDH was only available in a limited amount and the protein concentration of the provided sample was very low. However, a working group has been found which is able to provide FDH in a higher grade and purity. The task of assembling a fructose sensitive electrode on the basis of enzyme entrapment in the cyt *c*/DNA ML system will be addressed within the recently initiated cooperation project.

4.3   Formation of new signal chains by combining the cytochrome *c*/DNA multilayer system with PQQ-GDH

Since the reaction rate for the ET between FDH and cyt *c* was very low, reaching only 0.7 nA with both proteins immobilized on an electrode surface, a second enzyme - which was provided in a higher purity - was tested as reaction partner for cyt *c*. The interaction of the two proteins was investigated in solution and in the immobilised state. Here, the cyt *c*/DNA architecture was used as a matrix for the enzyme coupling, intending to allow an efficient communication of the enzyme with the electrode by protein-protein interaction (and without the addition of a soluble mediator). DNA was chosen as the anionic second building block, given that it is not electro active in the potential range of interest, in contrast to the polyelectrolyte, sulfonated polyanilline, which has also been used for such types of assemblies. Besides the very high stability of the cyt *c*/DNA ML system, it enables the adsorption of a vast amount of cyt *c* on the electrode surface. Therefore, this system provides promising conditions for the investigation of protein-protein ET between the enzymes and the redox protein.

4.3.1 Reaction of cytochrome *c* with PQQ-GDH in solution

In order to test the optimal conditions of the reaction between cyt *c* and the selected enzyme, exploratory investigations were performed with both bio-molecules in solution. For the evaluation of the reaction rate of cyt *c* and the enzymes, UV-vis spectroscopy was first applied. In the second step, cyt *c* was immobilised as a monolayer on a SAM modified AuE, the enzyme was kept in solution and the interaction was studied by CV.

4.3.1.1 Investigation of freely diffusing cytochrome *c* and PQQ-GDH

Since free PQQ is known to mediate the ET reaction between the two proteins, the reconstitution was performed with an equal molar ratio of PQQ and apoGDH, adapted from Olstroon et al. (Olsthoorn and Duine, 1996), avoiding a high concentration of free PQQ in solution. The procedure was performed at pH 5.0. Note that the reconstitution also works at pH 7.0, although the activity of the holo enzyme was approximately 50 % higher when reconstituted at pH 5.0.

For the evaluation of the reaction rate of cyt *c* and PQQ-GDH, UV-vis spectroscopy was applied, with both proteins in solution. After mixing cyt *c* and holoPQQ-GDH, glucose was added and the absorption change of the reduced cyt *c* was recorded at 550 nm. First, the pH-profile of the reaction was studied. **Figure 35** shows that the two proteins interact most efficiently at pH 4.0. If the pH value is changed towards pH 7.0 the reaction rate decreases stepwise. Going towards pH 3.0, results in a sudden decrease of activity, compared to pH 4.0. This may be due to the denaturation of cyt *c*, which was reported to start at pH 4.0 (Knapp and Pace, 1974). On the other hand, the enzyme may be inactivated below pH 4.0. However, data concerning the pH stability and the pH range of activity in more acidic media is not listed in literature for PQQ-GDH from *Acinetobacter calcoaceticus*.
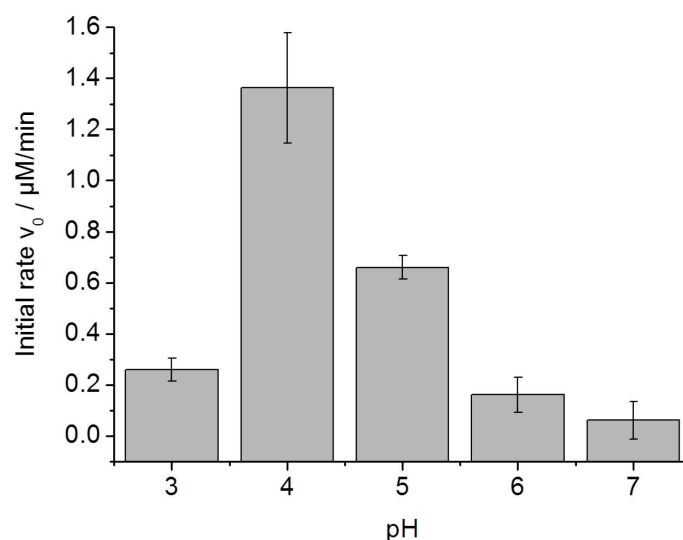
Figure 35: Initial rate (v_0) of cyt *c* reduction in the presence of PQQ-GDH and substrate in solutions of different pH values. The reaction rate was measured by following the cyt *c* reduction at 550 nm and calculated from the change in absorbance versus time, using the Lambert-Beer equation. Experimental conditions: 20 mM MES + 1 mM CaCl$_2$, [cyt *c*] = 20 µM, [PQQ-GDH] = 400 nM (44 U), [glucose] = 5 mM.

4.3.1.2 Investigation of cytochrome *c* monolayer electrodes and freely diffusing PQQ-GDH

Prior to the immobilisation of both components only one building block, the redox protein cyt *c* was adsorbed as a monolayer on a MU:MUA modified AuE. The ET reaction between the surface-bound cyt *c* and PQQ-GDH in solution was investigated. A small oxidative catalytic current occurs at the electrode after the addition of 1 mM glucose to the solution. This

indicates that free diffusing PQQ-GDH can also reduce cyt c, in the immobilised state. Given that PQQ-GDH can transfer electrons to modified electrodes directly, the reaction of PQQ-GDH and the electrode may occur via gaps in the cyt c monolayer. In order to reduce the probability for this process and ensure that the observed catalytic current is based upon the interaction of the two proteins, a cyt c/DNA bi-layer was assembled on the electrode (Au/MU:MUA/cyt c/DNA/cyt c). This more complex surface modification contains a higher amount of cyt c, which hinders the DET reaction of the larger PQQ-GDH with the modified gold surface. Consequently, the ET via cyt c becomes the dominant mechanism. Additionally, the enlarged surface may provide more interaction sites for the enzyme. The red graph in **figure 36b** represents a typical CV graph of a cyt c/DNA bi-layer electrode in buffer with enzyme in solution. In the presence of the substrate a clear catalytic current flows, starting from the oxidation peak of cyt c (blue line). Compared to the monolayer system (**figure 36a**) the catalytic current slightly increases. This observation indicates that a) cyt c mediates electrons from PQQ-GDH towards the electrode and b) that the cyt c bi-layer system provides a larger interface for the protein-protein interaction than the monolayer system.
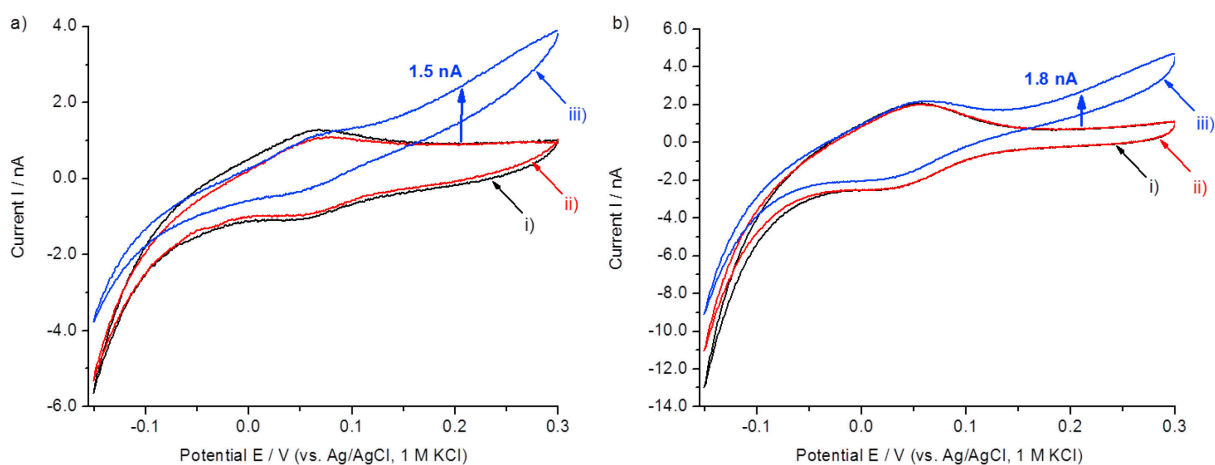
Figure 36: Cyclic voltammograms of different cyt c electrodes in the absence and presence PQQ-GDH. **a)** cyt c monolayer Au/MU:MUA/cyt c and **b**) cyt c bi-layer Au/MU:MUA/cyt c/DNA/cyt c. i) modified electrode in buffer; ii) electrode after the addition of [PQQ-GDH] = 400 nM (44 U); iii) catalytic current after the addition of glucose (c = 1 mM). Experimental conditions: 5 mM MES buffer + 1 mM CaCl$_2$, pH 5.0, SR = 10 mV/s, step potential = 0.3 mV.

4.3.1.3 Interaction of covalently bound cytochrome *c* and freely diffusing PQQ-GDH

Moreover, the interaction between PQQ-GDH and covalently immobilised cyt *c* was investigated. Covalent attachment of cyt *c* was achieved by cross-linking primary amine groups of cyt *c* with the carboxylic groups of MUA via EDC. This may result in binding of cyt *c*´s lysine residues near the heme region (Collinson et al., 1992). Thus, cyt *c* was fixed with its heme region-oriented towards the electrode. This orientation may hinder ET between the redox protein and an enzyme in solution. **Figure 37** shows that a small catalytic current occurs at an EDC fixed cyt *c* monolayer in the presence of PQQ-GDH and glucose in solution. It can be concluded that PQQ-GDH reduces the covalently immobilised redox protein although its heme site may not be directly accessible; however, the ET efficiency is significantly lower compared to the adsorbed state. As reported for peroxidase which also reduces covalently bound cyt *c* (Jiang et al., 1995), electron tunnelling via the enzyme or cyt *c* may also take place here. After the addition of 40 nM and 400 nM of PQQ, an increased catalytic current was observed which suggests that PQQ facilitates ET between the enzyme and fixed cyt *c* by mediating electrons towards the heme region. Thus, PQQ induces the increase of the oxidative catalytic current.

In the literature the ET reaction between a NADPH dependent cytochrome P450 reductase and covalently fixed cyt *c* was described. Here, the reaction was also hindered and the enzyme was disabled to reduce cyt *c*. Using adsorbed cyt *c*, the interaction was enabled (Jin et al., 1997). In the case of adsorbed cyt *c* and cyt *c* immobilised in the DNA ML system, the redox protein is flexible and may orient its heme edge towards the enzyme and the electrode. Therefore, mediator free ET between cyt *c* and PQQ-GDH is feasible with the adsorbed monolayer, as well as the ML assembly. Covalent coupling was not found to be beneficial for the assembly of a signal chain with PQQ-GDH. The combination of the enzyme with the cyt *c*/DNA ML system is addressed in the following chapter.
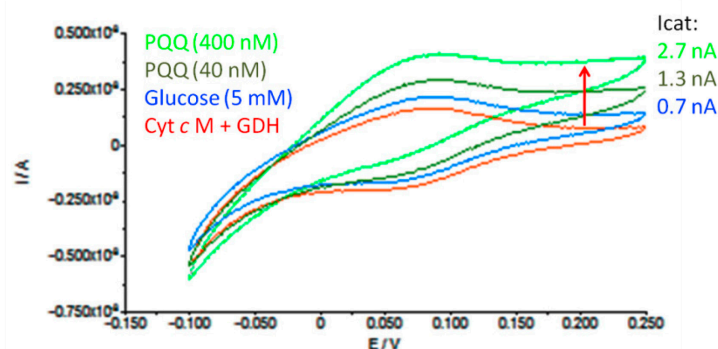
Figure 37: Cyclic voltammograms of an covalently fixed cyt *c* monolayer with PQQ-GDH in solution and in the presence of increasing PQQ concentrations. Red line: Au/MU:MUA/cyt *c* with [PQQ-GDH] = 400 nM (44 U) in solution (red line); Blue line: catalytic current electrode after the addition of glucose (*c* = 5 mM); dark green line: catalytic current after the addition of 40 nM PQQ; light green line: catalytic current after the addition of 400 nM of PQQ. Experimental conditions: 5 mM MES buffer + 1 mM CaCl$_2$, pH 5.0, SR = 10 mV/s, step potential = 0.3 mV.

4.3.2 Strategies for the coupling of the cytochrome *c*/DNA multilayer system with PQQ-GDH

In order to create a functional ET chain with PQQ-GDH based upon the cyt *c*/DNA ML system, several strategies for the coupling of the enzyme with the ML system were considered. Therefore, previous studies of enzyme coupling with ML systems have been analysed:

1) Dronov et al. described one possible assembly in mixed layers of cyt *c*/BOD with PASA as polyelectrolyte (Dronov et al., 2008b; Wegerich et al., 2011) (also see **chapter 2.4**). This method of incorporating enzymes in cyt *c* ML systems is very efficient, since a large amount of enzyme is immobilised on the electrode surface. The mixed assembly of the ML system was feasible since cyt *c* and BOD have opposing pI values enabling charge-charge interaction between the two proteins within the layers. Consequently an experiment of assembling mixed layers of cyt *c* and PQQ-GDH on a QCM chip was conducted. Therefore, a mixed solution of cyt *c* and PQQ-GDH (cyt *c*:PQQ-GDH) and a solution of DNA were alternately flushed over a MU:MUA modified QCM chip. The QCM measurement showed that a stable assembly of alternating cyt *c*:PQQ-GDH/DNA layers is not possible. Because cyt *c* and PQQ-GDH both have a basic pI, it is suggested that electrostatic repulsion may occur between cyt *c* and PQQ-GDH, destabilising the mixed layer system.

2) An alternating assembly of cyt *c* and PQQ-GDH may also be considered, although when inter-protein ET is expected to be the dominant mechanism, an alternating assembly of cyt *c* and an enzyme will not result in a functional system, given that the thick enzyme layer blocks the ET. This has already been shown for SOx (Spricigo et al., 2008).

3) XOD was combined with a cyt *c*/PASA ML by assembling a top layer on the ML system (Dronov et al., 2007). Due to the dimension of the PQQ-GDH and its basic pI, this strategy was considered to be suitable and promising for coupling PQQ-GDH with the cyt *c*/DNA ML system.

The assembled signal chains were investigated by means of CV, chronoamperometry and QCM to characterise their sensing properties. Hereby, the optimised reaction conditions between cyt *c* and the enzyme in solution were used as starting point.

4.3.3 Immobilisation of PQQ-GDH on top of the cytochrome *c*/DNA multilayer system

According to the previous considerations, electrodes with a defined number of cyt *c*/DNA layers and one terminating layer of PQQ-GDH were prepared. The schematic design of such (cyt *c*/DNA)$_n$-PQQ-GDH electrodes is shown in **figure 38**.
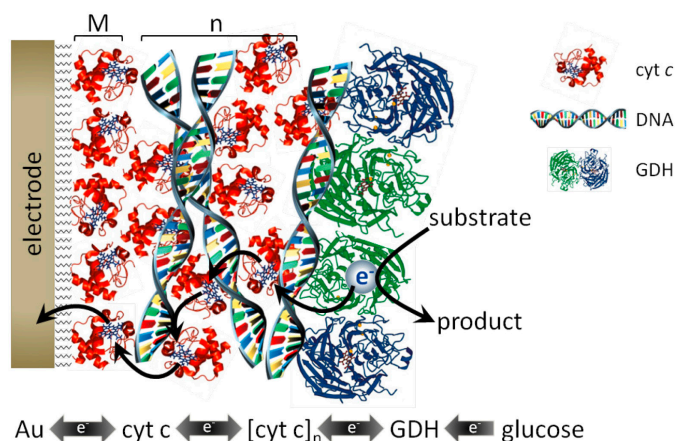
Figure 38: Schematic representation of the protein arrangement on the modified AuE: AuE/MU:MUA/(cyt *c*/DNA)$_n$/PQQ-GDH. Black arrows show electron pathway from PQQ-GDH via cyt *c* to electrode. M = Monolayer.

The cyt *c* ML assembly creates a rough film on the electrode, which provides a large, specific surface area for the interaction with the enzyme. The formation of this ML architecture was

investigated by QCM measurements. Therefore, the three components cyt *c*, DNA and PQQ-GDH were adsorbed on a QCM chip. The graphs in **figure 39** show a step-by-step accumulation of mass, after DNA or cyt *c* was passed through the flow cell.

For the last assembly step of the enzyme, the buffer was changed from KPi to MES + CaCl$_2$, since PQQ-GDH requires calcium ions for the stabilisation of its dimer structure and the binding of the cofactor. This caused a loss of mass on the chip surface. However, the same amount of DNA subsequently assembled and a huge accumulation of PQQ-GDH was recorded when PQQ-GDH was flushed over the surface. The (cyt *c*/DNA)$_4$/PQQ-GDH ML assembly remained stable during the following washing step. This demonstrates that PQQ-GDH can be immobilised efficiently on top of the cyt *c*/DNA ML system.
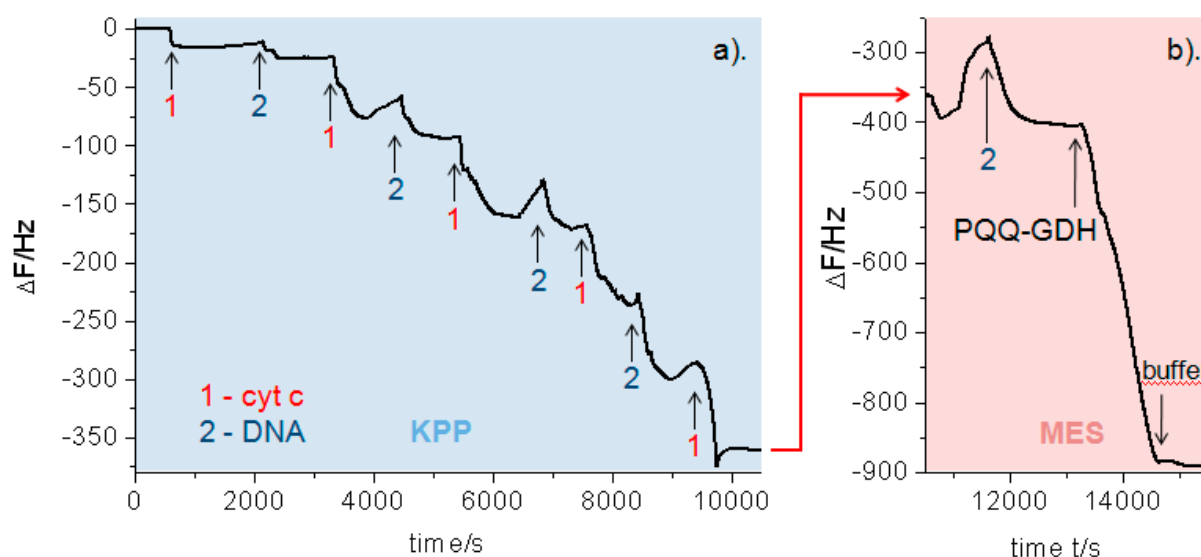
Figure 39: QCM measurement of the ML assembly formation. Frequency shift of 5 MHz crystal vs. reference crystal displays mass accumulation of each deposition step. Experimental conditions: [cyt *c*] = 20 µM, [DNA] = 2 mg/ml, [PQQ-GDH] = 2 µM. (**a**) 5 mM KPi buffer, pH 7 for monolayer assembly and 0.5 mM KPi buffer, pH 5 for ML assembly; (**b**) 0.5 mM MES buffer +1 mM CaCl$_2$, pH 5 for assembly of DNA/PQQ-GDH top layer.

4.3.3.1 Electrochemical characterisation of the (cytochrome *c*/DNA)$_n$/PQQ-GDH electrode

In order to investigate the electrochemical interaction of the PQQ-GDH top layer with the cyt *c*/DNA architecture, CV was applied first. The (cyt *c*/DNA)$_n$/PQQ-GDH bi-protein-electrodes generate a catalytic current in the presence of the substrate, *i.e.* glucose (**figure**

40). The PQQ-GDH top layer is easily accessible for glucose. Here, the ET cascade starts, whereby PQQ-GDH extracts electrons from the substrate at its active site and transfers them to a cyt *c* molecule in its neighbourhood. Cyt *c* subsequently transports electrons towards the electrode via other cyt *c* molecules while re-oxidising itself.

When electrodes with different numbers of cyt *c*/DNA layers below the PQQ-GDH top layer are compared, it is found that all systems show a catalytic current in the presence of the substrate, where the magnitude of the current increases depending on the number of cyt *c*/DNA layers. For the cyt c monolayer electrode, a very weak catalytic current is observed, which slightly increases at electrodes with one and two cyt *c*/DNA bi-layers (**figure 40; M, 1 and 2**). Clear catalytic currents are measured at electrodes modified with three and four layers of cyt *c* (see **figure 40; 3 and 4**) underneath the PQQ-GDH top-layer. Moreover, the cyt *c* surface concentration increased from 6 pmol/cm² of the monolayer up to 132 pmol/cm² of the electrode with five layers of cyt *c*. This high protein loading is the result of the effective binding between cyt *c* and DNA and illustrates the special feature of the cyt *c*/DNA ML compared to alternative ML systems. Here, the surface coverage reaches more than twenty times the monolayer coverage. Thus, the catalytic current of the cyt *c*/DNA ML with PQQ-GDH on top is influenced by the cyt *c* surface concentration. **Figure 40 S** shows a summary of the catalytic current measured with increasing numbers of cyt *c*/DNA layers. This suggests that the catalytic current increases with the number of layers assembled. Consequently, the ML system provides more interaction sites for the adsorption and reaction of PQQ-GDH, than a monolayer. Atomic force microscopy (AFM) measurements of cyt *c*/DNA ML systems on ultra flat gold indicate an increased roughness of the cyt *c*/DNA-ML system (**figure 41**), (roughness factor R_{rms} = 10.26 nm), compared to a cyt *c* monolayer. This correlated well with the high amount of electro active cyt *c* bound in the ML (as determined by CV) and suggests that a larger interface is provided for the enzyme to attach. Moreover the E_f of the PQQ-GDH modified cyt *c* ML electrodes was found to be 25 +/- 2 mV vs. Ag/AgCl. This is in agreement with the findings of Sarauli et al. who stated an E_f of 23 +/-2 mV vs. Ag/AgCl for up to six cyt *c*/DNA bi-layers (Sarauli et al., 2009) and indicates that the PQQ-GDH top layer does not severely affect cyt *c*'s microenvironment.
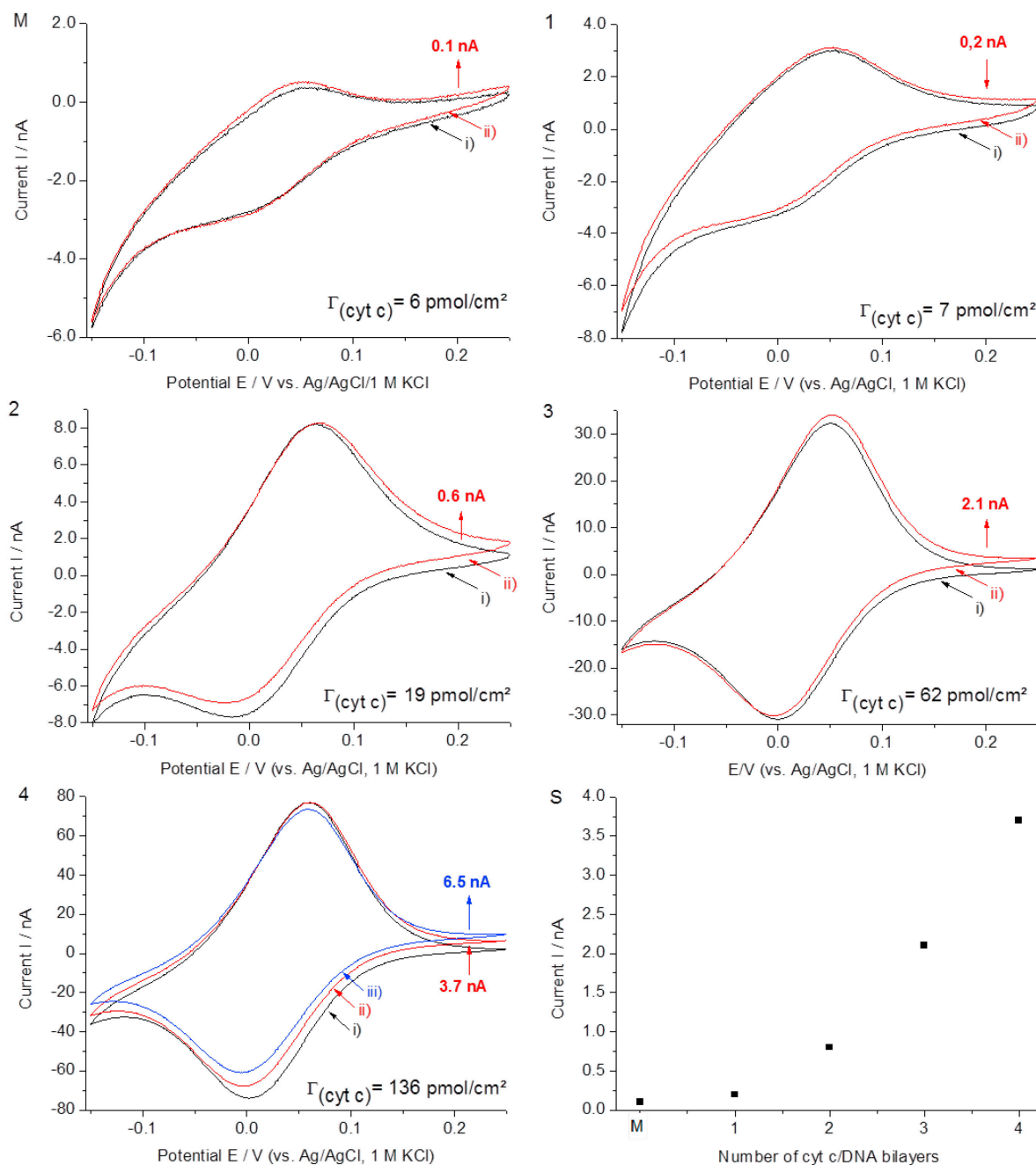
Figure 40: Cyclic voltammograms of different cyt *c*/DNA electrodes with an immobilised PQQ-GDH top layer, in the absence and presence of glucose. **M** represents a cyt *c* monolayer electrode (Au/MU:MUA/cyt *c*/DNA/PQQ-GDH) and **1-4** stands for ML electrodes (monolayer electrodes + n cyt *c*/DNA bi-layers) and PQQ-GDH on top. **S** summarises the catalytic currents measured in the presence of glucose, plotted against the number of cyt *c*/DNA bi-layers, assembled on the electrode. The response of the electrode to glucose was investigated at SR = 10 mV/s (step potential = 0.3 mV) in 5 mM MES + 1 mM $CaCl_2$, pH 5.0. i) Modified electrode in buffer, ii) catalytic current measured after the addition of glucose (*c* = 1 mM), iii) electrode in the presence of glucose and free PQQ (*c* = 1 µM). Cyt *c* surface concentration is determined at SR = 100 mV/s (step potential = 5 mV) in 5 mM MES + 1 mM $CaCl_2$, pH 7.0.

However, the magnitude of the catalytic current was moderate. Thus, it is concluded that although conditions for the communication of the enzyme and the redox protein were found, ET between both immobilised proteins was not efficient. Most likely, not all enzymes of the top layer are involved in the reduction of cyt c. Loew et al. reported on a PQQ-GDH ML electrode, which is dependent on the presence of diphenol and quinone as electron mediators (Loew et al., 2004). The addition of free PQQ to a (cyt c/DNA)$_4$/PQQ-GDH ML results in a further increase of catalytic current. This supports the idea that not all deposited PQQ-GDH molecules are able to exchange electrons with cyt c directly. Nevertheless, the comparatively high concentration necessary also indicates that the current generated in the absence of added PQQ is mainly a result of direct protein-protein interaction. It is rather unlikely that a high PQQ concentration resulted from denatured PQQ-GDH and remains stable in the ML system.
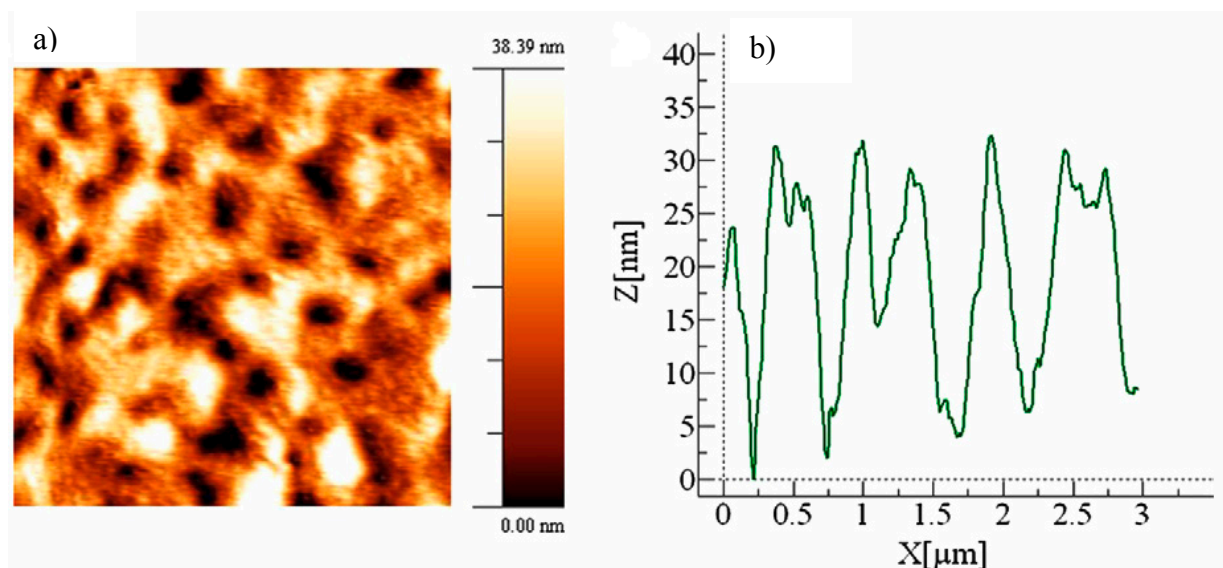
Figure 41: a) AFM-topography image (scan size 3x3 μm) of Au/MU:MUA/cyt c/(DNA–cyt c)$_4$ assembled on thiol-modified ultraflat gold surface (pH 5.0, [cyt c] = 20 μM, [DNA] = 0.2 mg/ml):. Roughness factors: R_{rms} = 10.26 nm; Rave = 8.34 nm (averaged for 10 lines); **b)** height profile of the Au/MU:MUA/cyt c/(DNA/cyt c)$_4$ ML structure.

4.3.3.2 Glucose-sensing properties of the (cytochrome c/ DNA)$_4$/PQQ-GDH electrode

For studies on the sensitivity towards glucose, chronoamperometry was applied. Electrodes with four layers of cyt c/DNA and a terminal PQQ-GDH layer were investigated, given that this was the most stable and efficiently working system. The modified electrode was placed

in a stirred measuring cell and glucose was added. It has to be mentioned that all PQQ-GDH modified electrodes provided a stable baseline, indicating that the assembly is strong enough to resist the shear forces which are applied by the buffer stirring. First, the pH dependency of the bi-protein ML system was tested. The highest current response was detected at pH 6.0. When the pH was changed towards the basic and acidic range, a clear decrease of catalytic activity occurred (**figure 42a**), suggesting the pH optimum of the immobilised bi-protein assembly to be at pH 6.0. This is different from the measurements performed in solution where we found a pH optimum for the cyt *c*/PQQ-GDH interaction of pH 4.0. This observation can be explained in different ways: in solution, PQQ-GDH can easily access many cyt *c* molecules in its close environment and reduce them directly; however, in the immobilised state, only the cyt *c* molecules of the periphery are reduced by the enzyme. The cyt *c*/cyt *c* pathway, leading the electrons towards the electrode, might have a pH optimum, which is different from the cyt *c*/PQQ-GDH reduction (around pH 7.0). The cyt *c*/PQQ-GDH ML system combines both types of ET, namely cyt *c*/cyt *c* and cyt *c*/PQQ-GDH-interaction. Therefore, the pH optimum of the ML system may be shifted towards pH 6.0.

Furthermore, the actual pH value inside the ML system may be more acidic compared to the pH of the solution, since the negatively charged DNA may attract protons. Such effects on the pH value in ML systems consisting of polyelectrolytes were reported in the literature (Redepenning et al., 1986; Ugo et al., 1993). Next, the glucose sensitivity of the (cyt *c*/DNA)$_4$/PQQ-GDH system was studied. It was found that a catalytic current already flows in the presence of concentrations as low as 25 nM glucose (**figure 42b**). At lower concentrations, no signal was recorded. When the glucose concentration was increased step-by-step, a correlating rise of the catalytic current was detected. At concentrations higher than 0.5 µM no major increase of the current is achieved.
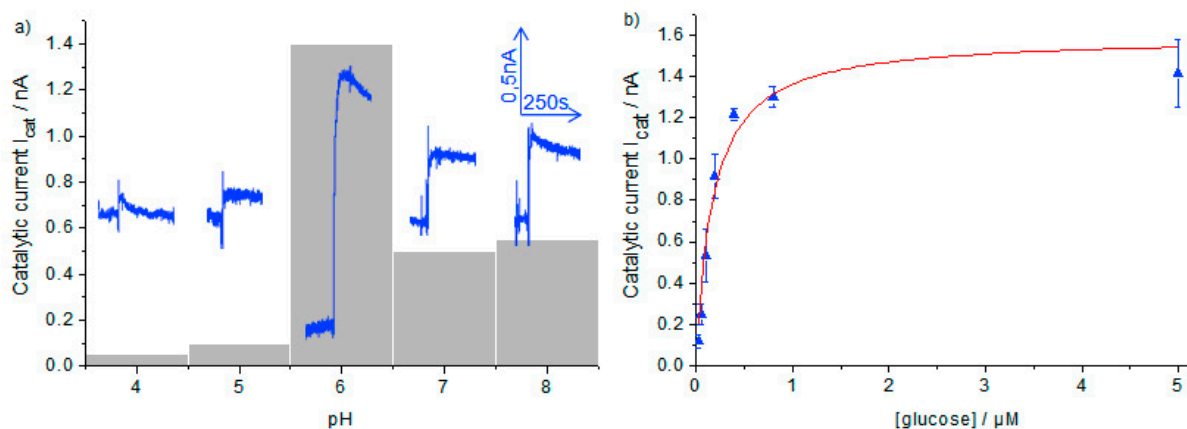
Figure 42: Response of a cyt *c* ML electrode with PQQ-GDH immobilised on top (Au/MU:MUA/(cyt *c*/DNA)$_4$/PQQ-GDH) to glucose. Amperometric measurement at a fixed potential (E = +0,2V vs. Ag/AgCl/1 M KCl). **a)** Response of the electrode to glucose (*c* = 1 mM) at different pH values. **b)** Response to different glucose concentrations at pH 6. Values (blue triangle) are fitted by y = I$_{max}$·[S]/(K$_m$+[S]) (red line) with I$_{max}$ = 1.62 ± 0.09 nA and K$_m$ = 176 ± 36 nM. Experimental conditions: 5 mM MES buffer + 1 mM CaCl$_2$.

The system was observed to follow the characteristic Michaelis–Menten kinetics. The apparent K$_m$ value for glucose was calculated to be 176 ± 36 nM. Compared to the value of the enzyme in solution (Matsushita et al., 1988) and immobilised on several electrodes (Flexer et al., 2011; Ivnitski et al., 2007; Jin et al., 1995; Tanne et al., 2010), this is rather low. The limited dynamic range occurs, given that protein-protein ET becomes the rate limiting process. This means that electron withdraw is not efficient in the system with PQQ-GDH immobilised on top of the cyt *c* ML system. However, the aim of this study is to show that a signal chain from an immobilised enzyme in a protein-architecture is feasible, which is shown by the experiments performed.

SUMMARY AND OUTLOOK

The arrangement of cyt *c* layers on electrode surfaces provides the basis for the creation of analytical signal chains. In this work, double-stranded DNA was used to assemble electro active cyt *c*/DNA multilayer (ML) architectures which have the following outstanding properties:

a) very high amount of redox active material, compared to other systems;

b) tunability of the protein amount by the number of layers assembled; and

c) simple and robust handling.

These features, together with the biocompatibility, create an advanced, fully electro active interface for enzyme binding.

The first part of this thesis particularly aimed at gaining insight into the interaction between the two building blocks on the molecular level to ascertain the nature of the forces in cyt *c*/DNA complexes, stabilizing the ML assembly. Although the electrostatic character of the cyt *c*/DNA interaction was already studied, little was known about the effect of the ionic strength and pH value. A model system was chosen in which the complex formation of cyt *c* and DNA was investigated by applying ds 41 bp oligonucleotides instead of calf thymus (ct) DNA which has been used for the ML construction.

For the assembly process of MLs on electrodes, the most efficient deposition was achieved at pH 5.0 and low ionic strength. Under the same conditions, persistent cyt *c*/DNA complexes were formed in solution. UV-vis spectroscopy and dynamic light scattering (DLS) measurements revealed that the complex formation proceeded within seconds and resulted in 3D-structures with an average diameter of 1250 ± 200 nm. The agglomeration was found to be non-reversible by increasing the pH value, agreeing with the stability of the cyt *c*/DNA ML system in solutions of neutral pH. Increasing the salt concentration to 50 mM NaCl resulted in the partial disruption of the complexes. Going to 100 mM NaCl further attenuated the interaction; however, even under such a high ionic strength, a minor remaining contact was monitored by DLS and nuclear magnetic resonance (NMR) measurements.

At pH 7.0, no agglomerates were formed, as indicated by UV-vis and DLS, permitting the characterization of the interaction by NMR spectroscopy. Using transverse relaxation-

optimised spectroscopy (TROSY)-heteronuclear single quantum coherence (HSQC) experiments, DNAs' binding sites on the protein were identified by revealing a total of 22 amino acids (AAs) with chemical shift perturbations (csps) in the cyt c spectrum. Here, positively charged lysine residues (K7, K8, K72, K73, K86, K87 and K100), were mainly affected, since they interact with the negative backbone charge of the DNA molecule. Moreover, neutral AAs in the close environment of the affected lysine residues also showed csps. Regarding the primary structure of the protein, the spotted interaction sites were mainly located at the N- and C-terminus of the protein. The csps were clearly dependent on the DNA concentration indicating the significance of the observed effect, as well as the transient character of the interaction. Hereby, a saturation of the chemical shifts was observed at a DNA/cyt c concentration ratio of 0.36. The spectral changes were consistent with a fast exchange process on the NMR time scale and suggest that cyt c and the oligonucleotide form a transient complex with a lifetime in the millisecond range.

Mapping the affected AA residues onto the crystal structure of cyt c, revealed that the interaction sites were mainly part of α-helical structures. Moreover, the α-helices were only partly found to be in interaction with the DNA molecule. In general, numerous interaction sites were found in this study, such as Lys 8, 72, 87 and Q16 were also elucidated in the interaction of cyt c with its natural binding partners, *i.e.* the enzymes cyt c oxidase and cyt c peroxidase.

At a slightly acidic pH (6.0) an increased number of 26 interaction sites was observed, demonstrating the impact of the pH on the character of the binding. The NMR spectrum recorded at pH 6.0 showed a similar pattern of csps as the one recorded pH 7.0; however, additional csps were already observed at lower DNA concentration including the basic AA residues K5, K73 and K88 as well as the neutral Y74 and A101, which neighbour basic ones. This increased number of resonances with csps at pH 6.0 suggested that at pH 5.0 even more interaction sites may be contacted, making up the strong interaction between cyt c and DNA, which enables the formation of cyt c/DNA complexes in solution and stabilises 3D cyt c/DNA architectures on electrode surfaces.

Although the interaction at neutral pH appeared to be much weaker, size exclusion chromatography (SEC) experiments verified that its strength is sufficient to change the elution of cyt c from the column when mixed with DNA in high concentrations. For the

deposition of cyt *c*/DNA architectures, this binding strength is not sufficient. Thus, acidic pH values are necessary for the LBL deposition of cyt *c*/DNA ML systems.

In the second part of this study, the sophisticated task of arranging proteins on electrode surfaces to create functional ET chains was addressed. Therefore, two enzyme types, fructose dehydrogenase (FDH) and PQQ dependent glucose dehydrogenase (PQQ-GDH), which differ in their cofactor (FAD vs. PQQ), size (140 kDa vs. 100 kDa), cellular location (membrane bound vs. soluble) and pI (acidic vs. basic), were tested as reaction partners of freely diffusing cyt *c* and cyt *c* immobilised on electrodes in mono- and MLs. The characterisation of the ET processes was performed by means of electrochemistry and the protein deposition was monitored by micro-gravimetric measurements.

Investigating the interaction between FDH and cyt *c*, the pH profile of the reaction with both proteins in solution indicated that FDH reduces cyt *c* most effectively at pH 4.0 and 7.0, while the reduction reaction also proceeded at intermediate pH values; however, less efficiently. These two pH optima suggest that two different ET pathways may exist.

Immobilizing cyt *c* in a monolayer while keeping FDH in solution resulted in the detection of a substrate induced catalytic response at pH 5.0 and pH 7.0. In acidic media the maximum catalytic current achieved rather small values and reached its maximum at very low substrate concentrations in the μM range. An apparent K_m of the reaction with immobilised cyt *c* was not determined, since electron withdrawing at the FDH active site becomes limiting at low substrate concentrations. In media of neutral pH a more pronounced catalytic response was recorded, following a clear substrate dependency. Here, an apparent K_m value of 250 μM was determined. Compared to the K_m of FDH in solution which was assayed with ferricyanide as electron acceptor (Ameyama et al., 1981), the obtained value is still rather low. This indicates that the ET from the active site of the enzyme to the reaction partner is the rate limiting process.

The distinct efficiency in bioelectrocatalysis of FDH with immobilised cyt *c* at pH 7.0 and pH 5.0, along with the two different pH optima determined by UV-vis spectroscopy with both proteins in solution, may be interpreted as differing ET pathways, as it was previously suggested by Ferapontova et al. (Ferapontova and Gorton, 2005). These may either proceed from the FAD active site via the heme groups to cyt *c* or directly from the active site to cyt *c*, skipping the heme centres. However, further investigation, e.g. working with the FAD

subunit only, will be necessary to entirely clarify the precise pathway of the suggested ET reactions.

With respect to the results obtained from TX-free solutions, a significant decrease in the catalytic activity was found in the presence of the detergent, indicating that the ET reaction between FDH and cyt c may be hindered by TX. Although it was reported that FDH is inactivated in the absence of TX (Ameyama et al., 1981), the enzyme appears to remain active in TX-free buffer, at least in the time range of the measurements. This finding may be an important point in the definition of favourable conditions for the investigation of protein-protein interaction and multilayer assembly.

Moreover, it was shown that ferricyanide acts as electron mediator between FDH and cyt c following the same pH dependency as the ET reaction via the redox protein. A direct reaction of ferri-/ferrocanide with the MU:MUA modified electrode occurred; however, only to a very small extent. DET reaction from FDH in solution on the MU:MUA modified electrode was not found under the present conditions.

Immobilising both components by adsorbing FDH on a cyt c monolayer electrode revealed that ET between the two proteins is feasible, even in the surface fixed state. Here, an apparent K_m value of 1.1 mM was found upon addition of fructose. For DET reactions with FDH immobilised on carbon based electrodes, such as multiwalled carbon nanotubes (MWCNTs) (Tominaga et al., 2009) and ketjen black (Kamitaka 2007), slightly higher apparent K_m values of 11.0 mM and 10.0 mM were determined. This indicates that the protein-protein reaction in the surface confined state is feasible; however, the ET efficiency is limited even at high fructose concentrations.

Co-immobilization of FDH and cyt c in a ML system was not realised, yet. For this purpose a highly active and pure enzyme preparation will be needed to guarantee an efficient ET between the reaction partners and to avoid the co-assembly contaminants. The commercially available FDH obtained from Sigma-Aldrich was of low protein content (*i.e.* 5.1 % (w/w) and additionally mixed with stabilizing agents and other proteins, making an efficient ML assembly initially problematic. The non-commercially available FDH provided by our cooperation partner from the Kyoto University at the end of the project is of high purity (> 90% protein content) and activity (150 U/mg (protein)). Therefore, it may fulfil the requirements for a ML assembly. Concerning the immobilization strategy of the two proteins, the assembly of mixed cyt c:FDH ML systems with DNA as negatively charged

polyelectrolyte may be feasible, since their opposing pIs should enable direct charge-charge interaction. This view is supported by the successful deposition of FDH on the cyt *c* monolayer. Thus, assembling a polyelectrolyte-free cyt *c*:FDH ML system, as it was shown with sulfite oxidase and cyt *c*, should be tested. These approaches will be addressed in our future project.

As second enzyme PQQ-GDH was chosen. ET between cyt *c* and PQQ-GDH was found to be most efficient at pH 4.0, when both molecules were in solution. When the pH value was changed towards 7.0, the reaction rate declined stepwise. Decreasing the pH value to 3.0 resulted in a sudden loss of activity which can be affiliated to the denaturation of the enzyme.

The next step in the development addressed the ET reaction between the surface-bound redox protein and the freely diffusing enzyme. Catalytic currents occurred upon oxidation of glucose, suggesting inter-protein ET even when one partner is adsorbed at an electrode surface. Providing an enlarged interface for protein-protein interaction, increased catalytic responses were observed at electrodes modified with a cyt *c*/DNA bi-layer.

For the PQQ-GDH immobilisation several assembly strategies were tested, e.g. a ML assembly of mixed cyt *c*/PQQ-GDH layers versus DNA. However, only the architecture of cyt *c*/DNA MLs with a terminating PQQ-GDH layer was found to be stable. This was verified by micro-gravimetric measurements, which showed that a substantial amount of the enzyme binds to the cyt *c*/DNA assembly. Finally, the substrate induced ET between the PQQ-GDH and cyt *c* of the underlying layers was achieved, as concluded from CV measurements. An increase in the numbers of cyt *c*/DNA layers underneath the PQQ-GDH top-layer, resulted in a subsequent elevation of the catalytic current. This effect can be explained by the increase in surface roughness of the 3D cyt *c*/DNA ML architecture, which provides a layer-dependent enlargement of the interface area for enzyme coupling.

Moreover, the sensor properties of the (cyt *c*/DNA)$_n$/PQQ-GDH ML electrode were analyzed. The ET reaction between the immobilised PQQ-GDH and cyt *c* proceeded most efficiently in solutions of pH 6.0. This observation differs from the pH optimum found in solution (4.0), and can be explained in different ways: either the cyt *c*/cyt *c* pathway, leading electrons towards the electrode might have a pH optimum which is different from the cyt *c*/PQQ-GDH reduction or the actual pH value inside the ML system may be more acidic compared to the pH of the solution. This pH shift may be caused by the negatively charged DNA backbone, which may attract protons from the solution. Besides this, the system was

observed to follow the characteristic Michaelis–Menten kinetics. The apparent K_m value was calculated to be 176 ± 36 nM, which is rather low in comparison to the values of PQQ-GDH in solution ($K_m = 24.5$ mM), indicating that ET from the active site of the enzyme on the reaction partner is the rate limiting process. The glucose sensitivity of the ML electrode was found to work reliably in a substrate concentration range between 25 nM and 0.5 μM.

Finally, the moderate catalytic current can be explained by the assembly strategy with PQQ-GDH on top of the cyt *c*/DNA ML system, resulting in a limited interaction area. The alternative approach of integrating the enzyme into the ML system, as it was shown for BOD and CDH provided a higher amount of enzyme on the electrode surface. However, this immobilization strategy was not feasible here. Despite this, the (cyt *c*/DNA)$_n$-PQQ-GDH electrode demonstrates that the creation of a signal chain, based upon the idea of co-immobilised proteins, is feasible.

In this study the characteristics of the cyt *c* and DNA interaction were defined on the molecular level for the first time. The binding sites of DNA on cyt *c* were identified and the interaction was found to be strongly dependent on the pH value as well as the ionic strength. Besides this, the feasibility of the inter-protein ET between the redox protein cyt *c* and two different types of enzymes was shown in solution and in the immobilised state, whereby the required conditions to enable the ET reaction were elucidated. Although combining FDH with the cyt *c*/DNA ML system did not succeed, yet, the basic conditions for this protein-protein interaction were defined. These results can be used as starting point for a ML assembly. Moreover, a functional and stable glucose sensitive ET chain was created by coupling PQQ-GDH to the cyt *c*/DNA ML system, indicating that its surface is suitable as interface for enzyme binding.

Future work may be directed to the investigation of cyt *c*/DNA interaction under the precise conditions of ML assembly. Therefore, solid state NMR or X-ray crystallography may be required. Based on the results of this study, the combination of FDH with the ML system will be addressed. Moreover, alternative types of enzymes may be tested as catalytic component of the ML assembly, aiming on the development of innovative biosensor applications.

APPENDIX

^{1}H-^{15}N TROSY-HSQC spectra recorded from ^{15}N-labled cyt *c* in the presence of DNA at different pH values and salt concentrations
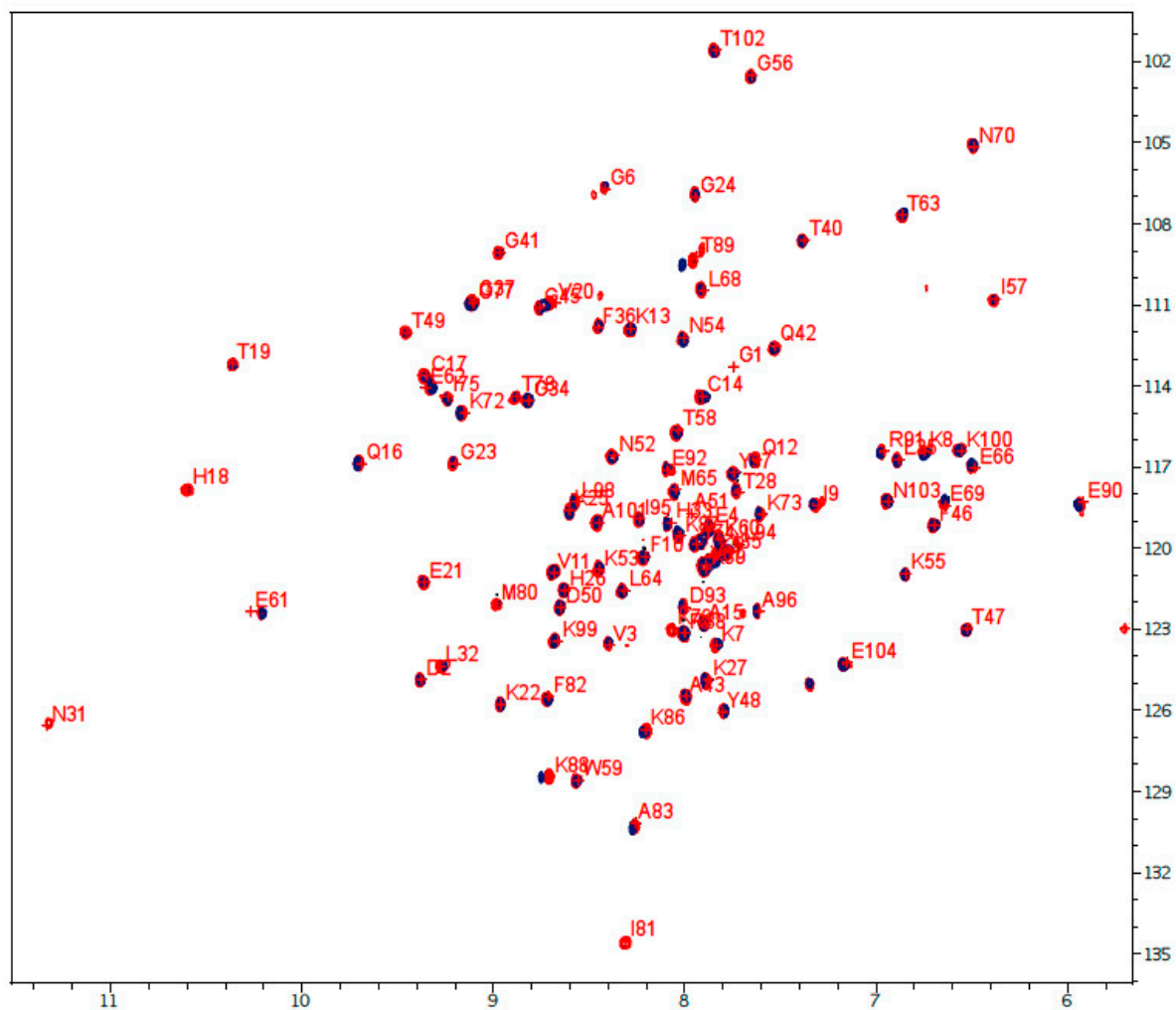
Figure A1: Spectrum from overlaid ^{1}H-^{15}N TROSY-HSQC spectra recorded at pH 5.0 and a high salt concentration of 100 mM NaCl. Samples containing 50 μM pure cyt *c* (red) and cyt *c* after addition of 6 μM DNA (blue) in 20 mM KPi + 100 mM NaCl.
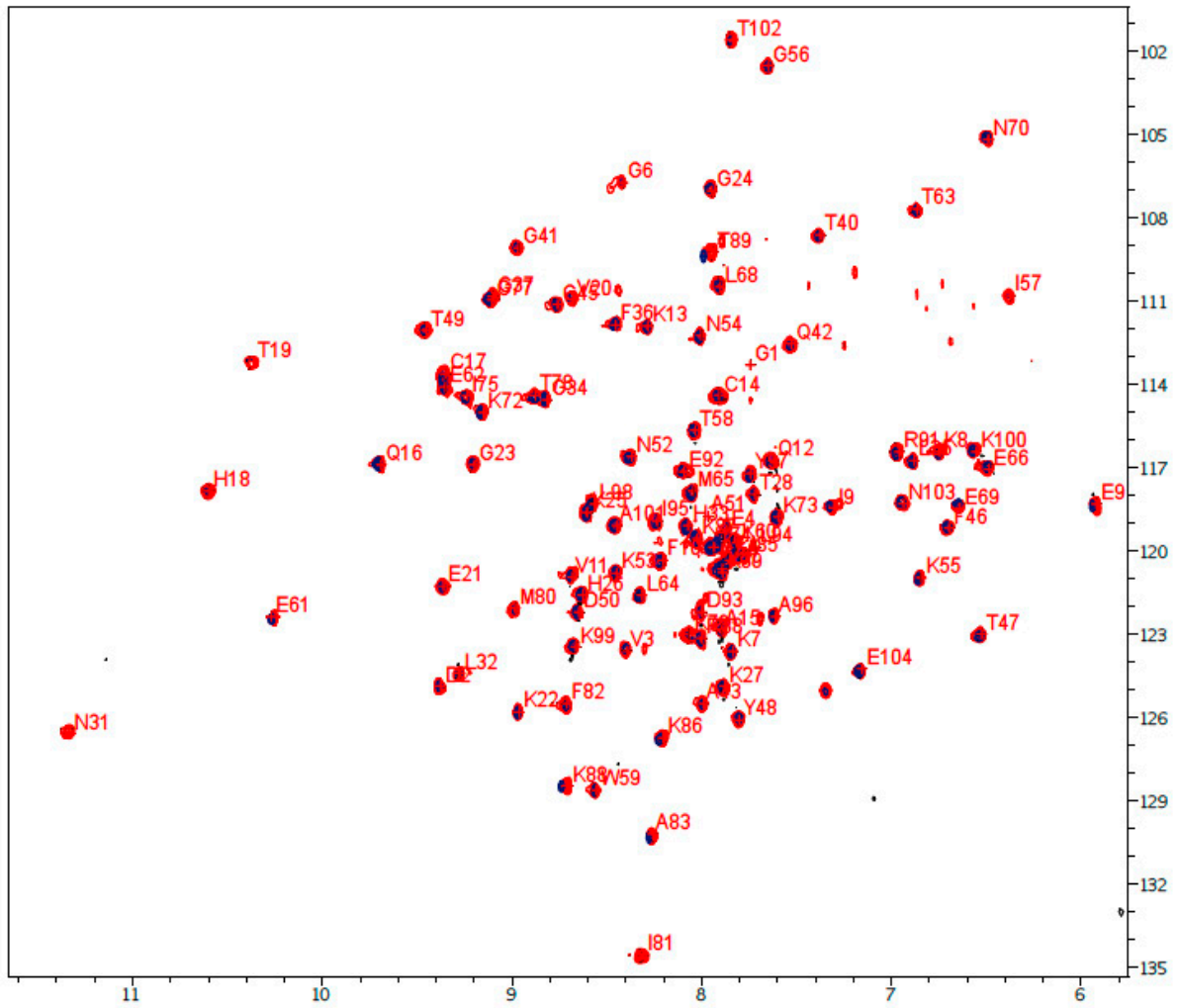
Figure A2: Spectrum from overlaid ¹H-¹⁵N TROSY-HSQC spectra recorded at pH 5.0 and a medium salt concentration of 50 mM NaCl. Samples containing 50 µM pure cyt *c* (red) and cyt *c* after addition of 6 µM DNA (blue) in 20 mM KPi + 50 mM NaCl.
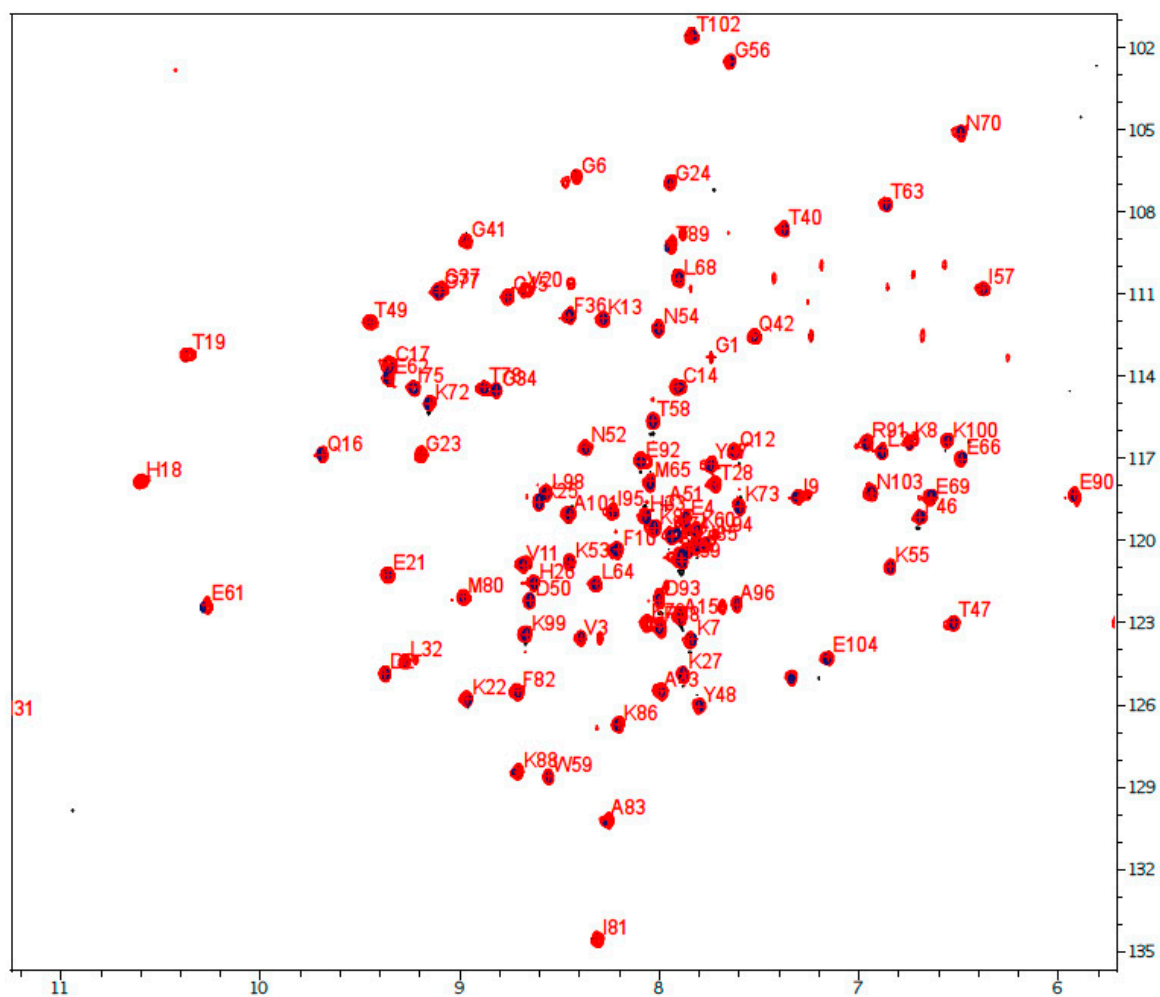
Figure A3: Spectrum from overlaid ${}^{1}H$-${}^{15}N$ TROSY-HSQC spectra recorded at pH 5.0 and the standard salt concentration for the NMR measurements used here (30 mM NaCl). Samples containing 50 μM pure cyt *c* (red) and cyt *c* after addition of 6 μM DNA (blue) in 20 mM KPi + 30 mM NaCl.
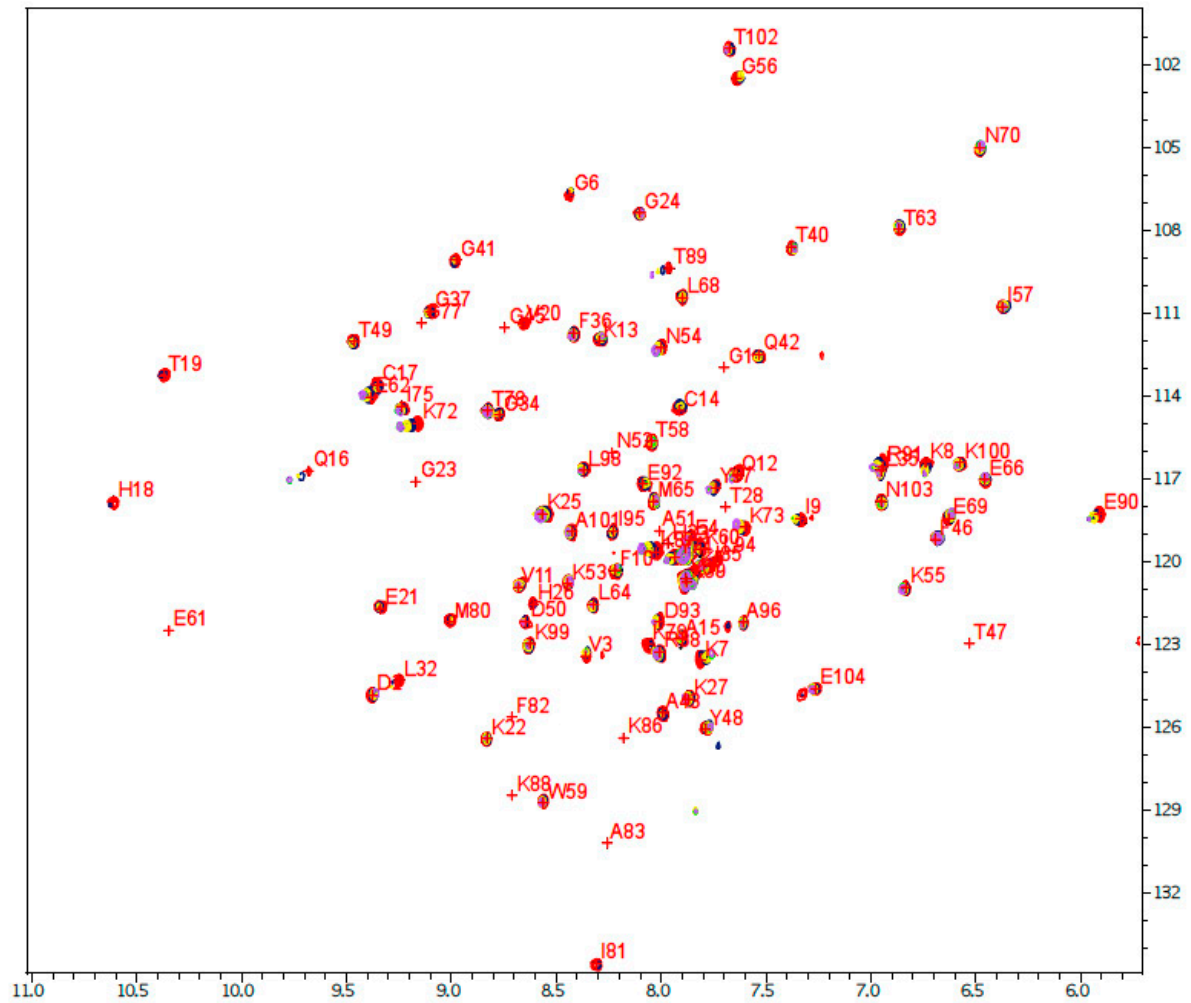
Figure A4: Spectrum from overlaid ¹H-¹⁵N TROSY-HSQC spectra recorded at pH 7.0 Samples containing 50 μM pure cyt *c* (red) and cyt *c* after titration with DNA: 3.0 μM (blue), 6 μM (yellow), 18 μM (purple) and 24 μM (green) in 20 mM KPi + 30 mM NaCl.
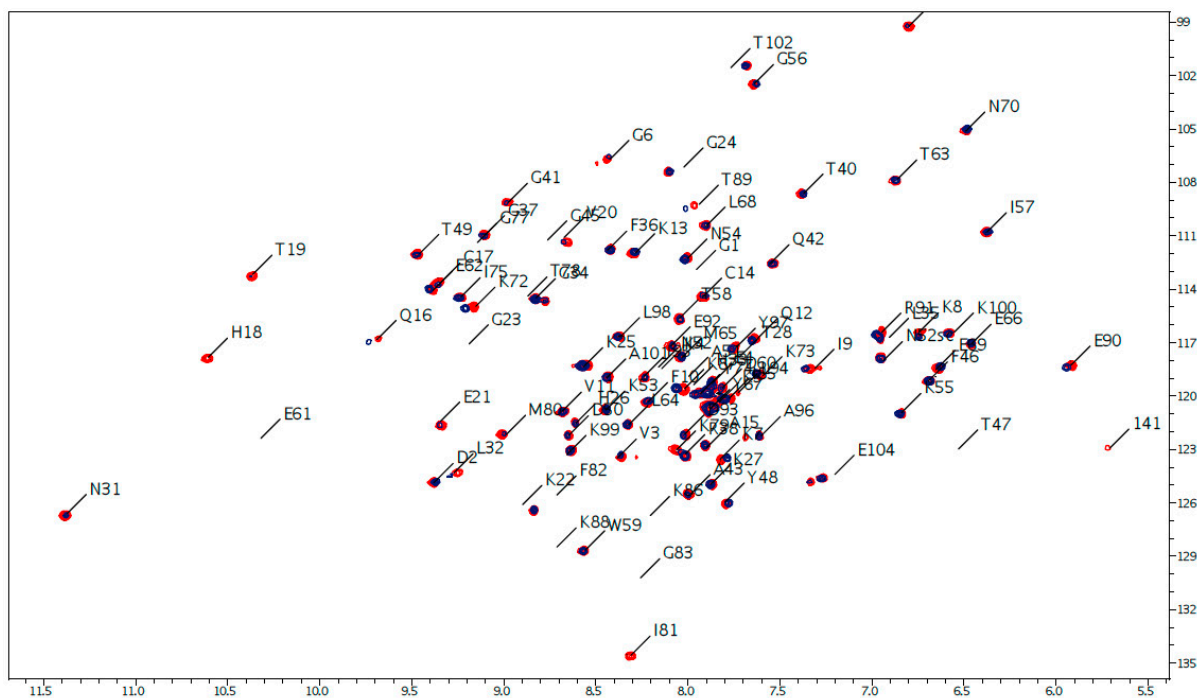
Figure A5: Spectrum from overlaid ^{1}H-^{15}N TROSY-HSQC spectra recorded at pH 7.0 Samples containing 50 µM pure cyt *c* (red) and cyt *c* after addition of 6 µM DNA (blue) in 20 mM KPi + 30 mM NaCl.
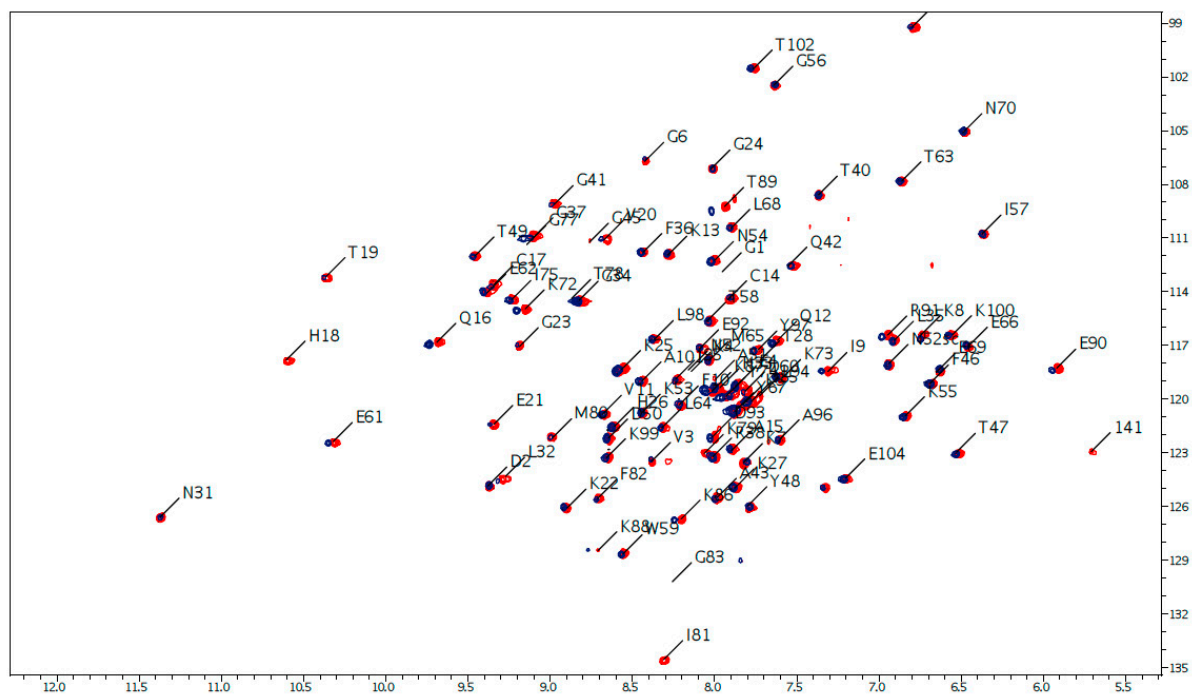
Figure A6: Spectrum from overlaid ^{1}H-^{15}N TROSY-HSQC spectra recorded at pH 6.0 Samples containing 50 µM pure cyt *c* (red) and cyt *c* after addition of 6 µM DNA (blue) in 20 mM KPi + 30 mM NaCl.

Investigation of cytochrome *c*/DNA ML formation using 41 bp oligonucleotides instead of ctDNA.

The cyt *c*/DNA ML assembly was performed on MU:MUA modified AuEs according to the protocol of Sarauli et al. with 0.5 mM KPi at pH 5.0 (Sarauli et al., 2009). Instead of ctDNA, ds 41 bp oligonucleotides, which were also used in the interaction study (see **4.1**), were used as negatively charged building blocks in concentrations of 0.2 mg/ml and 0.9 mg/ml. The so modified electrodes were analyzed by CV (SR = 100 mV/s, SP = 0.3 mV).

Using, 0.2 mg/ml of oligonucleotides, the same concentration as in the ML assembly with ctDNA was applied. The assembly of 6 cyt *c*/41 bp bi-layers did not result in an increased protein concentration on the electrode surface. compared to the cyt *c* monolayer (**figure A7**).
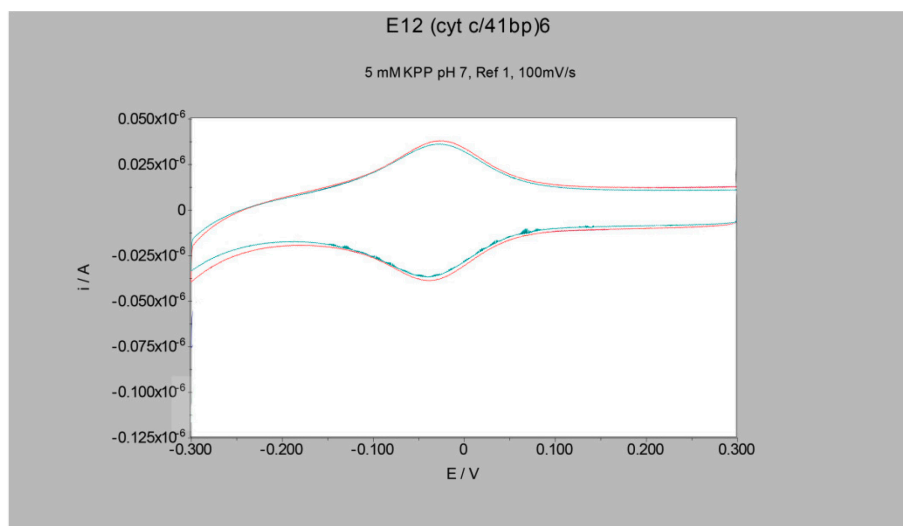
Figure A7: Cyclic voltammograms of a cyt *c* monolayer electrode (Au/MU:MUA/cyt *c*) (green line) and a cyt *c*/41 bp electrode consisting of 6 cyt *c*/DNA bi-layers (Au/MU:MUA/cyt *c*/[41 bp/cyt *c*]$_6$) (red line). Experimental conditions: [DNA] = 0.2 mg/ml, 5 mM KPi, pH 7.0, SR = 100 mV/s, step potential = 0.3 mV.

When the oligonucleotide concentration was increased to 0.9 mg/ml, and two bi-layers were assembled, the surface coverage increased, however, it remained in the range of a monolayer electrode (**figure 8, left**). This indicates that a ML assembly is not possible, even at a higher DNA concentration. Interestingly, at two bi-layer electrode, the redoxpeaks were found to increase with the number of scans, indicating a re-arrangement process on the electrode surface which improves ET of the immobilised cyt *c* within the system (**figure 8, right**).

Compared to the monolayer electrode, it was observed that the amount of redox active material on electrode surface was increased after the assembly of cyt c/41bp layers.
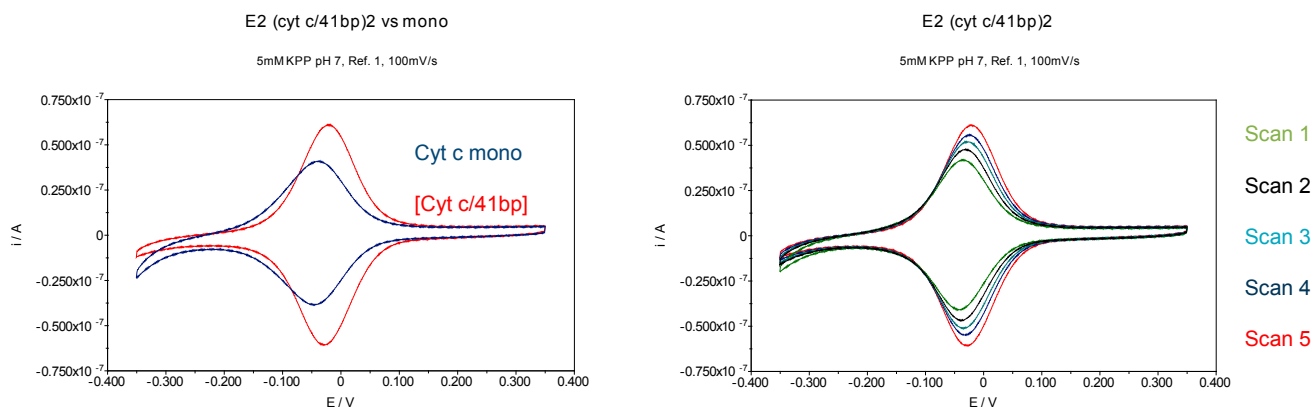
Figure A8, left: Cyclic voltammograms of a cyt c monolayer electrode (Au/MU:MUA/cyt c) (blue line) and a cyt c/41 bp electrode consisting of 2 cyt c/DNA bi-layers (Au/MU:MUA/cyt c/[41 bp/cyt c]$_2$) (red line). **Right:** Cyclic voltammograms of a cyt c/41 bp electrode consisting of 2 cyt c/DNA bi-layers (Au/MU:MUA/cyt c/[41 bp/cyt c]$_2$). The intensity of the redox peaks increased in dependency on the number of scans recorded: scan 1 = light green line, scan 2 = black line, scan 3 = cyan line, scan 4 = dark blue line, scan 5 = red line. Experimental conditions: [DNA] = 0.9 mg/ml, 5 mM KPi, pH 7.0, SR = 100 mV/s, step potential = 0.3 mV.

Comparison of commercially and non-commercially produced FDH

For the comparison of the interaction of commercially and non-commercially available FDH with immobilised cyt *c*, cyt *c* was adsorbed on a MU:MUA modified AuE as a monolayer (**see 4.2.3.1**). The cyt *c*/FDH interaction was studied at pH 7.0, since the pH profile of the reaction suggests an efficient enzymatic reduction of the redox protein at neutral pH. **Figure A9** shows the cyclic voltammogram of adsorbed cyt *c* after addition of FDH (red line), either non-commercial **a**) or commercial **b**). Upon the addition of increasing fructose concentrations (green lines), a clear, substrate dependent catalytic current occurs, starting at about -80 mV and reaching a maximum of 1.25 nA to 1.23 nA at substrate saturation.

Since the catalytic currents obtained at 200 mV (vs. Ag/AgCl 1M KCl) with non-commercial and commercial enzyme were similar and no significant differences in the maximum values were observed, This indicates that FDH from both stocks reduce the immobilised cyt *c* efficiently although it is trapped in a surface confined state.

Non-commercial FDH   Commercial FDH
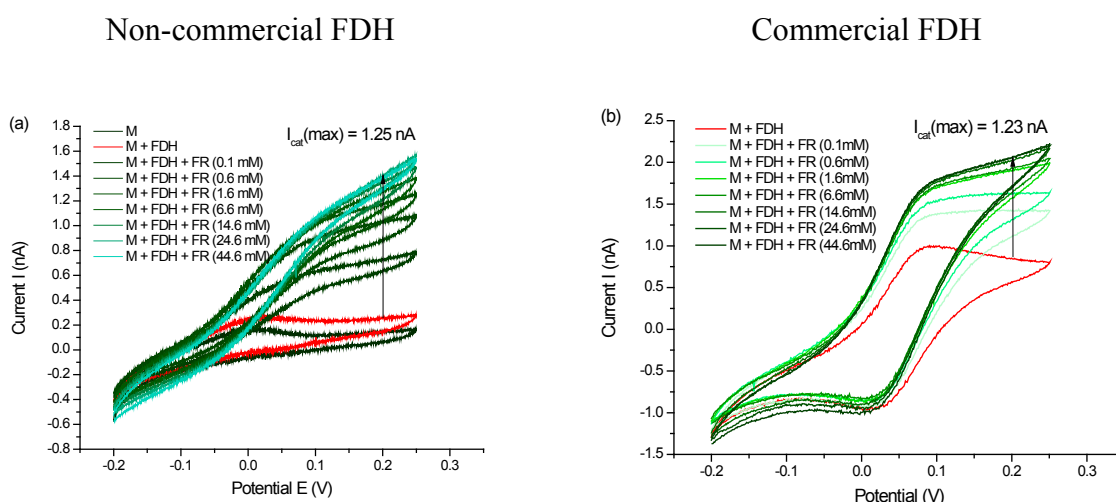
Figure A9: Cyclic voltammograms of cyt *c* monolayers (M) on a MU:MUA modified AuE surface with 4 U of (a) non-commercial FDH and (b) commercial FDH in solution. M (black lines), M with FDH in solution (red lines) and upon addition of 0.1 mM – 44.6 mM fructose (FR) (green lines). Experimental conditions: 5 mM KPi, pH 7.0, SR = 2 mV/s, step potential = 0.3 mV.

BIBLIOGRAPHY

Ameyama, M., E. Shinagawa, K. Matsushita, and O. Adachi, 1981, D-Fructose Dehydrogenase of Gluconobacter-Industrius - Purification, Characterization, and Application to Enzymatic Micro-Determination of D-Fructose: Journal of Bacteriology, v. 145, p. 814-823.

Andersen, F. F., B. Knudsen, C. L. P. Oliveira, R. F. Frohlich, D. Kruger, J. Bungert, M. Agbandje-McKenna, R. McKenna, S. Juul, C. Veigaard, J. Koch, J. L. Rubinstein, B. Guldbrandtsen, M. S. Hede, G. Karlsson, A. H. Andersen, J. S. Pedersen, and B. R. Knudsen, 2008, Assembly and structural analysis of a covalently closed nano-scale DNA cage: Nucleic Acids Research, v. 36, p. 1113-1119.

Anthony, C., 2001, Pyrroloquinoline quinone (PQQ) and quinoprotein enzymes: Antioxidants & Redox Signaling, v. 3, p. 757-774.

Ariga, K., T. Nakanishi, and T. Michinobu, 2006, Immobilization of biomaterials to nano-assembled films (self-assembled monolayers, Langmuir-Blodgett films, and layer-by-layer assemblies) and their related functions: Journal of Nanoscience and Nanotechnology, v. 6, p. 2278-2301.

Arnold, S., Z. Q. Feng, T. Kakiuchi, W. Knoll, and K. Niki, 1997, Investigation of the electrode reaction of cytochrome c through mixed self-assembled monolayers of alkanethiols on gold(111) surfaces: Journal of Electroanalytical Chemistry, v. 438, p. 91-97.

Balkenhohl, T., S. Adelt, R. Dronov, and F. Lisdat, 2008, Oxygen-reducing electrodes based on layer-by-layer assemblies of cytochrome c and laccasse: Electrochemistry Communications, v. 10, p. 914-917.

Bard, A. J., and M. Stratmann, 2007, Encyclopedia of electrochemistry: Encyclopedia of electrochemistry: Weinheim, Wiley-VCH, viii, 402 p. p.

Bayachou, M., R. Lin, W. Cho, and P. J. Farmer, 1998, Electrochemical reduction of NO by myoglobin in surfactant film: Characterization and reactivity of the nitroxyl (NO-) adduct: Journal of the American Chemical Society, v. 120, p. 9888-9893.

Beissenhirtz, M. K., B. Kafka, D. Schafer, M. Wolny, and F. Lisdat, 2005, Electrochemical quartz crystal microbalance studies on cytochrome c/polyelectrolyte multilayer assemblies on gold electrodes: Electroanalysis, v. 17, p. 1931-1937.

Beissenhirtz, M. K., F. W. Scheller, and F. Lisdat, 2004a, A superoxide sensor based on a multilayer cytochrome c electrode: Analytical Chemistry, v. 76, p. 4665-4671.

Beissenhirtz, M. K., F. W. Scheller, W. F. M. Stocklein, D. G. Kurth, H. Mohwald, and F. Lisdat, 2004b, Electroactive cytochrome c multilayers within a polyelectrolyte assembly: Angewandte Chemie-International Edition, v. 43, p. 4357-4360.

Berg, J. M., J. L. Tymoczko, and L. Stryer, 2012, Biochemistry: New York, W.H. Freeman, xxxii, 1054, 43, 41, 48 p. p.

Bi, Y. H., Z. L. Huang, and Y. D. Zhao, 2005, Interactions of Cytochrome c with DNA at glassy carbon surface: Biophysical Chemistry, v. 116.

Biscay, J., E. C. Rama, M. B. G. Garcia, A. J. Reviejo, J. M. P. Carrazon, and A. C. Garcia, 2012, Amperometric fructose sensor based on ferrocyanide modified screen-printed carbon electrode: Talanta, v. 88, p. 432-438.

Bonk, S., and F. Lisdat, 2009, Layer-by-layer assembly of electro-active gold nanoparticle/cytochrome c multilayers: Biosensors & Bioelectronics, v. 25, p. 739-744.

Brautigan, D. L., S. Fergusonmiller, and E. Margoliash, 1978, Definition of cytochrome-c binding domains by chemical modification .1. reaction with 4-chloro-3,5-dinitrobenzoate and chromatographic-separation of singly substituted derivates: Journal of Biological Chemistry, v. 253, p. 130-139.

Bushnell, G. W., G. V. Louie, and G. D. Brayer, 1990, High-resolution 3-dimensional structure of horse heart cytochrome-c: Journal of Molecular Biology, v. 214, p. 585-595.

Cai, X. M., and C. Dass, 2003, Conformational analysis of proteins and peptides: Current Organic Chemistry, v. 7, p. 1841-1854.

Calvo, E. J., V. Flexer, M. Tagliazucchi, and P. Scodeller, 2010, Effects of the nature and charge of the topmost layer in layer by layer self assembled amperometric enzyme electrodes: Physical Chemistry Chemical Physics, v. 12, p. 10033-10039.

Campuzano, S., S. A. Loaiza, M. Pedrero, F. J. M. de Villena, and J. M. Pingarron, 2004, An integrated bienzyme glucose oxidase-fructose dehydrogenase-tetrathiafulvalene-3-mercaptopropionic acid-gold electrode for the simultaneous determination of glucose and fructose: Bioelectrochemistry, v. 63, p. 199-206.

Caruso, F., K. Niikura, D. N. Furlong, and Y. Okahata, 1997, Assembly of alternating polyelectrolyte and protein multilayer films for immunosensing .2: Langmuir, v. 13, p. 3427-3433.

Chambers, J. P., B. P. Arulanandam, L. L. Matta, A. Weis, and J. J. Valdes, 2008, Biosensor recognition elements: Current Issues in Molecular Biology, v. 10, p. 1-12.

Clark, L. C., and C. Lyons, 1962, Electrode Systems for Continuous Monitoring in Cardiovascular Surgery: Annals of the New York Academy of Sciences, v. 102, p. 29-45.

Collinson, M., E. F. Bowden, and M. J. Tarlov, 1992, Voltammetry of covalently immobilized cytochrome-c on self-assebled monolayer electrodes: Langmuir, v. 8, p. 1247-1250.

Cooney, M. J., V. Svoboda, C. Lau, G. Martin, and S. D. Minteer, 2008, Enzyme catalysed biofuel cells: Energy & Environmental Science, v. 1, p. 320-337.

Creighton, T. E., 2010, The biophysical chemistry of nucleic acids & proteins [electronic resource]: [S.l.], Helvetian Press, 1 online resource 774 p.

Crowley, P. B., and M. A. Carrondo, 2004, The architecture of the binding site in redox protein complexes: Implications for fast dissociation: Proteins-Structure Function and Bioinformatics, v. 55, p. 603-612.

Crowley, P. B., E. Chow, and T. Papkovskaia, 2011, Protein Interactions in the Escherichia coli Cytosol: An Impediment to In-Cell NMR Spectroscopy: Chembiochem, v. 12, p. 1043-1048.

Damar, K., and D. O. Demirkol, 2011, Modified gold surfaces by poly(amidoamine) dendrimers and fructose dehydrogenase for mediated fructose sensing: Talanta, v. 87, p. 67-73.

Decher, G., M. Eckle, J. Schmitt, and B. Struth, 1998, Layer-by-layer assembled multicomposite films: Current Opinion in Colloid & Interface Science, v. 3, p. 32-39.

Degani, Y., and A. Heller, 1988, Direct Electrochemical Communication Between Chemically Modified Enzymes and Metal-Electrodes .2. Methods for Bonding Electron-Transfer Relays to Glucose-Oxidase and D-Amino-Acid Oxidase: Journal of the American Chemical Society, v. 110, p. 2615-2620.

Dickerson, R. E., M. L. Kopka, J. Weinzierl, J. Varnum, D. Eisenberg, and E. Margoliash, 1967, Location of the heme in horse heart ferricytochrome c by x-ray diffraction: The Journal of biological chemistry, v. 242, p. 3015-3023.

Dixon, M., J. M. Maynard, and P. F. W. Morrow, 1960, Cause of the instability of cytochrome-c reductase: Nature, v. 186, p. 1032-1033.

Dokter, P., J. Frank, and J. A. Duine, 1986, Purification and Characterization of Quinoprotein Glucose-Dehydrogenase from Acinetobacter-Calcoaceticus LMD-79.41 Biochemical Journal, v. 239, p. 163-167.

Dronov, R., D. G. Kurth, H. Moehwald, F. W. Scheller, J. Friedmann, D. Pum, U. B. Sleytr, and F. Lisdat, 2008a, Self-assembly of S-layer-enveloped cytochrome c polyelectrolyte multilayers: Langmuir, v. 24, p. 8779-8784.

Dronov, R., D. G. Kurth, H. Moehwald, F. W. Scheller, and F. Lisdat, 2007, A self-assembled cytochrome c/xanthine oxidase multilayer arrangement on gold: Electrochimica Acta, v. 53, p. 1107-1113.

Dronov, R., D. G. Kurth, H. Moehwald, F. W. Scheller, and F. Lisdat, 2008b, Communication in a protein stack: Electron transfer between cytochrome c and bilirubin oxidase within a polyelectrolyte multilayer: Angewandte Chemie-International Edition, v. 47, p. 3000-3003.

Dronov, R., D. G. Kurth, H. Moehwald, R. Spricigo, S. Leimkuehler, U. Wollenberger, K. V. Rajagopalan, F. W. Scheller, and F. Lisdat, 2008c, Layer-by-layer arrangement by protein-protein interaction of sulfite oxidase and cytochrome c catalyzing oxidation of sulfite: Journal of the American Chemical Society, v. 130, p. 1122-+.

Dronov, R., D. G. Kurth, H. Moehwald, R. Spricigo, S. Leimkuehler, U. Wollenberger, K. V. Rajagopalan, F. W. Scheller, and F. Lisdat, 2008d, Layer-by-layer arrangement by protein-protein interaction of sulfite oxidase and cytochrome c catalyzing oxidation of sulfite: Journal of the American Chemical Society, v. 130, p. 1122-1123.

Duine, J. A., 1988, Enzymology of PQQ and Quinoproteins: Journal of Cell Biology, v. 107, p. 441A-441A.

Duine, J. A., 1991, Quinoproteins - Enzymes Containing the Quinoid Cofactor Pyrroloquinoline Quinone, Topaquinone or Tryptophan-Trypthphan Quinone: European Journal of Biochemistry, v. 200, p. 271-284.

Eddowes, M. J., and H. A. O. Hill, 1977, Novel Method for Investigation of Electrochemistry of Metalproteins - Cytochrome-c: Journal of the Chemical Society-Chemical Communications, p. 771-772.

Erben, C. M., R. P. Goodman, and A. J. Turberfield, 2006, Single-molecule protein encapsulation in a rigid DNA cage: Angewandte Chemie-International Edition, v. 45, p. 7414-7417.

Feifel, S. C., A. Kapp, and F. Lisdat, 2014a, Electroactive Nanobiomolecular Architectures of Laccase and Cytochrome c on Electrodes: Applying Silica Nanoparticles as Artificial Matrix: Langmuir, v. 30, p. 5363-5367.

Feifel, S. C., A. Kapp, and F. Lisdat, 2014b, Protein Multilayer Architectures on Electrodes for Analyte Detection: Biosensors Based on Aptamers and Enzymes, v. 140, p. 253-298.

Feifel, S. C., A. Kapp, R. Ludwig, and F. Lisdat, 2014c, Nanobiomolecular Multiprotein Clusters on Electrodes for the Formation of a Switchable Cascadic Reaction Scheme: Angewandte Chemie-International Edition, v. 53, p. 5676-5679.

Feifel, S. C., and F. Lisdat, 2011, Silica nanoparticles for the layer-by-layer assembly of fully electro-active cytochrome c multilayers: Journal of Nanobiotechnology, v. 9.

Feifel, S. C., R. Ludwig, L. Gorton, and F. Lisdat, 2012, Catalytically Active Silica Nanoparticle-Based Supramolecular Architectures of Two Proteins - Cellobiose Dehydrogenase and Cytochrome c on Electrodes: Langmuir, v. 28, p. 9189-9194.

Feng, Z. Q., S. Imabayashi, T. Kakiuchi, and K. Niki, 1997, Long-range electron-transfer reaction rates to cytochrome c across long- and short-chain alkanethiol self-assembled monolayers: Electroreflectance studies: Journal of the Chemical Society-Faraday Transactions, v. 93, p. 1367-1370.

Ferapontova, E. E., and L. Gorton, 2005, Direct electrochemistry of heme multicofactor-containing enzymes on alkanethiol-modified gold electrodes: Bioelectrochemistry, v. 66, p. 55-63.

Ferri, S., K. Kojima, and K. Sode, 2011, Review of glucose oxidases and glucose dehydrogenases: a bird's eye view of glucose sensing enzymes: Journal of diabetes science and technology, v. 5, p. 1068-76.

Finklea, H., 1996, Electrochemistry of organized monolayers of thiols and related molecules on electrodes: Electroanalytical Chemistry: a Series of Advances, Vol 19, v. 19, p. 109-335.

Finzel, B. C., T. L. Poulos, and J. Kraut, 1984, Crystal-structure of yeast cytochrome-c peroxidase refined at 1.7-A resolution: Journal of Biological Chemistry, v. 259, p. 3027-3036.

Fisher, W. R., H. Taniuchi, and C. B. Anfinsen, 1973, Role of heme in formation of structure of cytochrome c: Journal of Biological Chemistry, v. 248, p. 3188-3195.

Flexer, V., F. Durand, S. Tsujimura, and N. Mano, 2011, Efficient Direct Electron Transfer of PQQ-glucose Dehydrogenase on Carbon Cryogel Electrodes at Neutral pH: Analytical Chemistry, v. 83, p. 5721-5727.

Flory, J. D., C. R. Simmons, S. Lin, T. Johnson, A. Andreoni, J. Zook, G. Ghirlanda, Y. Liu, H. Yan, and P. Fromme, 2014, Low Temperature Assembly of Functional 3D DNA-PNA-Protein Complexes: Journal of the American Chemical Society, v. 136, p. 8283-8295.

Frasca, S., T. von Graberg, J. J. Feng, A. Thomas, B. M. Smarsly, I. M. Weidinger, F. W. Scheller, P. Hildebrandt, and U. Wollenberger, 2010, Mesoporous Indium Tin Oxide as a Novel Platform for Bioelectronics: Chemcatchem, v. 2, p. 839-845.

Ge, B., and F. Lisdat, 2002, Superoxide sensor based on cytochrome c immobilized on mixed-thiol SAM with a new calibration method: Analytica Chimica Acta, v. 454, p. 53-64.

Gobel, G., I. W. Schubart, V. Scherbahn, and F. Lisdat, 2011, Direct electron transfer of PQQ-glucose dehydrogenase at modified carbon nanotubes electrodes: Electrochemistry Communications, v. 13, p. 1240-1243.

Gobi, K. V., and F. Mizutani, 2000, Efficient mediatorless superoxide sensors using cytochrome c-modified electrodes: surface nano-organization for selectivity and controlled peroxidase activity: Journal of Electroanalytical Chemistry, v. 484, p. 172-181.

Gooding, J. J., R. Wibowo, J. Q. Liu, W. R. Yang, D. Losic, S. Orbons, F. J. Mearns, J. G. Shapter, and D. B. Hibbert, 2003, Protein electrochemistry using aligned carbon nanotube arrays: Journal of the American Chemical Society, v. 125, p. 9006-9007.

Gorton, L., 1995, Carbon-Paste Electrodes Modified with Enzymes, Tissues, and Cells: Electroanalysis, v. 7, p. 23-45.

Gorton, L., A. Lindgren, T. Larsson, F. D. Munteanu, T. Ruzgas, and I. Gazaryan, 1999, Direct electron transfer between heme-containing enzymes and electrodes as basis for third generation biosensors: Analytica Chimica Acta, v. 400, p. 91-108.

Guto, P. M., and G. N. Kamau, 2010, Electrochemical Characterization of Myoglobin-Polylysine Films at a Temperature Range of 6-80 degrees C: Electroanalysis, v. 22, p. 1186-1190.

Habermuller, K., S. Reiter, H. Buck, T. Meier, J. Staepels, and W. Schuhmann, 2003, Conducting redoxpolymer-based reagentless biosensors using modified PQQ-dependent glucose dehydrogenase: Microchimica Acta, v. 143, p. 113-121.

Halamkova, L., J. Halamek, V. Bocharova, A. Szczupak, L. Alfonta, and E. Katz, 2012, Implanted Biofuel Cell Operating in a Living Snail: Journal of the American Chemical Society, v. 134, p. 5040-5043.

Heller, A., Y. Degani, D. W. Johnson, and P. K. Gallagher, 1987, Controlled Supression and Enhancement of the Photoactivity of Titanium-Dioxide (Rutile) Pigment: Journal of Physical Chemistry, v. 91, p. 5987-5991.

Hunte, C., S. Solmaz, and C. Lange, 2002, Electron transfer between yeast cytochrome bc(1) complex and cytochrome c: a structural analysis: Biochimica Et Biophysica Acta-Bioenergetics, v. 1555, p. 21-28.

Ikeda, O., Y. Shirota, and T. Sakurai, 1990, Electrical communication between horse heart cytochrome-c and electrodes in the presence of DNA and RNA: Journal of Electroanalytical Chemistry, v. 287, p. 179-184.

Ikeda, T., F. Matsushita, and M. Senda, 1991, Amperometric Fructose Sensor Based on Direkt Bioelectrocatalysis: Biosensors & Bioelectronics, v. 6, p. 299-304.

Ivnitski, D., P. Atanassov, and C. Apblett, 2007, Direct bioelectrocatalysis of PQQ-dependent glucose dehydrogenase: Electroanalysis, v. 19, p. 1562-1568.

Iwahara, J., and G. M. Clore, 2006, Detecting transient intermediates in macromolecular binding by paramagnetic NMR: Nature, v. 440, p. 1227-1230.

Iwahara, J., C. D. Schwieters, and G. M. Clore, 2004, Characterization of nonspecific protein-DNA interactions by H-1 paramagnetic relaxation enhancement: Journal of the American Chemical Society, v. 126, p. 12800-12808.

Iwahara, J., M. Zweckstetter, and G. M. Clore, 2006, NMR structural and kinetic characterization of a homeodomain diffusing and hopping on nonspecific DNA: Proceedings of the National Academy of Sciences of the United States of America, v. 103, p. 15062-15067.

Jasion, V. S., T. Doukov, S. H. Pineda, H. Y. Li, and T. L. Poulos, 2012, Crystal structure of the Leishmania major peroxidase-cytochrome c complex: Proceedings of the National Academy of Sciences of the United States of America, v. 109, p. 18390-18394.

Jeuken, L. J. C., 2003, Conformational reorganisation in interfacial protein electron transfer: Biochimica Et Biophysica Acta-Bioenergetics, v. 1604, p. 67-76.

Jiang, L., C. J. McNeil, and J. M. Cooper, 1995, Direct Electrochemical Coupling of Component of the Biological Electron-Transfer Chain to modified Surfaces - Molecular Recognition between Cytochrome-c Peroxidase and Cytochrome-c: Angewandte Chemie-International Edition in English, v. 34, p. 2409-2411.

Jin, W., F. Bier, U. Wollenberger, and F. Scheller, 1995, Construction and Characterization of a Multilayer Enzyme Electrode - Covalent Binding of Quinoprotein Glucose-Dehydrogenase onto Gold Electrodes: Biosensors & Bioelectronics, v. 10, p. 823-829.

Jin, W., U. Wollenberger, F. F. Bier, A. Makower, and F. W. Scheller, 1996, Electron transfer between cytochrome c and copper enzymes: Bioelectrochemistry and Bioenergetics, v. 39, p. 221-225.

Jin, W., U. Wollenberger, E. Kargel, W. H. Schunck, and F. W. Scheller, 1997, Electrochemical investigations of the intermolecular electron transfer between cytochrome c and NADPH cytochrome P450 reductase: Journal of Electroanalytical Chemistry, v. 433, p. 135-139.

Jin, W., U. Wollenberger, and F. W. Scheller, 1998, PQQ as redox shuttle for quinoprotein glucose dehydrogenase: Biological Chemistry, v. 379, p. 1207-1211.

Kalodimos, C., N. Biris, A. Bonvin, M. Levandoski, M. Guennuegues, R. Boelens, and R. Kaptein, 2004, Structure and flexibility adaptation in nonspecific and specific protein-DNA complexes: Science, v. 305, p. 386-389.

Kamau, G. N., M. P. Guto, B. Munge, V. Panchagnula, and J. F. Rusling, 2003, Myoglobin coadsorbed on electrodes from microemulsions provides reversible electrochemistry and tunable electrochemical catalysis: Langmuir, v. 19, p. 6976-6981.

Kamitaka, Y., S. Tsujimura, and K. Kano, 2007a, High current density bioelectrolysis of D-fructose at fructose dehydrogenase-adsorbed and Ketjen black-modified electrodes without a mediator: Chemistry Letters, v. 36, p. 218-219.

Kamitaka, Y., S. Tsujimura, N. Setoyama, T. Kajino, and K. Kano, 2007b, Fructose/dioxygen biofuel cell based on direct electron transfer-type bioelectrocatalysis: Physical Chemistry Chemical Physics, v. 9, p. 1793-1801.

Kas'ianenko, N. A., S. F. Bartoshevich, and E. V. Frisman, 1985, Effect of the pH of the medium on DNA conformation: Molekuliarnaia biologiia, v. 19, p. 1386-93.

Katz, E., D. D. Schlereth, and H. L. Schmidt, 1994, Electrochemical Study of Pyrroloquinoline Quinone Covalently Immobilized as a Monolayer onto a Cystamine-Modified Gold Electrode: Journal of Electroanalytical Chemistry, v. 367, p. 59-70.

Katz, E., and I. Willner, 2004, Biomolecule-functionalized carbon nanotubes: applications in nanobioelectronics: Chemphyschem : a European journal of chemical physics and physical chemistry, v. 5, p. 1084-104.

Katz, E., M. Zayats, I. Willner, and F. Lisdat, 2006, Controlling the direction of photocurrents by means of CdS nanoparticles and cytochrome c-mediated biocatalytic cascades: Chemical Communications, p. 1395-1397.

Kawai, S., M. Goda-Tsutsumi, T. Yakushi, K. Kano, and K. Matsushita, 2013, Heterologous Overexpression and Characterization of a Flavoprotein-Cytochrome c Complex Fructose Dehydrogenase of Gluconobacter japonicus NBRC3260: Applied and Environmental Microbiology, v. 79, p. 1654-1660.

Kawai, S., T. Yakushi, K. Matsushita, Y. Kitazumi, O. Shirai, and K. Kano, 2014, The electron transfer pathway in direct electrochemical communication of fructose dehydrogenase with electrodes: Electrochemistry Communications, v. 38, p. 28-31.

Khan, G. F., H. Shinohara, Y. Ikariyama, and M. Aizawa, 1991, Electrochemical-Behavior of Monolayer Quinoprotein Adsorbed on the Electrode Surface: Journal of Electroanalytical Chemistry, v. 315, p. 263-273.

Khrapunov, S., A. Dragan, A. Sivolob, and A. Zagariya, 1997, Mechanisms of stabilizing nucleosome structure. Study of dissociation of histone octamer from DNA: Biochimica Et Biophysica Acta-Gene Structure and Expression, v. 1351, p. 213-222.

Kim, Y.-P., S. J. Park, D. Lee, and H.-S. Kim, 2012, Electrochemical glucose biosensor by electrostatic binding of PQQ-glucose dehydrogenase onto self-assembled monolayers on gold: Journal of Applied Electrochemistry, v. 42, p. 383-390.

Knapp, J. A., and C. N. Pace, 1974, Guanidine hydrochloride and Acid Denaturation of Horse, Cow, and Candida-Krustei Cytochromes-c: Biochemistry, v. 13, p. 1289-1294.

Krylov, A. V., M. Beissenhirtz, H. Adamzig, F. W. Scheller, and F. Lisdat, 2004, Thick-film electrodes for measurement of superoxide and hydrogen peroxide based on direct protein-electrode contacts: Analytical and Bioanalytical Chemistry, v. 378, p. 1327-1330.

Kuzuya, A., and M. Komiyama, 2010, DNA origami: Fold, stick, and beyond: Nanoscale, v. 2, p. 310-322.

Lao, R., L. Wang, Y. Wan, J. Zhang, S. Song, Z. Zhang, C. Fan, and L. He, 2007, Interactions between cytochrome c and DNA strands self-assembled at gold electrode: International Journal of Molecular Sciences, v. 8, p. 1.

Laurinavicius, V., J. Razumiene, A. Ramanavicius, and A. D. Ryabov, 2004, Wiring of PQQ-dehydrogenases: Biosensors & Bioelectronics, v. 20, p. 1217-1222.

Lisdat, F., R. Dronov, H. Moehwald, F. W. Scheller, and D. G. Kurth, 2009, Self-assembly of electro-active protein architectures on electrodes for the construction of biomimetic signal chains: Chemical Communications, p. 274-283.

Lisdat, F., B. Ge, B. Krause, A. Ehrlich, H. Bienert, and F. Scheller, 2001, Nucleic acid-promoted electron transfer to cytochrome c: Electroanalysis, v. 13, p. 1225-1230.

Lisdat, F., B. Ge, and F. W. Scheller, 1999, Oligonucleotide-modified electrodes for fast electron transfer to cytochrome c: Electrochemistry Communications, v. 1, p. 65-68.

Lisdat, F., and U. Wollenberger, 1998, Trienzyme amplification system for the detection of catechol and catecholamines using internal co-substrate regeneration: Analytical Letters, v. 31, p. 1275-1285.

Littlefield, O., and H. Nelson, 2001, Crystal packing interaction that blocks crystallization of a site-specific DNA binding protein-DNA complex: Proteins-Structure Function and Genetics, v. 45, p. 219-228.

Liu, W. X., J. Rumbley, S. W. Englander, and A. J. Wand, 2003, Backbone and side-chain heteronuclear resonance assignments and hyperfine NMR shifts in horse cytochrome c: Protein Science, v. 12, p. 2104-2108.

Loew, N., F. W. Scheller, and U. Wollenberger, 2004, Characterization of self-assembling of glucose dehydrogenase in mono- and multilayers on gold electrodes: Electroanalysis, v. 16, p. 1149-1154.

Love, J. C., L. A. Estroff, J. K. Kriebel, R. G. Nuzzo, and G. M. Whitesides, 2005, Self-assembled monolayers of thiolates on metals as a form of nanotechnology: Chemical Reviews, v. 105, p. 1103-1169.

Luisi, B. F., W. X. Xu, Z. Otwinowski, L. P. Freedman, K. R. Yamamoto, and P. B. Sigler, 1991, Crystallographic analysis of the interaction of the glucocorticoid receptor with DNA: Nature, v. 352, p. 497-505.

Lutkenhaus, J. L., and P. T. Hammond, 2007, Electrochemically enabled polyelectrolyte multilayer devices: from fuel cells to sensors: Soft Matter, v. 3, p. 804-816.

Lvov, Y. M., Z. Q. Lu, J. B. Schenkman, X. L. Zu, and J. F. Rusling, 1998, Direct electrochemistry of myoglobin and cytochrome p450(cam) in alternate layer-by-layer films with DNA and other polyions: Journal of the American Chemical Society, v. 120, p. 4073-4080.

Malmgren, L., Y. Olsson, T. Olsson, and K. Kristensson, 1978, Uptake and retrograde axonal transport of various exogenous macromolecules in normal and crushed hypoglossal nerves: Brain Research, v. 153, p. 477-493.

Marcinkeviciene, J., and G. Johansson, 1993, Kinetic-Studies of the Active-Sites Functioning in the Quinohemoprotein Fructose Dehydrogenase: Febs Letters, v. 318, p. 23-26.

Marcus, R. A., 1993, Electron-Transfer Reactions in Chemistry - Theory and Experiment (Noble Lecture): Angewandte Chemie-International Edition in English, v. 32, p. 1111-1121.

Marcus, R. A., and N. Sutin, 1985, Electron Transfer in Chemistry and Biology: Biochimica Et Biophysica Acta, v. 811, p. 265-322.

Matsushita, K., E. Shinagawa, O. Adachi, and M. Ameyama, 1988, Quinoprotein D-Glucose Dehydrogenase in Acinetobacter-Calcoaceticus LMD 79.41 - The Membrane-Bound Enzyme is Distinct from the Solube Enzyme: Fems Microbiology Letters, v. 55, p. 53-57.

McGovern, R. E., H. Fernandes, A. R. Khan, N. P. Power, and P. B. Crowley, 2012, Protein camouflage in cytochrome c-calixarene complexes: Nature Chemistry, v. 4, p. 527-533.

Murata, K., M. Suzuki, K. Kajiya, N. Nakamura, and H. Ohno, 2009, High performance bioanode based on direct electron transfer of fructose dehydrogenase at gold nanoparticle-modified electrodes: Electrochemistry Communications, v. 11, p. 668-671.

Nahir, T. M., R. A. Clark, and E. F. Bowden, 1994, Linear-Sweep Voltammetry of Irreversible Electron-Transfer in Surface-Confined Species Using the Marcus Theory: Analytical Chemistry, v. 66, p. 2595-2598.

Nassar, A. E. F., W. S. Willis, and J. F. Rusling, 1995, Electron-Transfer from Electrodes to Myoglobin - Facilitated in Surfactant Films and Blocked by Adsorbed Biomacromolecules: Analytical Chemistry, v. 67, p. 2386-2392.

Olsthoorn, A. J. J., and J. A. Duine, 1996, Production, characterization, and reconstitution of recombinant quinoprotein glucose dehydrogenase (soluble type; EC 1.1.99.17) apoenzyme of Acinetobacter calcoaceticus: Archives of Biochemistry and Biophysics, v. 336, p. 42-48.

Oubrie, A., 2003, Structure and mechanism of soluble glucose dehydrogenase and other PQQ-dependent enzymes: Biochimica Et Biophysica Acta-Proteins and Proteomics, v. 1647, p. 143-151.

Oubrie, A., H. J. Rozeboom, K. H. Kalk, A. J. J. Olsthoorn, J. A. Duine, and B. W. Dijkstra, 1999, Structure and mechanism of soluble quinoprotein glucose dehydrogenase: Embo Journal, v. 18, p. 5187-5194.

Patel, C. N., M. C. Lind, and G. J. Pielak, 2001, Characterization of horse cytochrome c expressed in Escherichia coli: Protein Expression and Purification, v. 22, p. 220-224.

Pavletich, N. P., and C. O. Pabo, 1991, Zink finger DNA recognition - crystal-structure of a ZIF268 complex at 2.1-A: Science, v. 252, p. 809-817.

Pelletier, H., and J. Kraut, 1992, Crystal-structure of a complex between electron-transfer partners, cytochrome-c peroxidase and cytochrome-c: Science, v. 258, p. 1748-1755.

Pingarron, J. M., P. Yanez-Sedeno, and A. Gonzalez-Cortes, 2008, Gold nanoparticle-based electrochemical biosensors: Electrochimica Acta, v. 53, p. 5848-5866.

Poulos, T. L., S. T. Freer, R. A. Alden, S. L. Edwards, U. Skogland, K. Takio, B. Erikkson, N. H. Xuong, T. Yonetani, and J. Kraut, 1980, Crystal-structure of cytochrome-c peroxidase: Journal of Biological Chemistry, v. 255, p. 575-580.

Privett, B. J., J. H. Shin, and M. H. Schoenfisch, 2010, Electrochemical Sensors: Analytical Chemistry, v. 82, p. 4723-4741.

Pumera, M., A. Ambrosi, A. Bonanni, E. L. K. Chng, and H. L. Poh, 2010, Graphene for electrochemical sensing and biosensing: Trac-Trends in Analytical Chemistry, v. 29, p. 954-965.

Razumiene, J., A. Vilkanauskyte, V. Gureviciene, J. Barkauskas, R. Meskys, and V. Laurinavicius, 2006, Direct electron transfer between PQQ dependent glucose dehydrogenases and carbon electrodes: An approach for electrochemical biosensors: Electrochimica Acta, v. 51, p. 5150-5156.

Redepenning, J., R. Naegeli, and F. C. Anson, 1986, Ionic-Strength and pH Effects in Measurements of Formal Potentials for Redox Couples Incorporated in Nafion Films on Electrodes: Abstracts of Papers of the American Chemical Society, v. 192, p. 147-COLL.

Rusling, J. F., E. G. Hvastkovs, D. O. Hull, and J. B. Schenkman, 2008, Biochemical applications of ultrathin films of enzymes, polyions and DNA: Chemical Communications, p. 141-154.

Ruzin, S. E., 1999, Plant Microtechnique and Microscopy: New York, Oxford University Press.

Sakamoto, K., M. Kamiya, M. Imai, K. Shinzawa-Itoh, T. Uchida, K. Kawano, S. Yoshikawa, and K. Ishimori, 2011, NMR basis for interprotein electron transfer gating between cytochrome c and cytochrome c oxidase: Proceedings of the National Academy of Sciences of the United States of America, v. 108, p. 12271-12276.

Sarauli, D., M. Riedel, C. Wettstein, R. Hahn, K. Stiba, U. Wollenberger, S. Leimkuhler, P. Schmuki, and F. Lisdat, 2012a, Semimetallic TiO2 nanotubes: new interfaces for bioelectrochemical enzymatic catalysis: Journal of Materials Chemistry, v. 22, p. 4615-4618.

Sarauli, D., J. Tanne, D. Schaefer, I. W. Schubart, and F. Lisdat, 2009, Multilayer electrodes: Fully electroactive cyt c on gold as a part of a DNA/protein architecture: Electrochemistry Communications, v. 11, p. 2288-2291.

Sarauli, D., C. G. Xu, B. Dietzel, K. Stiba, S. Leimkuhler, B. Schulz, and F. Lisdat, 2012b, Thin films of substituted polyanilines: interactions with biomolecular systems: Soft Matter, v. 8, p. 3848-3855.

Sasaki, Y., T. Sugihara, and T. Osakai, 2011, Electron transfer mediated by membrane-bound D-fructose dehydrogenase adsorbed at an oil/water interface: Analytical Biochemistry, v. 417, p. 129-135.

Scheller, F. W., U. Wollenberger, A. Warsinke, and F. Lisdat, 2001, Research and development in biosensors: Current Opinion in Biotechnology, v. 12, p. 35-40.

Scheller, W., W. Jin, E. Ehrentreich-Forster, B. Ge, F. Lisdat, R. Buttemeier, U. Wollenberger, and F. W. Scheller, 1999, Cytochrome C based superoxide sensor for in vivo application: Electroanalysis, v. 11, p. 703-706.

Scherbahn, V., M. T. Putze, B. Dietzel, T. Heinlein, J. J. Schneider, and F. Lisdat, 2014, Biofuel cells based on direct enzyme-electrode contacts using PQQ-dependent glucose dehydrogenase/bilirubin oxidase and modified carbon nanotube materials: Biosensors & Bioelectronics, v. 61, p. 631-638.

Schubart, I. W., G. Goebel, and F. Lisdat, 2012, A pyrroloquinolinequinone-dependent glucose dehydrogenase (PQQ-GDH)-electrode with direct electron transfer based on polyaniline modified carbon nanotubes for biofuel cell application: Electrochimica Acta, v. 82, p. 224-232.

Scott, R. A., and A. G. Mauk, 1996, Cytochrome C: a multidisciplinary approach: Sausalito, Calif., University Science Books, 738 p.

Shan, C., H. Yang, J. Song, D. Han, A. Ivaska, and L. Niu, 2009, Direct Electrochemistry of Glucose Oxidase and Biosensing for Glucose Based on Graphene: Analytical Chemistry, v. 81, p. 2378-2382.

Shao, Y., K. Morita, Q. Dai, S. Nishizawa, and N. Teramae, 2008, Sequence dependence of cytochrome c electrochemistry on DNA modified electrodes: Effect of hydrogen bonding of a ligand to nucleobases opposite an abasic site: Electrochemistry Communications, v. 10, p. 438-442.

Shen, L., R. Huang, and N. F. Hu, 2002, Myoglobin in polyacrylamide hydrogel films: direct electrochemistry and electrochemical catalysis: Talanta, v. 56, p. 1131-1139.

Song, S., R. A. Clark, E. F. Bowden, and M. J. Tarlov, 1993, Characterization of cytochrome-c alkanethiolate structures prepared by self-assembly on gold: Journal of Physical Chemistry, v. 97, p. 6564-6572.

Song, S. L., H. Y. Liu, X. H. Guo, and N. F. Hu, 2009, Comparative electrochemical study of myoglobin loaded in different polyelectrolyte layer-by-layer films assembled by spin-coating: Electrochimica Acta, v. 54, p. 5851-5857.

Song, Y., L. Wan, Y. Wang, S. Zhao, H. Hou, and L. Wang, 2012, Electron transfer and electrocatalytics of cytochrome c and horseradish peroxidase on DNA modified electrode: Bioelectrochemistry, v. 85.

Spricigo, R., R. Dronov, F. Lisdat, S. Leimkuhler, F. W. Scheller, and U. Wollenberger, 2009, Electrocatalytic sulfite biosensor with human sulfite oxidase co-immobilized with cytochrome c in a polyelectrolyte-containing multilayer: Analytical and Bioanalytical Chemistry, v. 393, p. 225-233.

Spricigo, R., R. Dronov, K. V. Rajagopalan, F. Lisdat, S. Leimkuehler, F. W. Scheller, and U. Wollenberger, 2008, Electrocatalytically functional multilayer assembly of sulfite oxidase and cytochrome c: Soft Matter, v. 4, p. 972-978.

Steel, A., T. Herne, and M. Tarlov, 1998, Electrochemical quantitation of DNA immobilized on gold: Analytical Chemistry, v. 70, p. 4670-4677.

Stoll, R., B. M. Lee, E. W. Debler, J. H. Laity, I. A. Wilson, H. J. Dyson, and P. E. Wright, 2007, Structure of the Wilms tumor suppressor protein zinc finger domain bound to DNA: Journal of Molecular Biology, v. 372, p. 1227-1245.

Taniguchi, I., K. Toyosawa, H. Yamaguchi, and K. Yasukouchi, 1982, Voltammetric response of horse heart cytochrome-c at a gold electrode in the presence of sulfur bridged bipyridines: Journal of Electroanalytical Chemistry, v. 140, p. 187-193.

Tanne, C., G. Goebel, and F. Lisdat, 2010, Development of a (PQQ)-GDH-anode based on MWCNT-modified gold and its application in a glucose/O(2)-biofuel cell: Biosensors & Bioelectronics, v. 26, p. 530-535.

Thiel, A., A. Frutos, C. Jordan, R. Corn, and L. Smith, 1997, In situ surface plasmon resonance imaging detection of DNA hybridization to oligonucleotide arrays on gold surfaces: Analytical Chemistry, v. 69, p. 4948-4956.

Tolkatchev, D., P. Xu, and F. Ni, 2003, Probing the kinetic landscape of transient peptide-protein interactions by use of peptide N-15 NMR relaxation dispersion spectroscopy: Binding of an antithrombin peptide to human prothrombin: Journal of the American Chemical Society, v. 125, p. 12432-12442.

Tominaga, M., S. Nomura, and I. Taniguchi, 2009, D-Fructose detection based on the direct heterogeneous electron transfer reaction of fructose dehydrogenase adsorbed onto multi-walled carbon nanotubes synthesized on platinum electrode: Biosensors & Bioelectronics, v. 24, p. 1184–1188.

Tominaga, M., C. Shirakihara, and I. Taniguchi, 2007, Direct heterogeneous electron transfer reactions and molecular orientation of fructose dehydrogenase adsorbed onto pyrolytic graphite electrodes: Journal of Electroanalytical Chemistry, v. 610, p. 1-8.

Turner, A. P. F., 2000, Biochemistry - Biosensors sense and sensitivity: Science, v. 290, p. 1315-1317.

Ugo, P., L. M. Moretto, and G. A. Mazzocchin, 1993, Ion-Exchange Voltammetry of Cupper Ions in Chloride Media at Glassy-Carbon Electrodes Modified with Polycationic Ionomers: Analytica Chimica Acta, v. 273, p. 229-236.

Updike, S. J., and G. P. Hicks, 1967, Enzyme Electrode: Nature, v. 214, p. 986-&.

van Gelder, B., and E. C. Slater, 1962, The extinction coefficient of cytochrome c: Biochimica et biophysica acta, v. 58, p. 593-595.

Vanwetswinkel, S., N. A. J. van Nuland, and A. N. Volkov, 2013, Paramagnetic properties of the low- and high-spin states of yeast cytochrome c peroxidase: Journal of Biomolecular Nmr, v. 57, p. 21-26.

Viadiu, H., and A. K. Aggarwal, 2000, Structure of BamHI bound to nonspecific DNA: A model for DNA sliding: Molecular Cell, v. 5, p. 889-895.

Volkov, A. N., and N. A. J. van Nuland, 2013, Solution NMR study of the yeast cytochrome c peroxidase: cytochrome c interaction: Journal of Biomolecular Nmr, v. 56, p. 255-263.

Volkov, A. N., S. Vanwetswinkel, K. Van de Water, and N. A. J. van Nuland, 2012, Redox-dependent conformational changes in eukaryotic cytochromes revealed by paramagnetic NMR spectroscopy: Journal of Biomolecular Nmr, v. 52, p. 245-256.

Volkov, A. N., A. Wohlkonig, S. H. Soror, and N. A. J. van Nuland, 2013, Expression, Purification, Characterization, and Solution Nuclear Magnetic Resonance Study of Highly Deuterated Yeast Cytochrome c Peroxidase with Enhanced Solubility: Biochemistry, v. 52, p. 2165-2175.

Volkov, A. N., J. A. R. Worrall, E. Holtzmann, and M. Ubbink, 2006, Solution structure and dynamics of the complex between cytochrome c and cytochrome c peroxidase determined by paramagnetic NMR: Proceedings of the National Academy of Sciences of the United States of America, v. 103, p. 18945-18950.

Wang, L., and D. H. Waldeck, 2008, Denaturation of cytochrome c and its peroxidase activity when immobilized on SAM films: Journal of Physical Chemistry C, v. 112, p. 1351-1356.

Wegerich, F., P. Turano, M. Allegrozzi, H. Mohwald, and F. Lisdat, 2009, Cytochrome c Mutants for Superoxide Biosensors: Analytical Chemistry, v. 81, p. 2976-2984.

Wegerich, F., P. Turano, M. Allegrozzi, H. Mohwald, and F. Lisdat, 2011, Electroactive Multilayer Assemblies of Bilirubin Oxidase and Human Cytochrome C Mutants: Insight in Formation and Kinetic Behavior: Langmuir, v. 27, p. 4202-4211.

Wettstein, C., H. Moehwald, and F. Lisdat, 2012, Coupling of pyrroloquinoline quinone dependent glucose dehydrogenase to (cytochrome c/DNA)-multilayer systems on electrodes: Bioelectrochemistry, v. 88, p. 97-102.

Williams, R. J. P., 1989, Electron-Transfer in Biology: Molecular Physics, v. 68, p. 1-23.

Willner, I., E. Katz, and B. Willner, 1997, Electrical contact of redox enzyme layers associated with electrodes: Routes to amperometric biosensors: Electroanalysis, v. 9, p. 965-977.

Winkler, F. K., D. W. Banner, C. Oefner, D. Tsernoglou, R. S. Brown, S. P. Heathman, R. K. Bryan, P. D. Martin, K. Petratos, and K. S. Wilson, 1993, The crystal-structure of EcoRV endonuclease and of its complexes with cognate and non-cognate DNA fragments: Embo Journal, v. 12, p. 1781-1795.

Wollenberger, U., R. Spricigo, S. Leimkuhler, and K. Schronder, 2008, Protein electrodes with direct electrochemical communication: Biosensing for the 21st Century, v. 109, p. 19-64.

Worrall, J. A. R., U. Kolczak, G. W. Canters, and M. Ubbink, 2001, Interaction of yeast iso-1-cytochrome c with cytochrome c peroxidase investigated by N-15,H-1 heteronuclear NMR spectroscopy: Biochemistry, v. 40, p. 7069-7076.

Wu, Y. H., and S. S. Hu, 2007, Biosensors based on direct electron transfer in redox proteins: Microchimica Acta, v. 159, p. 1-17.

Xiao, Y., F. Patolsky, E. Katz, J. F. Hainfeld, and I. Willner, 2003, "Plugging into enzymes": Nanowiring of redox enzymes by a gold nanoparticle: Science, v. 299, p. 1877-1881.

Yamada, Y., K. Aida, and T. Uemura, 1967, Enzymatic studies on the oxidation of sugar and sugar alcohol. II. Purification and properties of NADPH-linked 5-ketofructose reductase: Journal of biochemistry, v. 61, p. 803-11.

Yeh, P., and T. Kuwana, 1977, Reversible Electrode-Reaction of Cytochrome-c: Chemistry Letters, p. 1145-1148.

Yue, H. J., D. H. Waldeck, K. Schrock, D. Kirby, K. Knorr, S. Switzer, J. Rosmus, and R. A. Clark, 2008, Multiple sites for electron tunneling between cytochrome c and mixed self-assembled monolayers: Journal of Physical Chemistry C, v. 112, p. 2514-2521.

Zayats, M., E. Katz, R. Baron, and I. Willner, 2005, Reconstitution of apo-glucose dehydrogenase on pyrroloquinoline quinone-functionalized Au nanoparticles yields an electrically contacted biocatalyst: Journal of the American Chemical Society, v. 127, p. 12400-12406.

Zhao, W., J. J. Xu, and H. Y. Chen, 2006, Electrochemical biosensors based on layer-by-layer assemblies: Electroanalysis, v. 18, p. 1737-1748.

LIST OF PUBLICATIONS

PUBLISHED MANUSCRIPTS

- **Wettstein, C.**; Kyne C.; Doolan AM.; Möhwald H.; Crowley PB.; Lisdat F., Study of Cytochrome c-DNA Interaction - Evaluation of Binding Sites on the Redox Protein. Nanoscale **2014**, 6, (22), 13779-13786. (DOI: 10.1039/C4NR05301J).

- Sarauli, D.; Riedel, M.; **Wettstein, C.**; Hahn, R.; Stiba, K.; Wollenberger, U.; Leimkuhler, S.; Schmuki, P.; Lisdat, F., Semimetallic TiO_2 nanotubes: new interfaces for bioelectrochemical enzymatic catalysis. Journal of Materials Chemistry **2012**, 22, (11), 4615-4618. (DOI: 10.1039/C2JM16427B).

- **Wettstein, C.**; Moehwald, H.; Lisdat, F., Coupling of pyrroloquinoline quinone dependent glucose dehydrogenase to (cytochrome c/DNA)-multilayer systems on electrodes. Bioelectrochemistry **2012**, 88, 97-102. (DOI:10.1016/j.bioelechem. 2012.06.003).

PREPARED MANUSCRIPTS

- **Wettstein, C.**; Kano, K.; Wollenberger, U.; Lisdat, F., Investigating the Interaction of Fructose Dehydrogenase with Immobilized Cytochrome **c. Biochimica biophysica acta**

- Sarauli, D.; **Wettstein, C.**; Peters, K.; Schulz, B.; Fattakhova-Rohlfing, D. and Lisdat, F, Conformational Change in Sulfonated Polyaniline Induced by Ca^{2+} Ions: Enhancement of the Bioelectrocatalytic Activity of Fructose Dehydrogenase. Chemistry of Materials.

CURRENT PROJECT

- **Wettstein, C.**; Lisdat, F., Assembly of Cytochrome c:FDH Multilayer Systems on Electrodes.

LIST OF ORAL PRESENTATIONS

- Deutsches Biosensorsymposium (DBS), Wildau (Germany) **2013**.

- Workshop on Biomimetic and Bioanalytical Systems, Luckenwalde (Germany) **2010, 2011, 2012, 2014**.

- Engineering of Functional Interfaces (ENFI), Linz (Austria) **2011.**

- Summer School of the Max-Planck Institute of Colloids and Interfaces Crete (Greece) **2010**, Wismar (Germany) **2011**, Leche (Italy) **2013.**

LIST OF POSTERS

- Deutsches Biosensorsymposium (DBS), Heilbad Heiligenstadt (Germany) **2011**, Munich (Germany) **2015**.

- International Conference on Electroanalysis (ESEAC), Portorož (Slovenia) **2012**.

- Annual Meeting of the International Society of Electrochemistry (ISE), Niigata (Japan) **2011**, Prague (Czech Republic) **2012**.

- Surface Modification for Chemical and Biochemical Sensing (SMCBS), Lochów (Poland) **2011**.

- Engineering of Functional Interfaces (ENFI), Linz (Austria) **2011**.

ERKLÄRUNG AN EIDESSTATT

Hiermit erkläre ich, dass die vorgelegte Arbeit bisher an keiner anderen Hochschule eingereicht sowie selbständig und ausschließlich mit den angegebenen Mitteln angefertigt wurde. Zitate, sowohl wörtlich als auch inhaltlich übernommen, sind als solche gekennzeichnet.

Berlin, 07.01.2015   Christoph Wettstein